
Electronic Thesis and Dissertation Repository

11-10-2023 10:30 AM

Head impact effects in Small Remotely Piloted Aircraft System (sRPAS) collisions: Gender specific risks and vulnerable population protection

MD Farhan Hoque Sagar, *Western University*

Supervisor: Mao, Haojie, *The University of Western Ontario*

A thesis submitted in partial fulfillment of the requirements for the Master of Engineering Science degree in Mechanical and Materials Engineering

© MD Farhan Hoque Sagar 2023

Follow this and additional works at: <https://ir.lib.uwo.ca/etd>



Part of the [Biomedical Engineering and Bioengineering Commons](#), [Materials Science and Engineering Commons](#), and the [Mechanical Engineering Commons](#)

Recommended Citation

Sagar, MD Farhan Hoque, "Head impact effects in Small Remotely Piloted Aircraft System (sRPAS) collisions: Gender specific risks and vulnerable population protection" (2023). *Electronic Thesis and Dissertation Repository*. 9861.

<https://ir.lib.uwo.ca/etd/9861>

This Dissertation/Thesis is brought to you for free and open access by Scholarship@Western. It has been accepted for inclusion in Electronic Thesis and Dissertation Repository by an authorized administrator of Scholarship@Western. For more information, please contact wlsadmin@uwo.ca.

Abstract

This study focuses on supporting the development of safety regulations for vulnerable populations during drone to head impacts. First, the small female head and neck model was compared to cadaveric data. Then, combined with lab's previous work, gender-based disparities in head impact responses were highlighted, with small females experiencing higher injury risk metrics, despite lower skull von Mises stress. Beyond small females, children of various ages and their head responses during impacts were also analyzed. In addition to the previously developed quadcopter drone model, a new Mavic Pro drone model was developed, and this model was integrated with human head models during comparison against cadaveric data. The Mavic Pro, despite its lower weight, demonstrated higher injury risks compared to the previously studied Phantom 3. Overall, in this study head kinematics, head injury criteria (HIC), rotational velocities, and brain strains were analyzed, indicating potential risks for vulnerable populations. These findings underscore the need for tailored safety measures, regulatory guidelines, and comprehensive injury prevention strategies in the field of drone operations.

Keywords

Head injury metrics, head kinematics, small remotely piloted aircraft, finite element analysis, impact biomechanics, vulnerable population, von Mises stress, brain strain, rotational velocities

Summary for Lay Audience

Drones have gained widespread popularity across various industries but concerns about the safety of drone-head collisions have prompted research into head injury risks and protection strategies. This study presents a comprehensive investigation into this critical area.

The study investigated gender-based differences in head injury risks. A computational model was meticulously tested against experimental data, showcasing its reliability in simulating brain motion, and predicting injury responses. Notably, small females exhibited a higher vulnerability to head injuries compared to males. The research progressed on the focus shifted to vulnerable populations, particularly children, in drone-related impacts. Advanced models simulated various impact scenarios and highlighted injury risks based on age groups. Findings underscore the significance of considering both linear and rotational kinematics in assessing head injuries. Furthermore, the study delved into the complex dynamics of drone-to-human impacts, emphasizing small remotely piloted aircraft systems (sRPAS). A highly detailed finite element model accurately replicated real-world impact dynamics and revealed that different drone models pose varying injury risks. The study underscores the importance of rigorous safety measures in drone design and operations.

Co-Authorship Statement

Chapter 2 (Investigation of Gender-Specific Head Injury Risks in Collisions with Small Remotely Piloted Aircraft Systems (sRPAS): Model Verification and Analysis) was co-authored by Yuhu Weng and Dr. Haojie Mao

Chapter 3 (Investigation of Differences in Head Impact Effects Among Vulnerable Populations in Small Remotely Piloted Aircraft Systems (sRPAS)) was co-authored by Dr. Haojie Mao

Chapter 4 (Investigating Head Injury Dynamics in Small Remotely Piloted Aircraft System(sRPAS) to Head Collisions: A Comparative Study of sRPAS Models) was co-authored by Kalish Gunasekaran and Dr. Haojie Mao

All manuscripts were drafted by MD Farhan Hoque Sagar and reviewed by Dr. Haojie Mao

Acknowledgments

I express my sincere gratitude to Dr. Haojie Mao, my supervisor, for his unwavering support and expert guidance throughout this journey. I am also thankful to Dr. Mike Shkrum, a valued member of my advisory committee, for his invaluable assistance and insightful suggestions. I acknowledge Kalish Gunasekaran for his assistance in my research with computational modeling. I acknowledge Transport Canada and National Research Council for their support on this research.

Table of Contents

Abstract.....	ii
Summary for Lay Audience.....	iii
Co-Authorship Statement.....	iv
Acknowledgments.....	v
Table of Contents.....	vi
List of Tables.....	x
List of Figures.....	xi
List of Appendices.....	xiv
List of Acronyms.....	xv
Chapter 1.....	1
1 Introduction.....	1
1.1 Brief Research Rationale.....	1
1.2 Brain and Head anatomy.....	1
1.2.1 Brain anatomy.....	1
1.2.2 Skull anatomy.....	3
1.3 sRPAS to human head impact studies.....	4
1.4 Review of FE Human Model.....	6
1.5 Injury Metrics.....	7
1.6 Research Objectives.....	10
1.7 Thesis Structure.....	10
Chapter 2.....	12
2 Investigation of Gender-Specific Head Injury Risks in Collisions with Small Remotely Piloted Aircraft Systems (sRPAS): Model Verification and Analysis.....	12
2.1 Introduction.....	14

2.2	Methods.....	17
2.2.1	Head model verification for Small Female.....	17
2.2.2	Average Male vs Small Female	24
2.3	Results.....	27
2.3.1	Head model verification.....	28
2.3.2	Male vs Female.....	30
2.4	Discussion.....	32
2.5	Conclusion	34
	Chapter 3.....	36
3	Investigation of Differences in Head Impact Effects Among Vulnerable Populations in Small Remotely Piloted Aircraft Systems (sRPAS)	36
3.1	Introduction.....	37
3.2	Methods.....	39
3.2.1	THUMS FE model.....	39
3.2.2	Impact setting.....	41
3.2.3	Mass-based scaling method	43
3.2.4	Skull stress	45
3.2.5	Comparison of head responses among children.....	45
3.3	Results.....	45
3.3.1	Resultant head linear acceleration verification	45
3.3.2	Resultant head rotational velocity verification	50
3.3.3	Skull stress	55
3.3.4	Comparing average values among child models of different ages	56

3.4 Discussion	58
3.5 Conclusion	60
Chapter 4.....	61
4 Investigating Head Injury Dynamics in Small Remotely Piloted Aircraft System(sRPAS) to Head Collisions: A Comparative Study of sRPAS Models	61
4.1 Introduction.....	62
4.2 Methods.....	64
4.2.1 Mavic Pro model development	64
4.2.2 Available cadaver data for verification.....	67
4.2.3 sRPAS to head impact	68
4.2.4 Mavic Pro vs Phantom 3	70
4.3 Results.....	71
4.3.1 Resultant linear acceleration verification.....	71
4.3.2 Resultant rotational velocity verification.....	71
4.3.3 Comparison of DJI Phantom and Mavic Pro	73
4.4 Discussion.....	77
4.5 Conclusion	80
Chapter 5.....	81
5 Conclusion	81
5.1 Summary and Conclusions	81
5.2 Limitations	82
5.3 Future Work.....	84
5.3.1 Expanded Impact Scenarios.....	84
5.3.2 Advanced sRPAS modeling and Material selection	84

5.3.3	Impact analysis for vulnerable populations	85
5.3.4	Cadaveric study.....	85
5.3.5	Sensitivity analysis and Injury metrics	85
5.4	Novelty, significance, and impact of work	86
References	88
Appendices	99
Curriculum Vitae	107

List of Tables

Table 2-1 Experimental Data for model verification	19
Table 2-2 sRPAS to THUMS female head impact setup.....	26
Table 3-1 sRPAS to Child head setups	41
Table 3-2 PMHS subjects	43
Table 4-1 Parts and material types.....	66
Table 4-2 General material properties	67
Table 4-3 Detailed material properties of polycarbonate	67
Table 4-4 sRPAS to head impact setups. FPS: Foot per second. OSU: Ohio State University	69
Table 4-5 sRPAS to female head setups. FPS: Foot per second.....	70

List of Figures

Figure 1-1 Anatomy of Brain (Adapted from Wikimedia commons)	2
Figure 1-2 Anatomy of Skull (Adapted from Wikimedia commons) [13]	4
Figure 1-3 FAA Hybrid III 50th percentile male dummy (ATD) (Adapted from Wikimedia commons)[18]	5
Figure 1-4 PMHS (Cadaver) experiments conducted by OSU [15]	6
Figure 2-1 Finite Element Model. (a) THUMS 4.02 Small female. (b) Head Only Model. (c) Head and Neck Model. (d-g) Experimental Setup For Head and Neck model verification. ..	19
Figure 2-2 Configuration of impact simulation (Frontal Impact)	22
Figure 2-3 Configuration of lateral drop simulations.	23
Figure 2-4 Neck Verification Model (Axial Loading).....	24
Figure 2-5 THUMS Male vs Female model	25
Figure 2-6 THUMS version 4.02 5th Percentile female model. (a) Full Model, (b-e) sRPAS impact directions.....	26
Figure 2-7 Average peak linear acceleration, HIC and skull stress comparison of male and female model.....	31
Figure 2-8 Average peak rotational velocity, BrIC and CSDM comparison of male and female model.....	32
Figure 3-1 THUMS 10YO, 6YO and 3YO model comparison	40
Figure 3-2 Typical impact directions for all child model	43
Figure 3-3 Head resultant linear acceleration of 10YO child. Experimental data were scaled digitized PMHS experiments data from ASSURE report.....	47

Figure 3-4 Head resultant linear acceleration of 6YO child. Experimental data were scaled digitized PMHS experiments data from ASSURE report.....	49
Figure 3-5 Head resultant linear acceleration of 3YO child. Experimental data were scaled digitized PMHS experiments data from ASSURE report.....	50
Figure 3-6 Head resultant rotational velocity of 10YO child. The experimental data were scaled digitized PMHS experiments data from ASSURE report.....	51
Figure 3-7 Head resultant rotational velocity of 6YO child. The experimental data were scaled digitized PMHS experiments data from ASSURE report.....	53
Figure 3-8 Head resultant rotational velocity of 3YO child. The experimental data were scaled digitized PMHS experiments data from ASSURE report.....	54
Figure 3-9 Skull stress contours comparison of three child models	56
Figure 3-10 Average peak linear acceleration, Average HIC and Average skull stress comparisons of all three-child model.....	57
Figure 3-11 Average peak rotational velocity, Average BrIC, Average CSDM and Average mean MPS comparisons of all three-child model.....	58
Figure 4-1 Mavic Pro finite element model. (a) Full FE model of Mavic Pro. (b) Exploded view. (c) Parts of Mavic Pro. (d) Motor assembly.....	65
Figure 4-2 Mavic Pro Frontal 58-degree Impact setting. (a) THUMS 4.02 50th percentile male model. (b) THUMS 4.02 5th percentile female model	70
Figure 4-3 (a) Mavic Pro. (b) Phantom 3.....	71
Figure 4-4 Head resultant linear acceleration verification. Experimental data were digitized based on ASSURE report.....	72
Figure 4-5 Head resultant rotational velocity verification. Experimental data were digitized based on ASSURE report.....	72

Figure 4-6 Comparison of Mavic Pro Vs Phantom 3 impact at 61fps (a) Peak linear acceleration, (b) HIC, (c) Skull stress..... 74

Figure 4-7 Comparison of Mavic Pro Vs Phantom 3 impact at 71fps (a) Peak linear acceleration, (b) HIC, (c) Skull stress..... 75

Figure 4-8 Comparison of Mavic Pro Vs Phantom 3 impact at 61fps (a) Peak rotational velocity, (b) BrIC, (c) Mean MPS 76

Figure 4-9 Comparison of Mavic Pro Vs Phantom 3 impact at 71fps (a) Peak rotational velocity, (b) BrIC, (c) Mean MPS. 77

List of Appendices

Appendix A: THUMS V4.02 small Female Head model verification Result	99
Appendix B: Material Property of Finite Element model.....	103
Appendix C: The summarized head kinematics, injury metrics, skull von Mises stress and brain strain value child model.....	104

List of Acronyms

ATD: Anthropomorphic test device

ASSURE: Alliance for System Safety of UAS through Research Excellence

BrIC: Brain injury criteria

CSDM: Cumulative strain damage measure

FAA: Federal Aviation Administration

FE: Finite element

HIC: Head injury criteria

MPS: Maximum principal strain

NIAR: National Institute for Aviation Research

OSU: Ohio State University

PMHS: Post mortem human surrogate

sRPAS: Small Remotely Piloted Aircraft Systems

THUMS: Total Human Model for Safety

Chapter 1

1 Introduction

1.1 Brief Research Rationale

The small remotely piloted aircraft (sRPAS) has undergone significant growth and development in recent years [1]. In 2022, the global market for commercial drones was valued at USD 8.15 billion, and it is anticipated to reach USD 47.38 billion by 2030 [2]. With drones experiencing a substantial increase in popularity and continued growth, it becomes essential to prioritize addressing safety concerns, especially regarding head impacts and injuries caused by these devices. Between 2015 and 2020, an estimated 4,250 drone-related injuries occurred in the US [3]. Among the individuals affected, 21% were below the age of 18, and a significant majority, constituting 84%, were male. Predominant injury diagnoses included lacerations (72%), followed by contusion/abrasion (10%), strain/sprain (5%), and internal injury (5%) [3]. Multiple reported incidents of drone-related injuries include a 13-year-old boy who sustained a skull fracture from a racing drone collision [1] and a 21-month-old girl who suffered a facial injury due to a toy drone [4]. These cases serve as clear examples of the potential risks associated with sRPAS operations in densely populated areas. Conducting a comprehensive analysis of collisions between sRPAS and humans is of utmost importance to identify relevant head injury metrics and establish effective safety regulations for sRPAS. This thesis focuses on investigating head injuries resulting from drone-to-head collisions in males, females, and vulnerable populations. It also involves calculating injury metrics and examining how different population groups experience head injuries due to drone-to-head impacts.

1.2 Brain and Head anatomy

1.2.1 Brain anatomy

The brain is an intricately complex organ composed of various interconnected components that work harmoniously to process, integrate, and coordinate information from different parts of the body, ensuring its optimal functioning (**Figure 1-1**). It

represents approximately 2% of our body weight, weighing around 1.36kg (3lb) [5]. Serving as the central command center of the body within the central nervous system (CNS), the brain is composed of an intricate network of neurons and supportive tissue, safeguarded by the skull, and surrounded by cerebrospinal fluid. It can be categorized into two primary divisions: gray matter and white matter. Gray matter encompasses nerve cells, glial cells, capillaries, and neuropil, while white matter consists of myelinated axons that establish connections between various regions of gray matter. Each distinct region of the brain possesses its own unique characteristics and functions, contributing to essential processes such as movement, cognitive processing, and everyday activities.

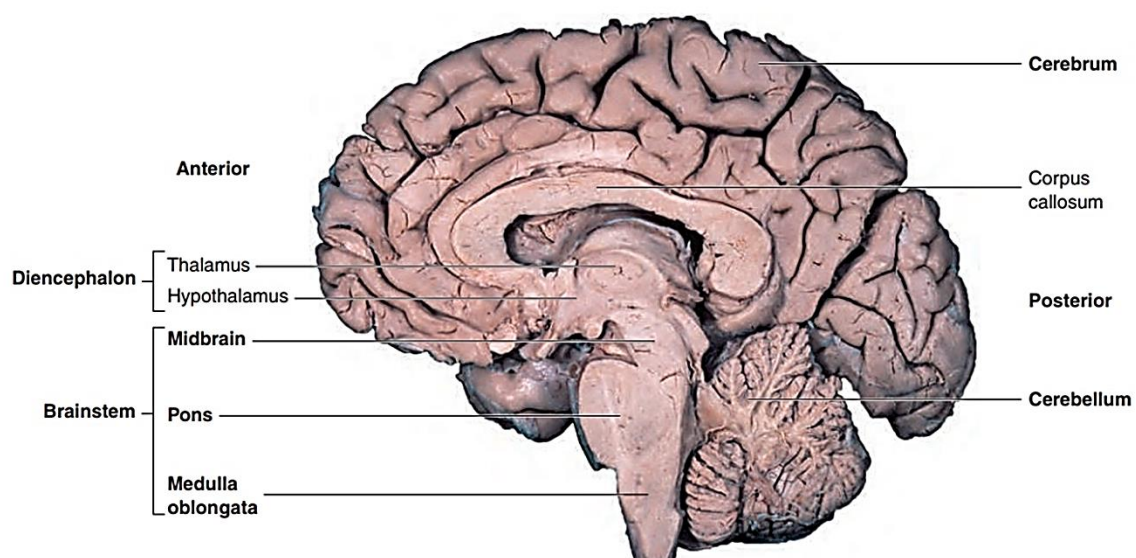


Figure 1-1 Anatomy of Brain (Adapted from Wikimedia commons)

The brain can be further categorized into three primary sections: the cerebrum, cerebellum, and brainstem. The cerebrum is the largest part and includes components such as the cortex, hippocampus, thalamus, basal ganglia, and corpus callosum. It primarily supports higher cognitive functions [6]. The cerebellum, located at the base of the brain and connected to the brainstem, plays a crucial role in coordinating movement and balance. The brainstem consists of the midbrain, pons, and medulla, and it connects the cerebrum to the spinal cord while regulating essential functions like auditory processing, eye movement, and sleep [7]–[9]. Previous research indicates that concussion

is often linked to deformation in specific areas of the brain, such as the corpus callosum, thalamus, midbrain, and brainstem [10]–[12].

Due to its delicate nature, the brain is vulnerable to injuries even from minor deformations. It responds differently to deformations compared to organs like the heart and muscles [13]. Understanding the brain's anatomy and properties is essential for studying impact injury mechanisms and establishing effective safety measures.

1.2.2 Skull anatomy

A skull is a bony structure that supports the face and surrounds the brain in a protective chamber. It is made up of 8 cranium bones and 14 face bones (**Figure 1-2**). The cranium houses the brain and the meninges as well as the cerebral vasculature. Anatomically, the cranium bone can be subdivided into calvarium and cranial base. Calvarium bones comprised of frontal, occipital and two parietal bones. The cranial base consists of the sphenoid, frontal, ethmoid, occipital, parietal, and temporal bones. These cranial bones collectively form a strong bony enclosure that surrounds and protects the brain. Three layers make up the skull. Trabecular bones make up the middle layer, whereas thick cortical bones make up the inner and outer layers. The rest of the skull is made up of facial bones that are connected to the skull. 13 of the 14 facial bones are fused or connected to the skull [5].

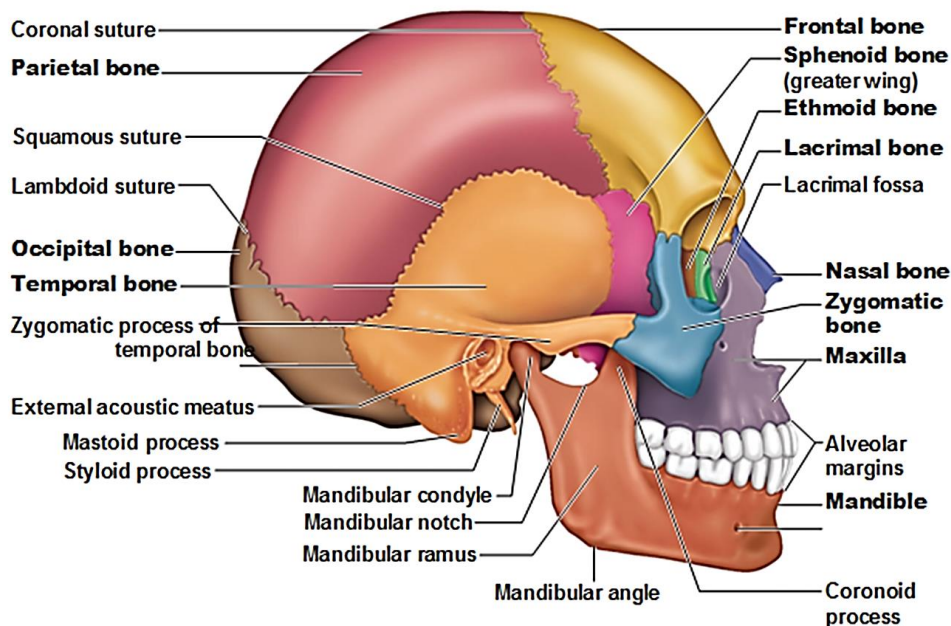


Figure 1-2 Anatomy of Skull (Adapted from Wikimedia commons) [13]

1.3 sRPAS to human head impact studies

Aviation regulatory authorities are currently addressing the challenge of balancing the advantages of Small Remotely Piloted Aircraft System (sRPAS) with the safety risks they pose to individuals and property. Various solutions have been proposed and put into action to ensure the safety of people on the ground. Before implementing regulations, authorities need to thoroughly examine studies on the impact of sRPAS on humans and understand the potential harm. It is important to determine the threshold values for impact energy, velocity, and sRPAS weight that can lead to serious accidents involving people on the ground. The FAA recently supported a consortium to investigate collisions between sRPAS and humans. The findings were reported in the ASSURE report, providing valuable data from cadaveric experiments [14]. The impacts caused by sRPAS are complex due to variations in impact energy, construction stiffness, velocity ranges, and sRPAS masses [14]. The University of Alabama in Huntsville (UAH) flight test reports recorded different failure modes, with vertical and downward angled impacts being the most probable scenarios. The Civil Aviation Safety Authority (CASA) in Australia has published an in-depth analysis of human injuries caused by impacts from

small, unmanned aircraft, which is one of the few reports providing data to support proposed rules and regulations. The analysis examined the principles of object collision and determined the outcomes in relation to kinetic energy and blunt criteria (BC) levels. The report reinforces Australia's regulation that unmanned aircraft systems (UAS) must maintain a minimum distance of 30 meters from individuals [16].

Various surrogates, such as anthropomorphic test devices (ATDs) and post mortem human surrogates (PMHSs), were utilized to simulate human responses in sRPAS collisions [15]. Each surrogate has its own strengths and limitations, but the main objective is to replicate human reactions in these collisions. This enables the evaluation of human tolerance and facilitates improvements in sRPAS design and safety measures.

Anthropomorphic test devices (ATDs), commonly known as dummies, were used by the National Institute for Aviation Research (NIAR) to assess the damage caused by sRPAS impacts [15]. They employed FAA Hybrid III 50th percentile male representative ATDs equipped with sensors to measure impact kinematics. While ATDs provide valuable insights and are easily repeatable [17], they have limitations in measuring skull and brain responses accurately. Another drawback is that ATD tests are time-consuming and costly. However, ATDs are commonly used in safety regulation tests to understand head responses during impacts.



Figure 1-3 FAA Hybrid III 50th percentile male dummy (ATD) (Adapted from Wikimedia commons)[18]

Post mortem human surrogate (PMHS) subjects have also been utilized to estimate injury risks from sRPAS impacts [15]. PMHS tests offer the advantage of studying human body responses and can represent injury characteristics such as skull fractures. However, conducting PMHS tests with entire cadavers is expensive, and the lack of neck muscle tension in cadaver subjects may affect head kinematics under impacts [19], [20].

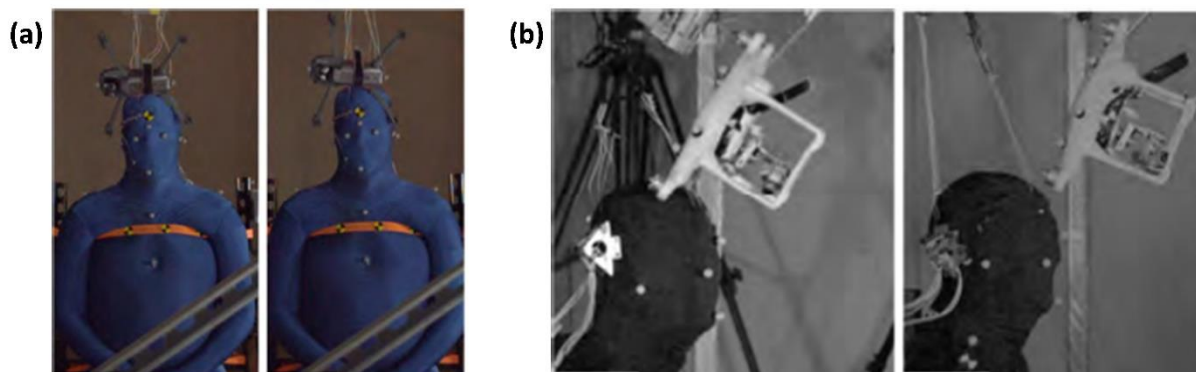


Figure 1-4 PMHS (Cadaver) experiments conducted by OSU [15]

1.4 Review of FE Human Model

Currently, biofidelic human models are being developed using computed tomography (CT) and magnetic resonance imaging (MRI) scans of volunteers. This study utilized the 5 finite element (FE) human models, including the THUMS version 4.02 50th percentile male, THUMS version 4.02 5th percentile small female, and THUMS version 4 3YO, 6YO, and 10YO models. Validation of these FE head models was performed using cadaver experiment data. The earliest 3D FE head model was developed by Ruan et al. from Wayne State University (WSU) in 1992 [21] and underwent subsequent refinements by Zhou et al., adding details such as grey matter and white matter. In 1997, Kang et al. developed the Université Loise Pasteur (ULP) human head model, which consisted of various components such as the skull, falx, tentorium, subarachnoid space, scalp, cerebrum, cerebellum, and brainstem [22]. The continuous improvement of FE techniques led to the development of the Kungliga Tekniska Högskolan (KTH) model in 2002 by Kleiven, which incorporated anatomical features and different material

properties [23]. In 2003, Takhounts and Eppinger created the simulated injury monitor (SIMon) model, representing the 50th percentile male [24]. Over time, these models were updated with improved geometry and material properties. A significant advancement occurred in 2013 with the development of the Global Human Body Models Consortium (GHBMC) FEM by Mao et al., which included key anatomical features and underwent validation against intracranial pressure data, brain displacements, nasal impacts, and frontal horizontal impacts [25]. Other validated head models, such as the Total Human Model for Safety (THUMS), Dartmouth Head Injury Model (DHIM) [26], University College Dublin Brain Trauma Model (UCDBTM) [27], and Strasbourg University Finite Element Head Model (SUFEHM) [28], are widely used in biomedical research.

1.5 Injury Metrics

Injury metrics are measurements used to quantify the severity of head impacts and can be represented by a single variable like linear acceleration or rotational velocity of the head, or a combination of variables. Traditionally, concussion prediction methods have relied on kinematics-based head injury metrics. These metrics are typically calculated based on the peak resulting kinematic response of the head during a traumatic impact. The development of these metrics was based on experimental data collected in the 1950s and 1960s, which were used to create a concussive tolerance curve known as the Wayne State tolerance curve (WSTC) [29]. Although the methods and analysis used to develop the WSTC have faced criticism, they have proven effective in reducing the occurrence of head injuries. According to the WSTC, the head can withstand higher peak acceleration for a short duration but will lead to injury if the same acceleration is sustained for a longer period [30]. Head injury metrics are based on either the translational or rotational motion of the head, or a combination of both. Additionally, tissue-based metrics have been developed through finite element (FE) analysis or in vitro experiments, focusing on parameters such as brain tissue stress and strain.

Gadd was the first to apply the WSTC to a head injury metric [31]. He proposed a weighted metric that would depend more on acceleration magnitude than duration. This metric became known as the severity index (SI). The equation is stated below:

$$SI = \int a(t)2.5dt$$

Where 'a' is head acceleration as a function of time, The weighting factor of 2.5 was based mainly on the slope of the straight-line approximation of log-log plot of the animal data used in the WSTC. It is good for predicting severe skull fracture and brain trauma, but it is not a good predictor for mTBI [32].

One of the conventional metrics used in the automotive industry for over three decades and popular in many industrial and research areas for predicting traumatic brain injury (TBI) is head injury criteria (HIC) [33]. The algorithm for the HIC calculates not only the severity of the head injury, but also the level of risk that is imposed by the collateral impact. The governing HIC equation is stated below:

$$HIC = \max_{t_1, t_2} \left\{ (t_2 - t_1) \left[\frac{1}{t_2 - t_1} \int_{t_1}^{t_2} a(t) dt \right]^{2.5} \right\}$$

Where 'a(t)' is the acceleration as a function of time and 't₁' and 't₂' are the bounds of the time interval that maximizes the HIC value over the duration of the pulse.

Initially, the Head Injury Criterion (HIC) had no time interval limit when it was first adopted by NHTSA, with a maximum limit set at 1000. In 1986, NHTSA proposed to limit the time interval to 36 ms after observing that long-duration accelerations with low magnitude were producing HIC values above the threshold, contrary to volunteer data [34]. Around the same time, a 15-17 ms limit was suggested since none of the injurious points on the WSTC had HIC durations greater than 13 ms. To maintain similar failure rates for cars, the introduction of HIC15 accompanied the reduction of the maximum HIC values.

Initially, the focus on head injury metrics was primarily based on linear acceleration, disregarding rotational acceleration, despite early theories recognizing the importance of both [35]. This limitation was due to the lack of comprehensive data and challenges in

accurately measuring rotational kinematics [36]. However, through the utilization of scaled animal models and collaboration with NHTSA, a rotational brain injury criterion called Brain Injury Criteria (BrIC) was developed. BrIC incorporates peak angular velocity and critical values that are directionally dependent on the anatomical planes of anthropomorphic test dummies [37]. BrIC has played a crucial role in understanding vehicle and dummy motion when developing restraint system tests. Recently, BrIC has been updated and adopted as a new head injury criterion in automobile oblique impact crash tests by the New Car Assessment Program [38]. The governing BrIC equation is stated below:

$$BrIC = \sqrt{\left(\frac{\omega_x}{\omega_{xc}}\right)^2 + \left(\frac{\omega_y}{\omega_{yc}}\right)^2 + \left(\frac{\omega_z}{\omega_{zc}}\right)^2}$$

Here, ω_x , ω_y , and ω_z are peak rotational velocity and ω_{xc} , ω_{yc} , and ω_{zc} are the critical rotational velocity in X, Y, Z axes [37].

Additional kinematics-based injury metrics encompass the Generalized Acceleration Model for Brain Injury Threshold (GAMBIT), which considers both linear and rotational acceleration of the head [39]. Another metric is the Head Impact Telemetry Severity Profile (HITSP), that combines factors such as linear and rotational acceleration, impact duration, and location [40].

Finite element (FE) models are utilized to predict the mechanical response of brain tissue during impacts, offering the potential to improve injury predictions by simulating specific mechanisms of brain injury rather than relying solely on overall head kinematics [41].

One such correlation has been identified between Diffuse Axonal Injury (DAI) and the tensile strains endured by a cumulative volume of brain tissue surpassing a predefined critical threshold. To predict the likelihood of DAI, the Cumulative Strain Damage Measure (CSDM) evaluates the strain levels within a specific fraction of the brain tissue's volume [24].

1.6 Research Objectives

To enhance comprehension of head responses and injury risks arising from sRPAS-related impacts on human heads, aimed at aiding the development of safety regulations, this thesis concentrated on the following objectives:

#1 The verification of the THUMSv4.02 small female head model through assessment against nine experimental loading conditions.

#2 Conducting a comparison between the average male and small female models, highlighting disparities in head kinematics and injury metrics.

#3 Verifying the model using scaled PMHS experimental data and mainstream injury metrics such as HIC and BrIC. This verification process aimed to facilitate the application of the model in assessing sRPAS.

#4 Collision-induced head injuries, thereby providing data to support safety regulations for vulnerable groups, particularly children.

#5 Developing a high-fidelity quadcopter sRPAS FE model, seamlessly integrated with a high biofidelity human model (THUMS) to understand sRPAS to head impacts.

#6 A comparative analysis between the previously modeled sRPAS (Phantom 3) and the newly developed sRPAS (Mavic Pro) model. This comparison aimed to discern differences in injury metrics, such as HIC and BrIC, when collisions with the head occur and variations in head kinematics are present.

1.7 Thesis Structure

Chapter 1 introduces the context of head injuries and the impact of small remotely piloted aircraft systems (sRPAS) on human heads. It also introduces key investigative methods including tests on Post Mortem Human Subjects (PMHS), dummy tests, and Finite Element (FE) models.

In Chapter 2, the verification process of the THUMS V4.02 small female head and neck model is outlined, compared against nine experimental studies. The study further

compares the head responses of the 50th percentile male and 5th percentile small female models. A combined sRPAS model with the small THUMS female model is developed. The chapter concludes by comparing head kinematics and injury metrics between the average male and small female models.

In Chapter 3, a comparison is drawn between the head responses of 10-year-old, 6-year-old, and 3-year-old child models. The sRPAS model is integrated with all three THUMS child models, verified using scaled OSU PMHS male experiment data. Head kinematics and injury metrics across the child models are compared.

Chapter 4 explains the development process of a new representative quadcopter sRPAS FE model. This model is combined with the THUMS model to simulate PMHS experiments by OSU. The FE models are verified using linear acceleration and rotational velocity curves from PMHS tests. The chapter also compares the head responses to impacts from previously developed sRPAS (Phantom 3) and newly developed sRPAS (Mavic Pro) on both average male and female models.

Chapter 5 concludes the thesis research by summarizing the findings and discussing the study's limitations. It also highlights future research directions, significance, and the novel contributions of the study.

Chapter 2

2 Investigation of Gender-Specific Head Injury Risks in Collisions with Small Remotely Piloted Aircraft Systems (sRPAS): Model Verification and Analysis

Abstract

Drones have become immensely popular and are being utilized across various industries, but the concern regarding potential risks associated with drone-head collisions has necessitated research into head injury mechanisms and protective strategies. This study focuses on first verifying the THUMS 4.02 small female head model and then comparing it with the verified average male model. Nine different loading cases were carefully selected from a range of experimental head impacts to thoroughly assess the model's predictive capabilities. Brain motion was verified by comparing the model's predictions of brain displacement with data obtained from blunt impact experiments conducted by Hardy et al (2001 & 2007). Furthermore, brain pressure predictions were verified against intracranial data reported by Nahum et al (1977). The force deflection responses were verified by comparing the model's simulations with lateral impact tests conducted by Yoganandan et al. (1995). Additionally, the neck model was verified using dynamic axial loading experiments reported by Nightingale et al (1997). The results demonstrated that the computational model accurately predicted brain displacement within the range of experimental measurements, indicating its reliability in simulating brain motion. Model predictions revealed a close match between the model's predictions and the experimental values, thereby reinforcing the model's accuracy. The model also demonstrated a strong alignment between the predicted force and measured force of skull impacts. Lastly, the model's predictions of neck forces closely corresponded to the experimental measurements. A comparative analysis of the average male and small female models revealed that small females experienced higher levels of linear acceleration, rotational velocity, and head injury criteria values, such as head injury criteria (HIC), brain injury criteria (BrIC), and brain strains, compared to males. These findings provide valuable insights into the head kinematics and injury metrics, shedding

light on the gender differences within the models. The results of this study significantly contribute to the understanding of head injury mechanisms and can serve as a foundation for the development of more effective head protection strategies for individuals of both genders.

2.1 Introduction

Traumatic brain injuries (TBI) impose a significant societal burden globally, affecting approximately 1.4 million individuals in the United States annually [42]. Road traffic accidents, sports-related incidents, falls, bullet strikes, explosions, and other external forces are the leading causes of TBI [43]. While TBIs from drone impacts are relatively less common than those in the mentioned scenarios, the anticipated rapid growth of small remotely piloted aircraft (sRPAS) and the consequential impact of TBI underscore the importance of understanding the biomechanical responses of sRPAS to head impacts for enhanced protection.

In studying TBI, the development of computational techniques has facilitated the creation of numerical head models, particularly finite element (FE) models, enabling comprehensive biomechanical investigations. Researchers worldwide have employed diverse approaches to develop human head FE models. These models are now the most advanced numerical representations, providing insights into brain deformations and strain/stress distributions associated with the risk of head injuries. While significant advancements have been made in FE modeling of the human head, there remains a need for continued research to elucidate head injury mechanisms and explore different forms of head protective equipment. The initial endeavor to simulate human head response using FE modeling was undertaken by Hardy et al. and Marcal et al. (1973) [44]. They developed a two-dimensional (2D) FE head model, solely incorporating the skull. Building upon their work, Shugar et al. (1975) [45] enhanced the model by introducing an elastic fluid-filled brain, presumed to be securely attached to the skull. Advancements in medical imaging, along with the availability of sophisticated pre-processing FE software and modeling techniques, have streamlined the process of creating new FE models, enabling faster and more efficient model development within reduced timeframes. In 2016, Miller et al. devised custom software codes that automated the generation of hexahedral meshes from image data, emphasizing the need for high-density meshes to accurately depict the curved and smooth surfaces of the brain [46]. Additionally, Mao et al. (2013) introduced a multi-block method incorporating O-grid blocks to create FE meshes for the brain model, ensuring the smoothness of its external

surfaces [25]. The majority of head models have been constructed with the intention of assessing specific facets of head injury. Among the various finite element (FE) human head models, only a few intricate models have been subjected to validation encompassing both brain motion and brain pressure [47], [48]. Notably, Zhang et al. extensively investigated various head responses, including those of the brain, skull, and facial regions [49]. Similarly, Mao et al. [25] delved into multiple aspects of head responses, such as brain pressure, relative skull-brain motion, skull response, and facial response. Fernandes et al. (2018) developed an FE head model and validated it through experimental cadaver impact tests. The validation included comparing intracranial pressure across frontal, parietal, occipital, and posterior fossa regions [50]. Iwamoto et al. (2015) developed and validated THUMS Version 5, an FE model of the human body. Validation involved comparing the model to 36 series of data from post-mortem human subjects (PMHS) [51]. While the model demonstrated good biofidelity in regional or full-body responses to side impacts, the discrepancies between model prediction and measurements in local responses, such as brain displacements, are observed.

Drones have become increasingly popular in recent years and are being used in various fields and industries. Their applications range from recreational, hobbyist use, to professional photography, videography, surveillance, delivery services, agriculture, and even infrastructure inspections. Drones are now a multi-billion-dollar industry [52]. While drones offer numerous benefits and opportunities, there have been instances of injuries and accidents resulting from drone impacts. Extensive research has been conducted on the collision between unmanned aircraft systems and the human head due to the rising utilization of drones in commercial and recreational settings, which has raised concerns about the potential risks of drone-head collisions. If an unsuspecting passerby is struck by a free-falling or rapidly accelerating sRPAS, the resulting head trauma could be severe, potentially leading to concussion or even death in certain situations. Injuries can occur both directly from the impact of drones and indirectly while handling them, with a higher incidence of injuries reported to be caused by direct impact [53], [54]. These lightweight drones are operated above individuals, posing a risk of impacting heads at speeds that can exceed 20 m/s [15].

The Federal Aviation Administration (FAA) has been pursuing a risk-based approach to determine safety operation parameters for sRPAS and to update its regulatory framework for commercial operations involving sRPAS [55]. The FAA initiated a significant project aimed at investigating the impact of sRPAS on human heads. The latest findings are summarized in the Alliance for System Safety of UAS through Research Excellence (ASSURE) report [15]. Various tests were conducted involving different sRPAS, impact scenarios, and impact partners, including a simplified Anthropomorphic Test Device (ATD) representing the head and neck of an average-sized male, an ATD representing the FAA's average-sized male, and Post Mortem Human Surrogates (PMHS). The PMHS experiments offered a valuable opportunity to develop and validate finite element (FE) simulations of sRPAS impacting human heads. Weng et al. (2021) validated an sRPAS FE model using data obtained from the ASSURE report, which provided a unique opportunity for the development of validated computational models [56]. Xin proposed a mathematical model to predict the level of injury resulting from drone-to-human impacts [57], while Magister (2010) proposed a modeling method to assess sRPAS-related injuries based on blunt ballistic impacts [58].

Gender-specific risks for Traumatic Brain Injury (TBI) have been reported in the literature, with higher concussion risks found among female athletes participating in sports such as baseball, basketball, ice hockey, and soccer [59]–[61]. In ice hockey specifically, the incidence of concussions in females was approximately 1.1 to 2.2 times higher than in males [59], [62]–[64]. Several factors may contribute to this discrepancy, including the smaller neck size and lower body mass of females [59], [65]. However, there is currently a lack of impact studies specifically examining the effects of sRPAS on females in the existing literature. [15]. Yoganandan and Pintar (2005) utilized scaling laws to develop acceleration, deflection, and force-time responses for small females [66]. Similar scaling laws have been employed to evaluate head responses across different species [67].

The objectives of this study include the verification of the THUMS V4.02 FE head model against a wide range of impact scenarios to ensure its biofidelity and stability. Additionally, the study aims to investigate the differences between average males and

small females under the same sRPAS-to-head impact scenarios. The simulations of sRPAS impacting small females were verified by comparing them to scaled PMHS data as conducted by Weng et al. (2021) [68]. Various parameters including head kinematics, head injury metrics, skull stress, and brain strain were summarized and compared between average males and small females.

2.2 Methods

The method section of this study primarily included two crucial aspects. Firstly, it focused on the verification of the THUMS 4.02 small female head model. Secondly, it pertained to the comparison between average male and small female subjects.

2.2.1 Head model verification for Small Female

2.2.1.1 Finite Element Model

The 5th percentile small female model from the Total Human Model for Safety (THUMS) version 4.02 [69] was used for this study. This female model was created by integrating various component models, including the head, torso, and extremity models. The female model consists of 2,514,045 elements and 878,461 nodes, with a total mass of 49kg. The THUMS model incorporates a three-layered structure for the skull, characterizing the outer and inner components as shells with an elastic-plastic material model featuring optional damage parameters. The intermediate spongy bone (diploe) is represented as a solid entity, employing an elastic viscoplastic material model. Within the brain region, both white and grey matter are defined using nearly incompressible and viscoelastic material properties. The skin and flesh portions are modeled as hyperelastic material. The nodes of the inner skull and arachnoid nodes are interconnected through tied contacts, while a low shear modulus cerebrospinal fluid (CSF) layer is introduced to facilitate controlled motion on the brain surface. Additional details regarding the material modeling of the FE model are available in Appendix B (**Table B 1**). The integration of the head and torso models occurs at the occipital condyle, where the inferior section of the head model is affixed to the neck model. The neck muscles are represented using 1D elements, with their attachment points to bony structures aligned with anatomical insertion points, ensuring biomechanical accuracy. Hexahedral elements were employed

in the generation of a solid mesh, conforming to prescribed guideline values. Tetrahedral elements were specifically chosen for the representation of internal organs and cortical bones, owing to the inherent complexity of their geometries, which posed challenges in achieving the required element quality. Furthermore, tetrahedral elements were utilized to model the flesh surrounding joints, facilitating seamless remeshing in response to changes in posture. **Figure 2-1 (a)** depicts the entire body model. For head verification, this study focused on the head-only model (**Figure 2-1 (b)**), while for neck verification, head and neck model was extracted from the THUMS version 4.02 5th percentile small female model (**Figure 2-1 (c)**). THUMS version 4.02 features improved mesh quality compared to version 4.01 and version 4 for the brain, skull, and epidermis parts. In version 4.02, the element lengths for these parts range from 1.2 to 5 mm, while in V4.01 and V4, the element length for the brain part specifically is 3 to 7 mm. Given the improved mesh quality and different element sizes in version 4.02, the main goal of this thesis involved the verification of the model through a range of impact experiments. **Figure 2-1** illustrates the different loading conditions utilized for head and neck model verification for version 4.02.

2.2.1.2 Experimental data for model verification

To verify the accuracy of the head and neck model, nine real-world head impact scenarios were simulated. The predictions of the finite element (FE) head and neck model were assessed by comparing the relative motion between the skull and brain, brain pressure, force deflection and drop test. The **Table 2-1** provides a summary of all the loading cases derived from the experimental studies. To comprehend the methods utilized in each loading condition within the experimental setup, concise descriptions of the experimental studies are provided.

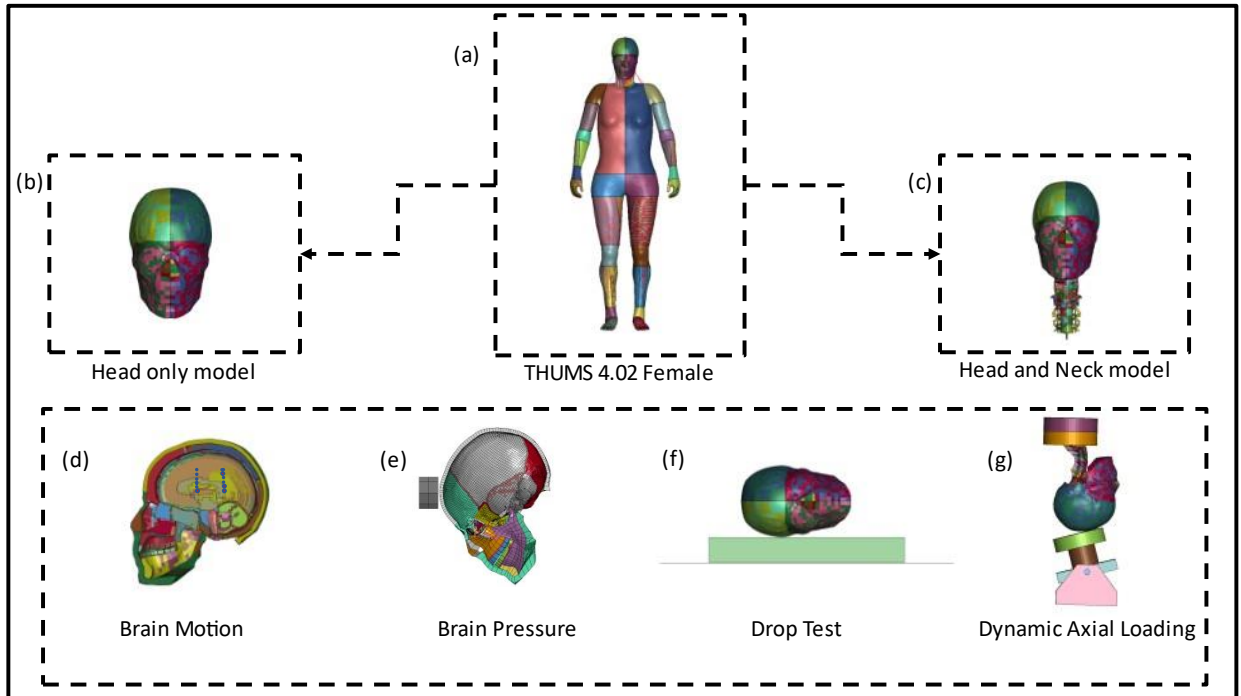


Figure 2-1 Finite Element Model. (a) THUMS 4.02 Small female. (b) Head Only Model. (c) Head and Neck Model. (d-g) Experimental Setup For Head and Neck model verification.

Table 2-1 Experimental Data for model verification

Model Verification Target	Author, year	Description	Loading Case (Simulation Settings)
Brain Motion	Hardy, 2001,2007 [47], [70]	Coronal Plane, aligned to CG Test id: 380-T3	1
		Coronal Plane, offset to CG Test id: 380-T4	1
		Horizontal Plane, offset to CG Test id: 380-T5	1
		Coronal Plane, offset to CG Test id: 393-T4	1

Brain Pressure	Nahum, 1977 [48]	Frontal Impact on Forehead Test id: 37	1
Force Deflection	Yoganandan, 2004 [71]	Lateral Impact, velocity: 3.5 m/s, 4.9 m/s, 6 m/s	3
Neck Verification	Nightingale, 1997 [72]	Drop test, Test id: D41- R+15 and N18-R+15	1

2.2.1.3 Mass based scaling method

For the study of head impact, various experimental studies employed different types of cadavers with varying masses. In order to verify the THUMS V4.02 small female FE head and neck model, it was necessary to account for these differences. Thus, a mass-based scaling law was utilized to scale the cadaveric data. According to literature findings, the 5th percentile small female is reported to have an average body weight of 49 kg [69].

The equations for calculating the mass-based scaling factor of head kinematics are shown below [66], [67]:

$$\text{Mass Ratio: } \lambda_m = \frac{M(\text{Cadaver})}{M(\text{THUMS})}$$

$$\text{Linear acceleration factor: } \lambda_a = (\lambda_m)^{-\frac{1}{3}}$$

$$\text{Angular velocity factor: } \lambda_\omega = (\lambda_m)^{-\frac{1}{3}}$$

$$\text{Time ratio factor: } \lambda_T = (\lambda_m)^{\frac{1}{3}}$$

Where $M(\text{Cadaver})$ and $M(\text{THUMS})$ represent the body mass of cadaver subject and THUMS FE model.

Predicted Head kinematics are shown below:

$$\text{Linear acceleration of FE female model: } a(\text{THUMS}) = \frac{a(\text{Cadaver})}{\lambda_a}$$

$$\text{Angular velocity of FE female model: } \omega(\text{THUMS}) = \frac{\omega(\text{Cadaver})}{\lambda_{\omega}}$$

$$\text{Time of FE female model: } T(\text{THUMS}) = \frac{T(\text{Cadaver})}{\lambda_T}$$

Where, $a(\text{Cadaver})$ and $a(\text{THUMS})$ represent the linear acceleration of Cadaver and THUMS FE model; $\omega(\text{Cadaver})$ and $\omega(\text{THUMS})$ represent the angular velocity of Cadaver and THUMS FE model. $T(\text{THUMS})$ and $T(\text{Cadaver})$ represent the time history of THUMS FE model and Cadaver.

2.2.1.4 Brain Motion

Hardy et al. (2001,2007) conducted classical experiments providing skull-to-brain displacement data to verify model-predicted brain displacements [47], [70]. Although displacements are not directly linked to strains, the reasonable prediction of brain motion would support that the stiffness of the computational brain model is appropriately defined providing more confidence in trusting strain predictions. Using a high-speed x-ray system combined with radio-opaque neutral-density-targets (NDTs), brain deformation could be visualized during blunt impacts. Impacts from various directions were conducted.

Hardy et al. (2001,2007) documented details of cadaveric heads in their published work. In Hardy et al.'s 2001 study, Cadaver C755 and C383 were used during impacts along the sagittal plane [70]. Although details of cadavers were not reported in the paper, a further investigation was conducted and pinpointed cadaver info in Hardy's PhD thesis [47]. Data from female cadavers are deemed useful for model verification. However, it should be noted that these female cadavers are not entirely at the 5th percentile size and hence scaling was needed. All available female cadaver data under these impact settings that have been adopted by the research community were used for verification.

2.2.1.5 Brain Pressure

The impact of a rigid mass on the skull was examined by Nahum et al. (1977), who employed a rigid impactor covered with multiple padding materials to deliver an anterior-posterior blow to the frontal bone in the mid-sagittal plane [48]. To compare the predicted brain pressure of the FE head model of THUMS 4.02 female, six cases of

Nahum's frontal angled head impact were used. The skull was inclined forward by 45° to align the Frankfurt anatomical plane horizontally. An impact force from Nahum et al.'s experiment no. 37 was applied to the forehead to verify the THUMS version 4.02 5th percentile female model, with impact boundary conditions illustrated in **Figure 2-2**.

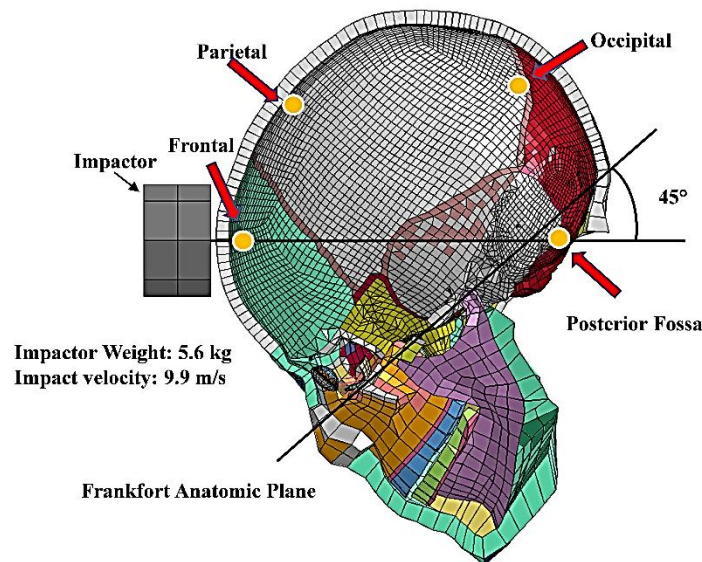


Figure 2-2 Configuration of impact simulation (Frontal Impact)

2.2.1.6 Force Deflection

Yoganandan et al. (2004) performed impact tests on the lateral side of the cranium of unembalmed post-mortem human subjects to ascertain the force and acceleration corridors at varying velocities for this region of the head [71]. The experiment involved the use of multiple triaxial accelerometers that were exposed to progressively increasing velocities through free-fall techniques, with impacts directed towards a force plate. The force plate was covered with a 40-durometer padding material. To verify the accuracy of the finite element (FE) head model, three loading scenarios from Yoganandan et al.'s experiment were replicated through simulation (**Figure 2-3**). The force deflection values

predicted by the FE head model for these loading scenarios were then compared to the corresponding experimental observations.

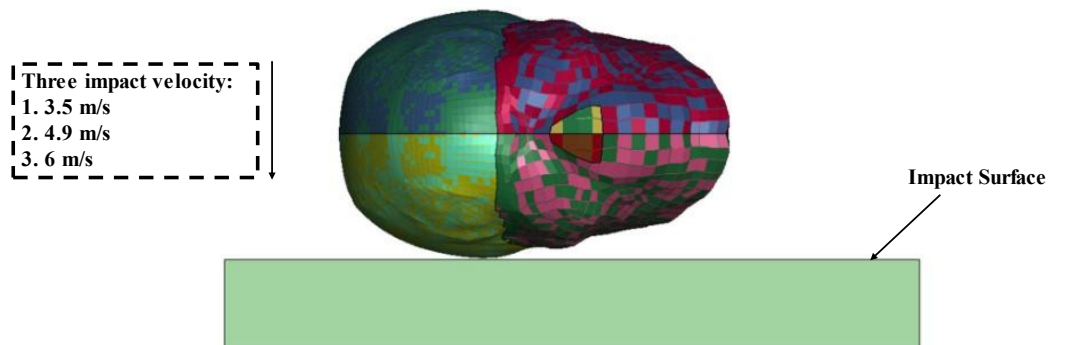


Figure 2-3 Configuration of lateral drop simulations.

2.2.1.7 Neck model verification

Nightingale et al. (1997) used unembalmed head and neck specimens from 22 cadavers to study the dynamics of head and cervical spine impact and the effect of head inertia and impact surface on injury risk [72]. The specimens were subjected to impacts using a drop tower with a drop mass, and the impact surface was varied between a rigid flat surface and a deformable surface. To verify the accuracy of the THUMS FE head and neck model, two tests, specifically D41-R+15 and N18-R+15, were selected from Nightingale et al.'s experiment. The impact boundary conditions for these tests were illustrated in the **Figure 2-4** Subsequently, the force values predicted by the FE head and neck model for these two loading scenarios were compared against the experimental observations.

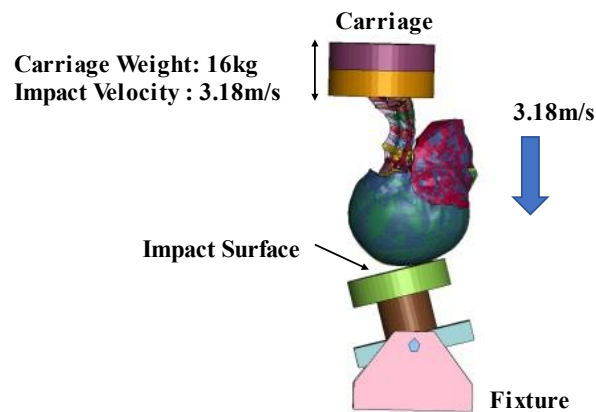


Figure 2-4 Neck Verification Model (Axial Loading)

2.2.2 Average Male vs Small Female

2.2.2.1 Finite Element model

The study utilized both the Total Human Model for Safety (THUMS) version 4.02 5th percentile small female model and the 4.02 50th percentile male adult model. The comparison of these THUMS male and female models is depicted in the **Figure 2-5**. Section **2.2.1.1** of the study provides information about the THUMS small female FE model. Similarly, the THUMS V4.02 adult male model features highly detailed brain meshes, with the element length of the brain part ranging from approximately 1.2 to 5mm. This particular model consists of 777,156 nodes and 1,975,599 elements, with a total mass of 77.6 kilograms. The head model verification involved several experiments, including translational impact experiments conducted by Nahum et al. (1977) to verify brain pressure [48], translational impact experiments conducted by Yoganandan et al. (1995) to verify skull impact forces, and translational and rotational impact experiments conducted by Hardy et al. to verify brain-skull relative motion [47], [70]. The neck part of the THUMS model was verified through dynamic axial loading experiments conducted by Nightingale et al. (1997) [72].

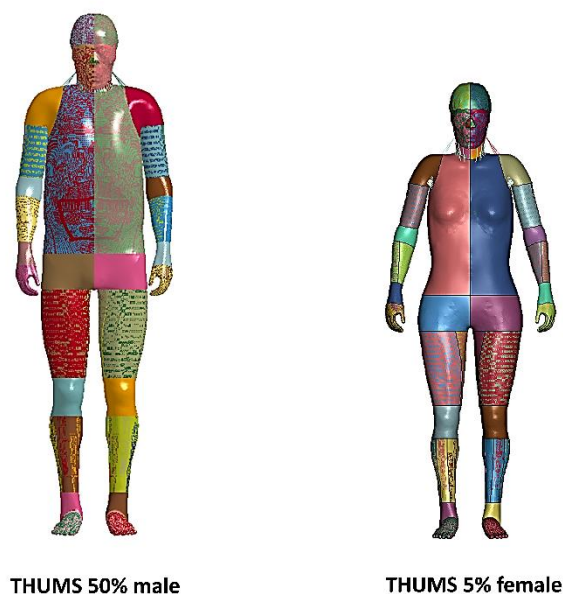


Figure 2-5 THUMS Male vs Female model

2.2.2.2 Impact Settings

During the preprocessing phase, the integration of the sRPAS model and THUMS model was carried out using LS-PrePost version 4.3 (LSTC/ANSYS, Livermore, CA). Initial steps involved positioning the sRPAS model in relation to the human head, establishing the sRPAS flying velocities, and specifying contact conditions between the sRPAS and the human head. Weng et al. (2021) [56] conducted a study where a quadcopter-style sRPAS was developed and applied it to the THUMS male 50th percentile human body model. A total of 17 impacts scenarios were simulated, following the cadaveric setting for model verification. The detailed test data of sRPAS to human collision in cadaveric tests can be found in the comprehensive ASSURE report, which was conducted by the Ohio State University. However, it should be noted that there were no available female cadaver data in the ASSURE report. To account for this, the THUMS 5th percentile female model was used, and four typical sRPAS to head impact directions were simulated (**Figure 2-6**), mirroring the male scenarios. The same 17 impact cases from Weng et al. (2021) were replicated for the THUMS female model. In order to ensure consistency in impact locations between male and female models, a proportional method was employed. A reference line passing through the head's center of gravity was selected, and the impact

locations were determined based on the angles between the reference line and the approaching direction of the sRPAS. The THUMS whole-body model employs a standard 1×10^{-7} s time step using an explicit approach, striking a balance between computational efficiency and acceptable added mass. Contact is implemented in a penalty-based mode with default thickness and stiffness. **Table 2-2** provides an overview of the 17 cases used for simulation, including the impact locations, impact velocity, and impact angle, which closely align with the male impact cases as simulated in Weng et al.'s setup [56].

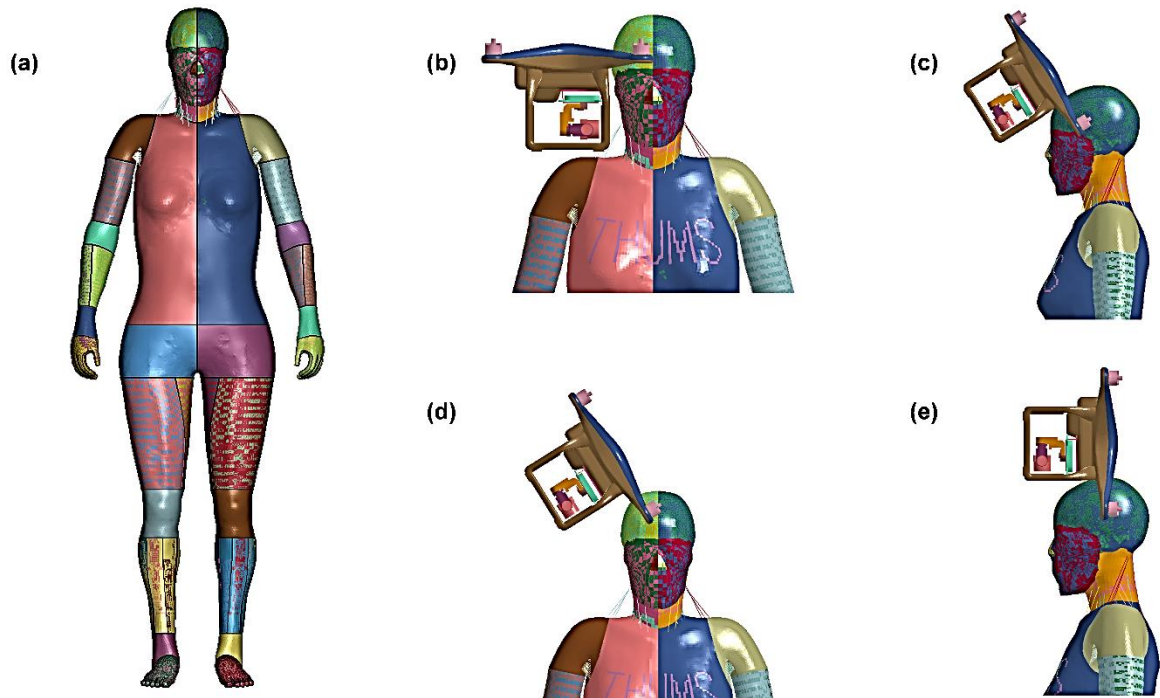


Figure 2-6 THUMS version 4.02 5th Percentile female model. (a) Full Model, (b-e) sRPAS impact directions.

Table 2-2 sRPAS to THUMS female head impact setup

Case #	Impact Direction	Impact Angle (Degree)	Sex	Impact Velocity (m/s-FPS)
1	Lateral	0	Female	16.8-55.1

2	Lateral	0	Female	18.3-60.1
3	Lateral	0	Female	21.1-69.2
4	Front	58	Female	17.5-57.3
5	Front	58	Female	18.0-59.2
6	Front	58	Female	18.3-59.9
7	Front	58	Female	21.4-70.1
8	Lateral	58	Female	18.7-61.2
9	Lateral	58	Female	21.9-72
10	Top	90	Female	16.8-55.2
11	Top	90	Female	19.5-63.9
12	Top	90	Female	21.5-70.5
13	Lateral	58	Female	18.6-60.9
14	Lateral	58	Female	21.9-72
15	Front	58	Female	21.9-71.8
16	Top	90	Female	19.7-64.5
17	Top	90	Female	21.5-70.5

2.3 Results

The simulations for impact scenarios and model verification were performed utilizing LS-DYNA. Computers with Intel Xeon 8-core CPUs and 24-core CPUs were used to solve simulations.

2.3.1 Head model verification

2.3.1.1 Brain Motion

For all verification cases, the computational head model was driven according to experimentally measured head kinematics, representing the exact head movements during experimental impacts. Brain displacement, in regard to the skull was then analyzed, and compared to the experimental data. The position of each NDT was reported in Hardy et al.'s study (2001,2007) [47], [70]. This positional data could be used for direct verification of the specific small female head model after being properly scaled to small female head geometry. Verification results are presented in **Appendix A (Figure A 1)**. Brain-skull displacements are generally difficult for computational models to match. This is partially due to the challenge in collecting displacement data from perfused cadavers. The comparison between simulation and experimental results showed mixed agreement, with some cases displaying good resemblance and others showing poor alignment in terms of brain displacements. Specifically, experiments like 380-T3, NDT-4 in the Y direction, and NDT-11 in the Z direction indicated inferior simulation results, with peak deformations ranging from 2 mm to 3 mm compared to the experimental data. Similar discrepancies were observed in experiments 380-T4, 380-T5, and 393-T4. Most of the phase patterns matched between experiments and predictions. The model predicted peak deformations were in the range of 3 to 6 mm, which agreed with experimental data.

2.3.1.2 Brain Pressure

The THUMS FE head model exhibited a general correspondence with the brain pressure measurements reported by Nahum et al. (1977) [48]. However, the exact locations of the pressure sensors during their experimental tests were not provided in detail. The verification of the model was conducted through the selection of representative elements from every brain region. Subsequently, the average value of these elements was calculated to generate the pressure curve for each respective region of the brain. The pressure magnitude predicted in FE model and cadaver experiments matched well, and the peak pressure values were generally close (as shown in the **Appendix A- Figure A 2**). The FE head model predicted a peak pressure of 156kPa in the frontal brain region,

slightly higher than the experimental value of 140kPa. In contrast, for the posterior fossa region, the predicted peak magnitude of -58kPa was in close proximity to the experimental value of -44kPa. Similarly, for the parietal region, the FE model predicted a peak pressure of 70kPa, while the experimental peak value was slightly higher at 83kPa. The predicted peak value for the right occipital region in the FE model was -49kPa, which was only slightly greater than the experimental peak value of -42kPa. On the other hand, for the left occipital region, the peak magnitude of the FE head models closely aligned with the experimental value, with the simulation peak value of -47kPa and the experimental value of -44kPa. Additionally, the curve shapes of the simulation and experimental results exhibited a close resemblance.

2.3.1.3 Force Deflection

The force-deflection curves predicted by the finite element (FE) model for lateral skull impact were found to be in good agreement with those reported by Yoganandan et al. (2004) [71], as depicted in the **Appendix A (Figure A 3)**. As the impact velocity increased, the FE head model consistently predicted higher impact forces. Although the duration of model predictions is generally longer than those reported experimentally, the model-predicted peak forces agree with experimental measurements, indicating the accuracy in predicting forces.

2.3.1.4 Neck model verification

Under vertical compression impacts, the model predicted force deflection values agreed with peak experimental measurements (as shown in **Appendix A- Figure A 4**). The study found that the FE head model accurately predicted the head peak force for N18-R+15 at approximately 8.5KN, which matched the experimental value. However, for D41-R+15, the experimental peak force was slightly higher at 8.75KN compared to the predicted value. The model-predicted neck force was approximately 15% lower than the experimental value for N18-R+15, on the other hand for D41-R+15, the neck force for the experimental peak force was almost 65% higher than the model-predicted value at around 4KN. In conclusion, the simulation and experimental results showed a close resemblance.

2.3.2 Male vs Female

2.3.2.1 Male vs Female head kinematics and injury metrics

The results, as depicted in **Figure 2-7** and **Figure 2-8**, present an analysis of several variables, including peak linear acceleration, peak rotational velocity, HIC, BrIC, maximum skull stress, and CSDM. The provided bar charts present a comprehensive comparison of various variables among 17 male and female cases. Among the cases analyzed, there were four different conventional sRPAS-to-head impact scenarios: three cases with a Lateral 0-degree angle, five cases with a Frontal 58 degrees angle, four cases with a Lateral 58 degrees angle, and five cases with Top 90 degrees impacts. This study provides valuable insights into head kinematics, injury metrics, and injury responses in relation to the average male and small female.

In **Figure 2-7 (a, b)**, the average peak linear acceleration across all 17 cases indicates that small females experienced 26.9% higher linear acceleration and 86.5% higher Head Injury Criterion (HIC) values compared to the average male model. However, the results differ for skull stress, where the small female model experienced less skull stress in the lateral 0 degree, frontal 58 degree, and top 90 degree impacts. An exception is observed in lateral 58 degree impacts, where the small female model experienced higher skull stress compared to the male model. Overall, when considering the average of all 17 impacts, the male model exhibited a 4.74% higher average skull stress compared to the female model (**Figure 2-7 (c)**).

According to **Figure 2-8 (a)**, the average peak rotational velocity in all four impacts was higher for small females compared to the male model. When considering the average rotational velocity across all 17 cases, small females experienced approximately 35.7% higher peak rotational velocity than males. Similar trends were observed in the average BrIC values, where small females had 41.7% higher BrIC values than males (**Figure 2-8 (b)**). Regarding brain strain, both CSDM10 and CSDM15 metrics indicated that females generally experienced higher values. On average, small females had 43.0% and 113.5% higher CSDM10 and CSDM15 values, respectively, when considering all 17 cases (**Figure 2-8(c, d)**). The MPS analysis revealed that the lateral 0-degree impact resulted in

the highest brain strain for both males and females. Females exhibited higher brain strain than males in lateral 0-degree and frontal 58-degree impacts, while males experienced higher brain strain in the Top 90-degree cases. However, the average MPS for all cases was similar for both genders (**Figure 2-8(e)**).

Overall, these findings highlight the differences in head kinematics and injury metrics between male and female models, providing valuable insights for further analysis and research.

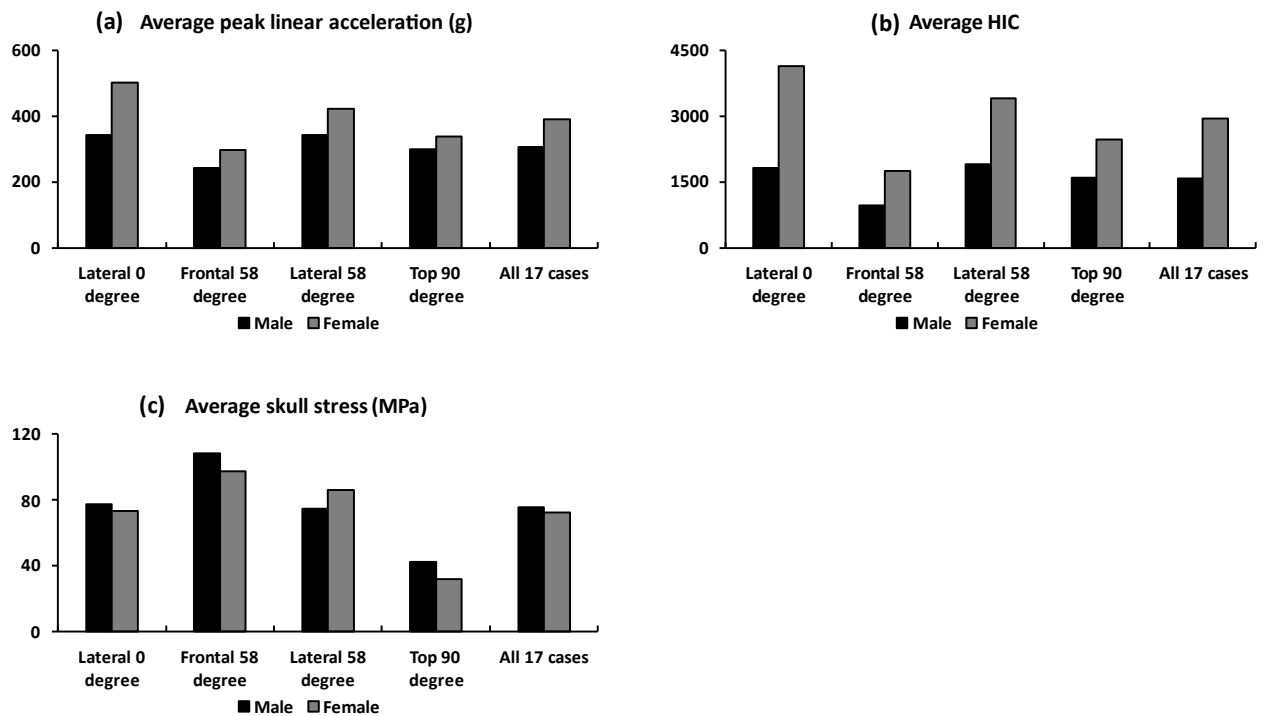


Figure 2-7 Average peak linear acceleration, HIC and skull stress comparison of male and female model.

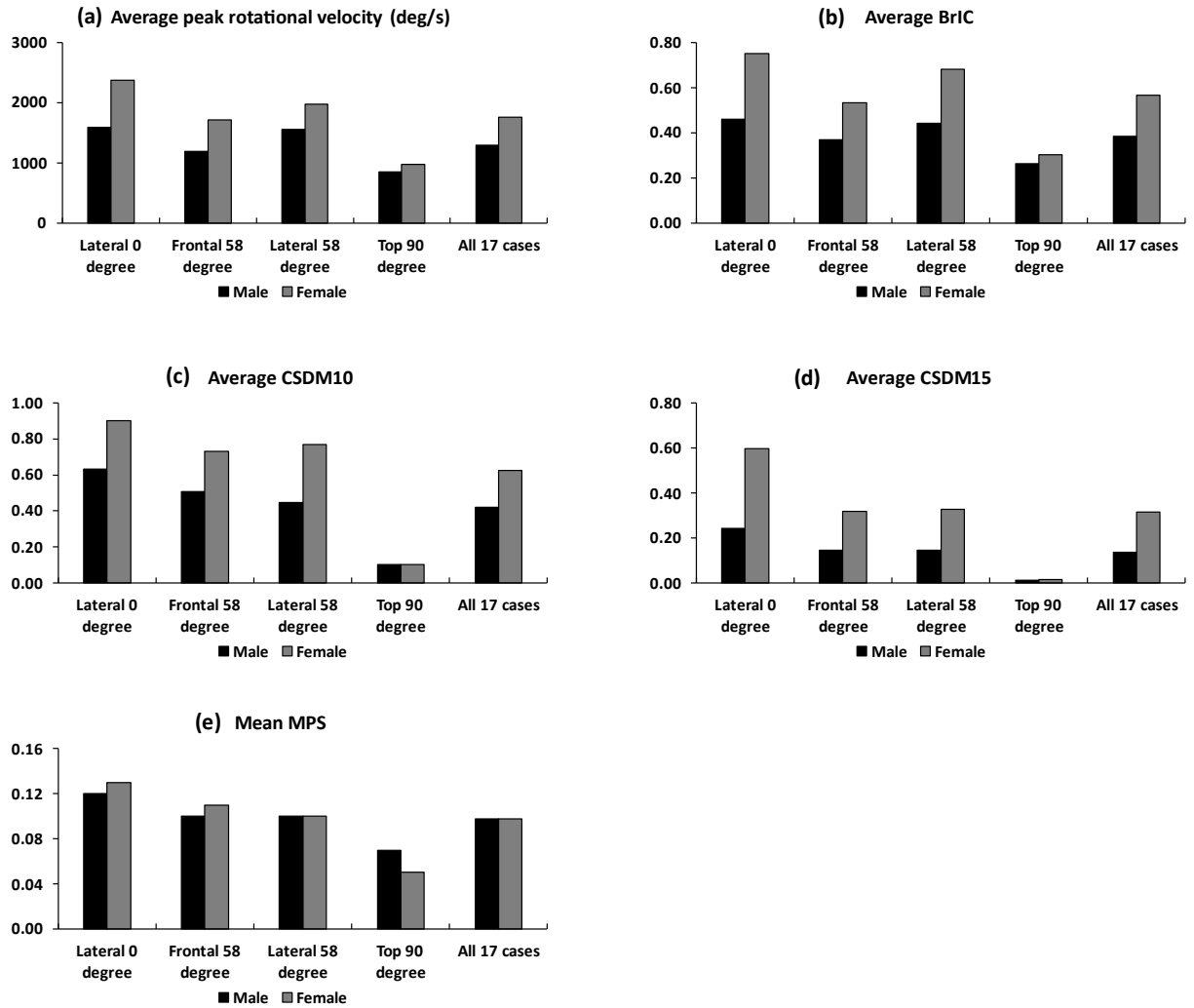


Figure 2-8 Average peak rotational velocity, BrIC and CSDM comparison of male and female model.

2.4 Discussion

The present study aimed to verify the THUMS 4.02 small female head model and compare it with the average male model in the context of drone head collisions. The findings offer significant insights into head injury mechanisms and shed light on gender difference within the models. To the best of the author's knowledge, this study served as the first one in understanding head responses between an average male and a small female during sRPAS-to-head impacts.

The FE head model underwent rigorous verification against nine different loading cases to ensure its ability to accurately predict various head responses. The brain displacement predictions exhibited strong agreement with the experimental studies. It should be noted that the FE head model employed in this research specifically represents a small female, and the verification was conducted solely using female cadaver displacement data from the studies conducted by Hardy et al. (2001,2007) [47], [70]. To address the different sizes and weights of the cadaver heads, a scaling method was employed for brain displacement verification. However, it is important to acknowledge a limitation in the methodology as only mass scaling was employed to address differences in head size. This choice introduces a constraint as varying head sizes do not necessarily correlate directly with differences in head mass. Therefore, the results may not fully encapsulate the intricacies associated with variations in both head size and mass, and this limitation should be considered when interpreting the findings. Future studies may benefit from incorporating a more comprehensive scaling approach to enhance the generalizability and applicability of the results across a broader range of anatomical variations. Brain pressure predictions also exhibited a strong match with experimental values, further confirming the model's accuracy. The distribution of intracranial pressure showed maximum compressive positive pressures at the coup site and negative pressures at the contrecoup site, consistent with findings by Nahum et al. (1977) [48]. Furthermore, the force deflection analysis utilized three impact cases from Yaganandan et al.'s (2004) study to verify the FE head model, and the results demonstrated a close agreement with experimental data [71]. The neck model was also verified, and the predicted neck forces closely corresponded to the experimental measurements, further verifying the accuracy and reliability of the neck model.

The comparison between the average male and small female models revealed interesting differences in head kinematics and injury metrics. Small females experienced higher levels of linear acceleration, rotational velocity, and head injury criteria values such as HIC and BrIC compared to males. The higher linear acceleration and rotational velocity in small females could be attributed to differences in anthropometry and biomechanical properties between genders. The smaller neck size and lower body mass of females may play a role in their increased susceptibility to head injuries [59], [65]. Across all 17

impact scenarios, small females experienced 26.9% higher linear acceleration on average. Moreover, the average HIC for small females, at 2946, was significantly larger than that of the average male. Although the impact duration of small females is typically shorter due to their lighter head mass, the HIC value remained much higher than that of the average male. Interestingly, the data also demonstrated that small females suffered 4.74% lower von Mises skull stress compared to the male model. Normally, the impact duration of small female would be much shorter than that of male because of the lighter head mass [59]. It can be considered that under sRPAS to human head impact, despite having larger HIC and peak linear acceleration values than the average male, the small female model exhibited lower risks of skull fractures. Hence, the conventional HIC limit used in auto safety might not be suitable for sRPAS impact scenarios.

The analysis of 17 male and female impact cases revealed generally low brain strains. Notably, lateral and frontal impacts caused higher average strains for both males and females compared to top impacts. This implies that the assessment of brain injury risks should prioritize frontal and lateral impacts over top impacts. Additionally, when comparing CSDM10 and CSDM15 values between small females and average males, it was evident that small females had higher CSDM values, indicating greater brain injury risks.

2.5 Conclusion

The verification results of the small female head model were encouraging. The computational model predicted brain displacement within the range of experimental measurements, indicating its reliability in simulating brain motion. The brain pressure predictions also showed a close match with the experimental values, further reinforcing the model's accuracy. Additionally, the force-deflection responses and neck forces closely corresponded to the experimental measurements, demonstrating the verification of the neck model. The comparison between the average male and small female models revealed interesting differences in head kinematics and injury metrics. Small females experienced higher levels of linear acceleration, rotational velocity, and head injury criteria values such as HIC and BrIC compared to males. It is essential to consider these gender differences in head injury responses while developing safety regulations and

protective equipment. The findings could also be valuable for industries that extensively use drones, such as surveillance, agriculture, and infrastructure inspections. Safety protocols and guidelines should be tailored to account for the unique injury risks faced by both males and females.

Chapter 3

3 Investigation of Differences in Head Impact Effects Among Vulnerable Populations in Small Remotely Piloted Aircraft Systems (sRPAS)

Abstract

This research aimed to investigate head injury risks in vulnerable populations, particularly children, due to sRPAS-related impacts. Finite element (FE) models of 10-year-old, 6-year-old, and 3-year-old children were utilized to simulate different impact scenarios. The resulting linear accelerations and rotational velocities were compared to scaled data from male post-mortem human subject (PMHS) experiments. The simulations generally captured the trends in the scaled data, although some variations were observed. The 6-year-old and 10-year-old models exhibited higher peak linear accelerations and head injury criterion (HIC) values, indicating a higher risk of injury compared to the 3-year-old model. However, the 3-year-old model displayed higher brain strain metrics (BrIC, CSDM10, CSDM15, and CSDM20) compared to the older models. The study emphasizes the importance of considering rotational kinematics in assessing head injuries and highlights the unique injury risks posed to different age groups.

3.1 Introduction

Head injury severities may vary among different populations under similar impact conditions. This is due to variations in body size, body mass, and stiffness. Traumatic brain injury (TBI) is a common and significant cause of both mortality and morbidity among children and young adults. Despite its recognized impact on health, there is limited information regarding the occurrence and prevalence of TBIs, especially among the most vulnerable age groups such as infants, children, and young adults. A recent review conducted by the World Health Organization highlighted the need for more comprehensive and high-quality research on TBI to facilitate effective planning of primary healthcare services and the development of prevention programs [73]. The reported incidence of TBI in children and young adults ranges from 100 to 300 cases per 100,000 individuals annually [73], [74].

In recent times, there has been a surge in the popularity of drones, also referred to as unmanned aerial vehicles (UAV), unmanned aircraft systems (UAS), or sRPAS, for recreational as well as commercial purposes. Drones are agile vehicles that can move swiftly, reaching speeds of up to 45 m/s, and are permitted to have a maximum weight of 55 pounds (25 kilograms) according to regulations [75]. The widespread use of drones has led to an increase in accidents resulting from drone impacts, making it a prevalent issue today. In addition to affecting males and females, vulnerable populations such as children are also susceptible to head injuries caused by drone impacts. Therefore, it is crucial to investigate head injuries in both males and females, as well as focus on vulnerable groups like children, to comprehensively understand the impact of drone-related head injuries. A 13-year-old boy experienced a skull fracture because of being struck by a racing drone [1]. In April 2003, a 14-year-old girl lost her life in England because of an uncontrollable model aircraft accident.[76]. During the landing of a large video drone, a 9-year-old boy sustained injuries from its propeller, resulting in lacerations to his right eyelid, right cornea, left ear, nasal bridge, and neck [77]. A 21-month-old girl experienced facial injury when a recreational toy drone collided with her right side, resulting in mild eyelid edema and normal bilateral blink to light visual acuity [4].

Child crash test dummies conventionally serve as instrumental tools for evaluating the safety performance of children in vehicular crash scenarios. A thorough examination of injuries in different body areas requires the use of mathematical models, providing insights beyond what crash test dummies can offer. Numerous finite element (FE) models designed for adults have been developed and successfully used to analyze how humans respond in crash situations. The importance of a child FE model becomes clear when evaluating the risk of injury for a child. Notably, drone impact injuries to the head are not confined to adults, as evidenced by accident reports highlighting the susceptibility of children across different age groups to such injuries. Several child FE models for specific body regions, like the head or neck, accurately depicted the detailed anatomical structure of a child. The Total Human Model for Safety (THUMS) emerges as a comprehensive human FE model, validated across an array of impact scenarios. In this study, three child FE models from THUMS, 3-year-old, 6-year-old, and 10-year-old children, commonly used in the field to represent child population, were selected. Ito et al. (2017) developed finite element models for children, comparing their whole-body kinematics and head injury risks to those of an adult male model. The study explores differences in head injury mechanisms for child pedestrians in various vehicle-to-pedestrian collision scenarios, considering different age groups (3, 6, and 10 years old), pedestrian models, and collision speeds [78]. The utilization of FE models, as opposed to conventional crash test dummies, augments the understanding of stress-strain analyses, and facilitates a more nuanced evaluation of injury risks. Katsuhara et al. (2019) examined head injury mechanisms in car-cyclist collisions, employing a 10-year-old THUMS child model and an adult Finite Element model to simulate diverse scenarios and gain insights into the intricacies of such injuries [79].

To better protect children during drone-to-head impacts, this study aimed to understand children's head responses during blunt impacts. The method aligned with that used in the previous Chapter. The difference was that in this study children's human body models, including 10, 6 and 3 YO models, were used to simulate drone-to-head impacts. Head kinematics and brain responses were analyzed and compared.

3.2 Methods

3.2.1 THUMS FE model

The Total Human Model for Safety (THUMS) version 4 child models, including 10, 6, and 3 years old, were used. For the THUMS 10-year-old FE model, a dataset of a 10-year-old male measuring 137 cm in height was selected. Likewise, a dataset of a 6-year-old female measuring 114 cm in height and weighing 20 kg was chosen for the THUMS 6-year-old FE model. Lastly, for the THUMS 3-year-old child FE model, a dataset of a 3-year-old female with a height of 94 cm and a weight of 13.5 kg was utilized. The full-body model was generated by integrating component models, which include the head, torso, and extremity models. The THUMS 10-year-old FE model comprises approximately 913,000 nodes and 2.1 million elements. It has a height of 138.3 cm and a weight of 34 kg, closely resembling the 50th percentile size of a 10-year-old American [80]. The THUMS 6-year-old FE model consists of around 510,000 nodes and 1.4 million elements, with a height of 117.2 cm and a weight of 24.6 kg, approximating the 50th percentile size of a 6-year-old American [81]. The THUMS 3-year-old FE model includes roughly 840,000 nodes and 2.6 million elements. It has a height of 98.3 cm and a weight of 15.8 kg, which closely aligns with the 50th percentile size of a 3-year-old American [82]. **Figure 3-1** depicts the full body model of the THUMS 10-year-old, 6-year-old, and 3-year-old FE models.

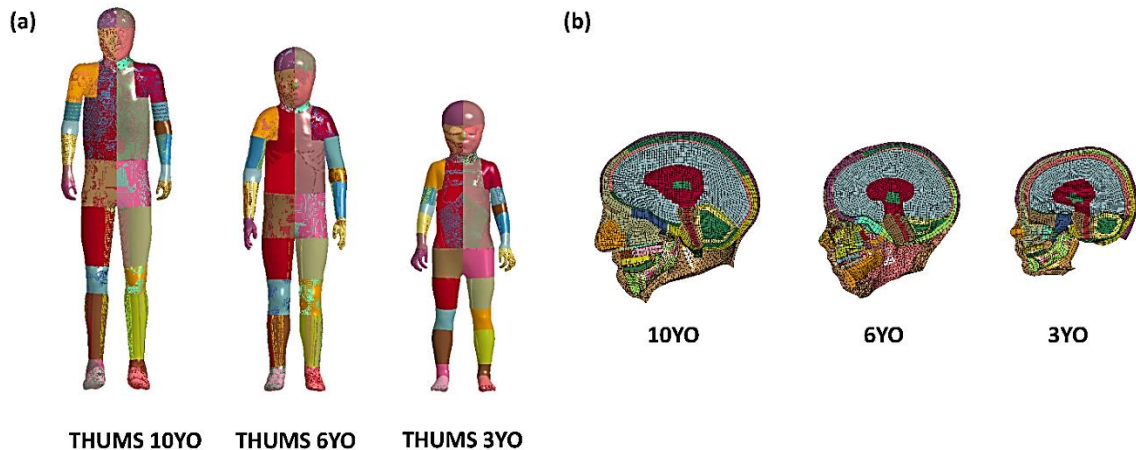


Figure 3-1 THUMS 10YO, 6YO and 3YO model comparison

The head modeling of the THUMS child FE models was based on THUMS Version 4.02 AM50. Details of the THUMS Male FE model were provided in section 2.2.2.1, and the child models followed a similar structure. These models incorporated various components such as the epidermis (skin), skull, mandible, eyeballs, teeth, meninges, cerebrum, cerebellum, brainstem, and cerebrospinal fluid (CSF). The brain was divided into white matter and gray matter, with varying element lengths. The brain portion of the THUMS 10-year-old FE model had elements measuring 0.9 to 3.3 mm in length. In the THUMS 6-year-old FE model, the brain element lengths ranged from 0.75 to 4.2 mm. On the other hand, in the THUMS 3-year-old model, the brain element lengths were between 0.6 and 3.7 mm. The brain was modeled as an incompressible and viscoelastic material.

The head model of the THUMS child FE model was validated through two different experiments, including a lateral compression test performed by Loyd et al. (2011) to validate force responses of the skull [83], and three head drop tests conducted by Loyd et al. (2011) to validate acceleration responses of the head model [83]. The neck of the THUMS child model was validated using axial loading experiments conducted by Luck et al. (2008, 2013) to validate the force responses [84].

3.2.2 Impact setting

The integration of the sRPAS and THUMS child models during the preprocessing stage in this research involved utilizing both HyperMesh and LS-PrePost version 4.3 (LSTC/ANSYS, Livermore, CA). In the initial stages, the boundary and loading conditions encompassed positioning the sRPAS model in relation to the child's head, defining impact velocities for the sRPAS, and specifying contact conditions between the sRPAS and the child model's head. Four typical sRPAS to head impact directions were simulated. Each child FE model underwent a total of 17 simulations, with the specific configurations outlined in **Table 3-1**. Given the absence of child cadaver data in the ASSURE report, a proportional method was employed to ensure consistent impact locations across both male and all child models. This approach mirrored the methodology used for small female simulations described in section 2.2.2.2. To determine the impact locations, a vertical line passing through the center of gravity was selected as a reference, and the angles between the vertical centerline and the approaching directions of the sRPAS were considered. Following the simulations, the linear acceleration in the x, y, and z directions underwent filtering using a low-pass CFC (channel frequency class) 1000Hz filter, and subsequently, the resultant acceleration was calculated based on the filtered x, y, and z data. Additionally, rotational velocities were filtered using a CFC 180 Hz filter.

Table 3-1 sRPAS to Child head setups

Case #	Impact Direction	Impact Angle (Degree)	THUMS Child FE model	Impact Velocity (m/s-FPS)
1	Right	0	10YO,6YO,3YO	16.8-55.1
2	Right	0	10YO,6YO,3YO	18.3-60.1
3	Right	0	10YO,6YO,3YO	21.1-69.2
4	Front	58	10YO,6YO,3YO	17.5-57.3

5	Front	58	10YO,6YO,3YO	18.0-59.2
6	Front	58	10YO,6YO,3YO	18.3-59.9
7	Front	58	10YO,6YO,3YO	21.4-70.1
8	Right	58	10YO,6YO,3YO	18.7-61.2
9	Right	58	10YO,6YO,3YO	21.9-72
10	Top	90	10YO,6YO,3YO	16.8-55.2
11	Top	90	10YO,6YO,3YO	19.5-63.9
12	Top	90	10YO,6YO,3YO	21.5-70.5
13	Right	58	10YO,6YO,3YO	18.6-60.9
14	Right	58	10YO,6YO,3YO	21.9-72
15	Front	58	10YO,6YO,3YO	21.9-71.8
16	Top	90	10YO,6YO,3YO	19.7-64.5
17	Top	90	10YO,6YO,3YO	21.5-70.5

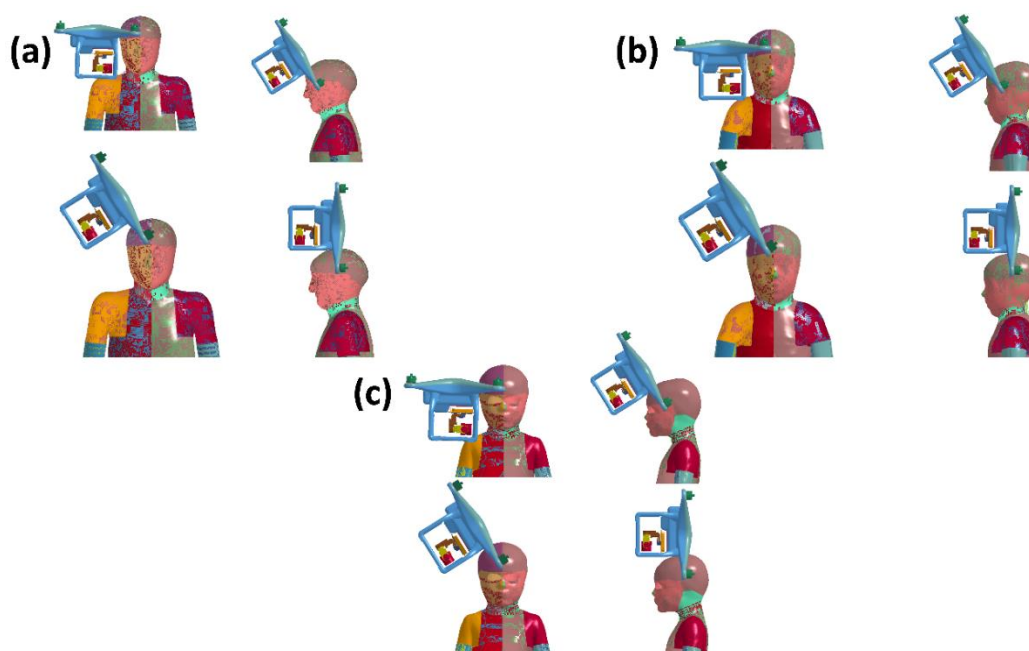


Figure 3-2 Typical impact directions for all child model

3.2.3 Mass-based scaling method

No PMHS experiments were conducted on child subjects; thus, the existing male PMHS cadaveric data were scaled using a mass-based scaling law. The Ohio State University (OSU) PMHS experiments only recorded the whole-body masses of subjects, so these masses were utilized to calculate the scaling factors. **Table 3-2** provides a summary of detailed information about the subjects from the OSU PMHS experiments, including their age, standing height, and body mass. According to the literature, the weight of the 10-year-old child model is 34 kg, the 6-year-old child model weighs 24.6 kg, and the 3-year-old model weighs 15.8 kg [80]–[82].

Table 3-2 PMHS subjects

Subject	Age	Standing Height (inch)	Body mass (lb)
1	60	70	170

2	73	66	163
3	67	71	143
4	67	72	193
5	74	74	195

The equations for calculating the mass-based scaling factor of head kinematics [66], [67] are shown below.

$$\text{Mass ratio: } \lambda_m = \frac{M_{male}}{M_{child}}$$

$$\text{Linear acceleration factor: } \lambda_a = (\lambda_m)^{-\frac{1}{3}}$$

$$\text{Angular velocity factor: } \lambda_\omega = (\lambda_m)^{-\frac{1}{3}}$$

$$\text{Time ratio (factor): } \lambda_T = (\lambda_m)^{\frac{1}{3}}$$

Where M_{male} and M_{child} represented for the body mass of male subject and child subject.

The equations of the predicted head kinematics are shown below:

$$\text{Linear acceleration of child: } \alpha_{child} = \frac{\alpha_{male}}{\lambda_a}$$

$$\text{Angular velocity of child: } \omega_{child} = \frac{\omega_{male}}{\lambda_\omega}$$

$$\text{Time of female: } T_{child} = \frac{T_{male}}{\lambda_T}$$

Where, α_{child} and α_{male} represented for the linear acceleration of male and child; ω_{child} and ω_{male} represented for angular velocity of male and child; T_{child} and T_{male} represented for time history of male and child under impact.

3.2.4 Skull stress

The maximum skull stress during the collision was found using LS-PrePost software. This stress is usually maximum right at the start of the collision. The highest von Mises stresses from skull shells were determined and their time histories were plotted. We picked the nine elements with maximum stress points. The highest value on the average curve was considered the maximum skull stress.

3.2.5 Comparison of head responses among children

The study involved 17 identical scenarios for each child model, along with a consistent set of four impact settings across all child models. These scenarios encompassed various impact angles: 3 cases of lateral impacts at 0 degrees, 5 cases of frontal impacts at 58 degrees, 4 cases of lateral impacts at 58 degrees, and 5 cases of top impacts at 90 degrees.

The comparative analysis considered multiple factors, including average peak linear acceleration, average HIC, average skull stress, average peak rotational velocity, average CSDM, and average Maximum Principal strain.

3.3 Results

A total of 51 simulations, comprising 17 cases for each child model, were performed using LS-DYNA. Computers with Intel Xeon 8-core CPUs and 24-core CPUs were used to solve simulations. When using 2 CPUs, it took approximately 20 hours to solve 40-millisecond impact cases.

3.3.1 Resultant head linear acceleration verification

3.3.1.1 10 years old model

In the lateral 0-degree impact cases (referred to as cases 1, 2, and 3 in **Figure 3-3**), the impact durations were slightly longer in the simulation compared to the scaled PMHS results. Case 1 and case 3 exhibited impact durations of 2.6 milliseconds, while case 2 had a duration of 2.5 milliseconds. Although the peak linear acceleration matched well with the PMHS results for cases 1 and 2, the simulation result for case 3 was 25% lower than the corresponding scaled PMHS result.

In the frontal impact cases at 58 degrees (specifically, cases 4, 5, 6, and 7 as depicted in **Figure 3-3**), the simulation time histories exhibited two peaks, which aligned well with the impact duration seen in the scaled results obtained from male PMHS. In case 5, the simulation results displayed a peak value at approximately 2.5 milliseconds, whereas the scaled PMHS result exhibited a peak at around 6 milliseconds. The peak values in the simulation closely matched those of the scaled PMHS data, except for cases 4 and 5, where the simulation yielded peak values that were 42% lower for case 4 and 49% lower for case 5 compared to the scaled PMHS results.

In the lateral impact cases at 58 degrees (specifically, cases 8, 9, 13, and 14 as depicted in **Figure 3-3**), the simulation results exhibited two peaks with an impact duration of approximately 3.9 milliseconds. In cases 8 and 9, the peak values closely matched the corresponding scaled data from male PMHS. In cases 13 and 14, although the shape of the curve in the simulation closely resembled the scaled PMHS data, there were slight differences in terms of magnitude. Specifically, case 13 overpredicted the scaled data by 29%, while case 14 underpredicted the scaled PMHS data by 13%.

Case 15 presents a unique impact scenario compared to the other cases discussed. In this particular case, the sRPAS impacts the head near the coronal suture. The impact duration closely matched the scaled results obtained from male PMHS. However, the simulation results underpredicted the result, with the peak value in the simulation being 302g's compared to the scaled result of 594g's.

In the top 90-degree scenarios (10, 11, 12, 16, and 17 shown in **Figure 3-3**), the simulation results consistently underestimated the peak values, except for case 17, which had a comparable peak value to the scaled PMHS data. For cases 10, 11, 12, and 16, the simulated peak values were respectively 52%, 73%, 99%, and 22% lower than the corresponding scaled PMHS data.

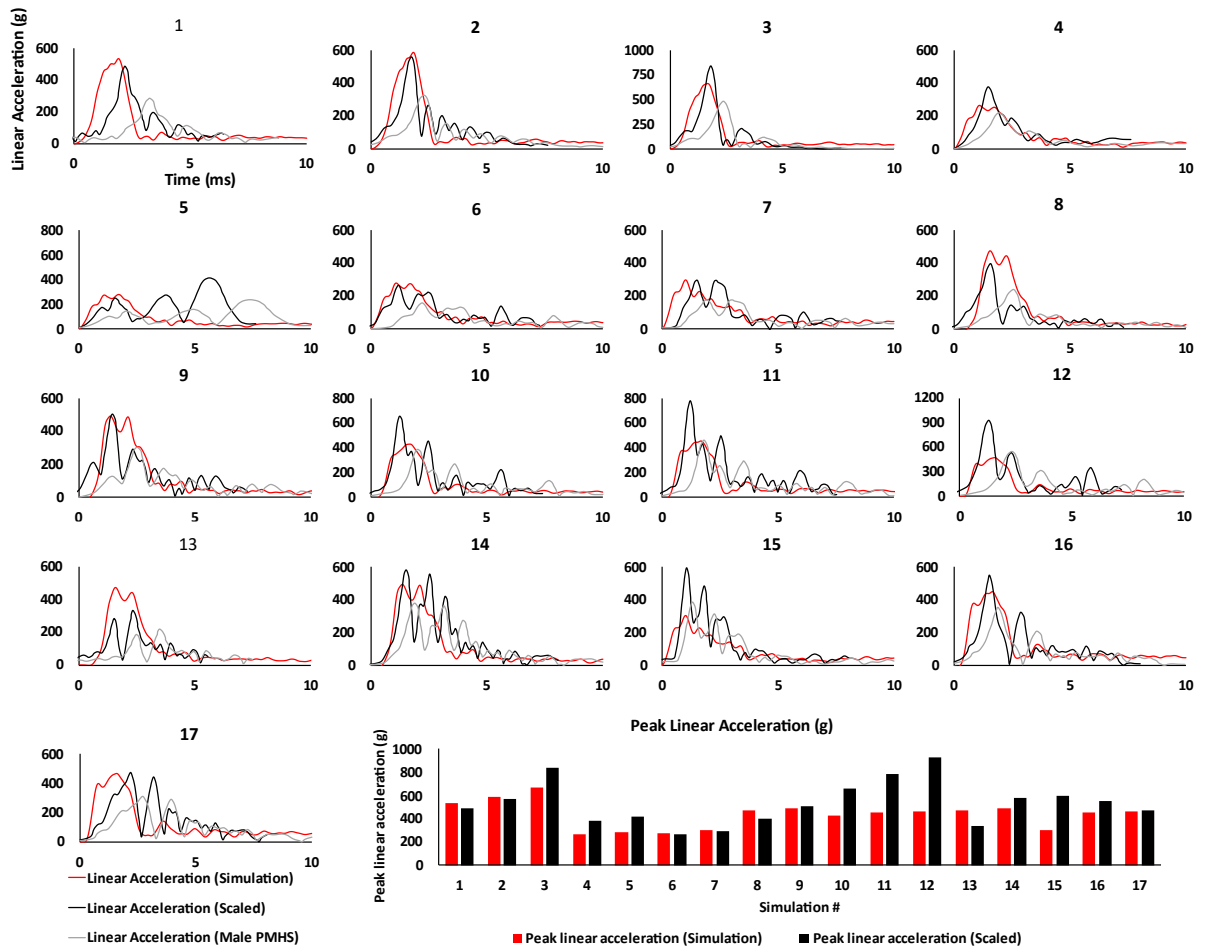


Figure 3-3 Head resultant linear acceleration of 10YO child. Experimental data were scaled digitized PMHS experiments data from ASSURE report.

3.3.1.2 6 years old model

In the lateral 0-degree scenarios (1, 2, and 3 shown in **Figure 3-4**), the simulated linear acceleration closely matched the pattern of the scaled data. However, in all three cases, the simulated peak results underpredicted the scaled PMHS peak results. Specifically, for cases 1, 2, and 3, the simulated peak values were underestimated by 18%, 21%, and 50%, respectively, compared to the scaled PMHS data.

In the frontal 58-degree impact cases (cases 4, 5, 6, and 7 shown in **Figure 3-4**), the simulated results exhibited two peaks in their time histories. The overall curve patterns closely resembled the scaled PMHS results, except for case 5, where the scaled curve had three peaks instead. In terms of peak values, case 4 agreed with the scaled peak value, while case 6 had a peak value that was 24% higher, and case 7 had a peak value that was 20% higher than their respective scaled PMHS peak values.

In the lateral 58-degree impact scenarios (cases 8, 9, 13, and 14 shown in **Figure 3-4**), the duration of the impact was approximately 3 milliseconds, which was closely matched by both the simulated and scaled results. The simulated peak value for case 8 closely aligned with the corresponding scaled PMHS peak value. However, for cases 9 and 14, the peak linear accelerations were underestimated by 31% and 50% respectively, compared to the scaled PMHS experiments. Conversely, for case 13, the simulated peak linear acceleration was overestimated by 14% when compared to the corresponding scaled PMHS result.

In case 15, the initial position of the sRPAS was near the coronal suture rather than the face. The predicted curve shape closely resembled the scaled PMHS curve. However, the simulated peak value was underpredicted by 63% compared to the scaled PMHS result.

In the top 90-degree impact scenarios (cases 10, 11, 12, 16, and 17 shown in the **Figure 3-4**), both the simulations and scaled PMHS experiments exhibited a similar impact duration of approximately 3 milliseconds. However, in all five cases, the simulated results consistently underpredicted the scaled PMHS results.

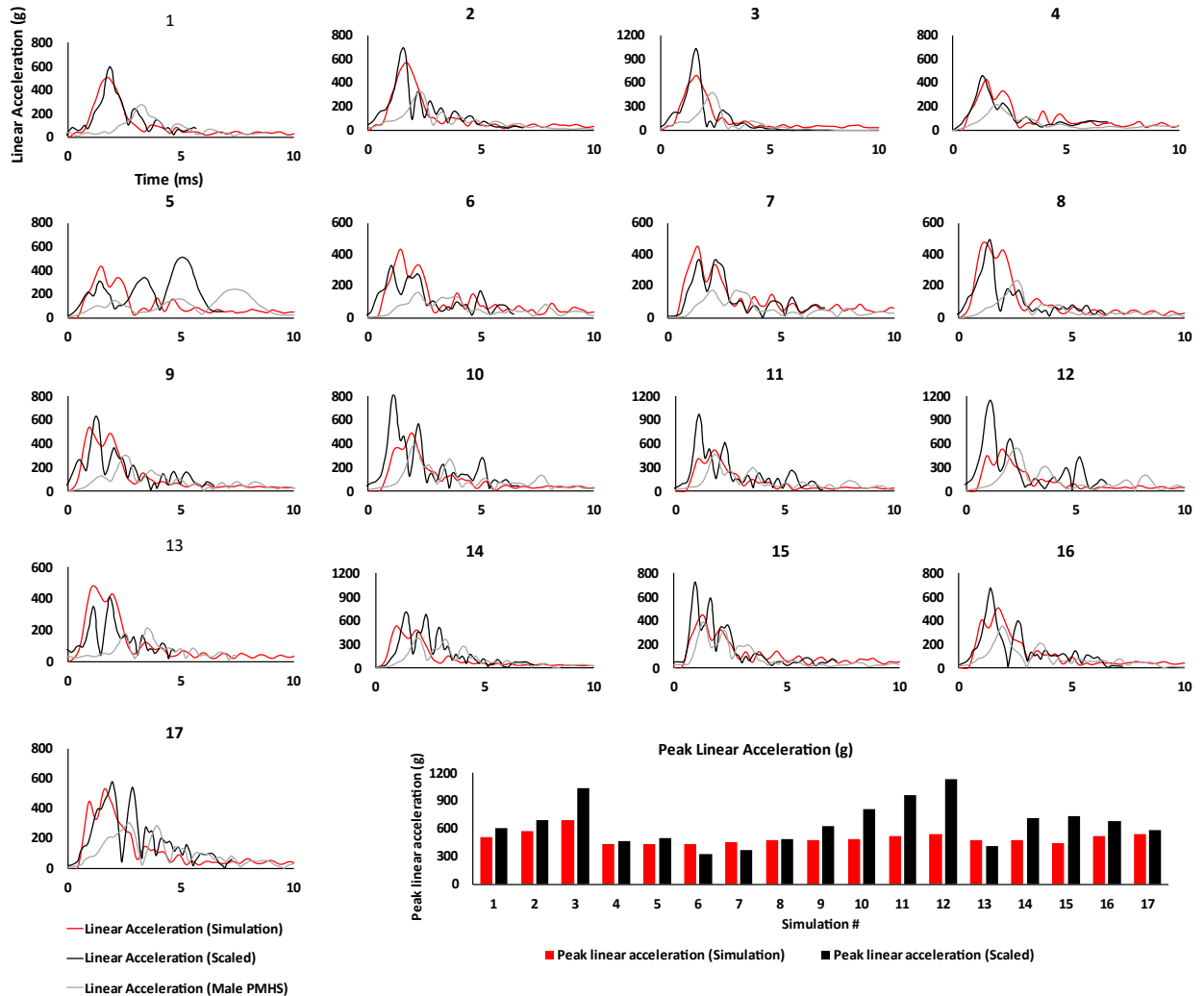


Figure 3-4 Head resultant linear acceleration of 6YO child. Experimental data were scaled digitized PMHS experiments data from ASSURE report.

3.3.1.3 3 years old model

In all 17 cases analyzed, the majority of the simulated results underpredicted the scaled PMHS results. However, two cases involving a frontal 58-degree impact (case 6 and case 7 shown in **Figure 3-5**) had simulated peak linear accelerations that were higher by 9% compared to the scaled values. Notably, in the top 90-degree impact scenario (Case 13 shown in **Figure 3-5**), the simulated peak linear acceleration matched well with the scaled value.

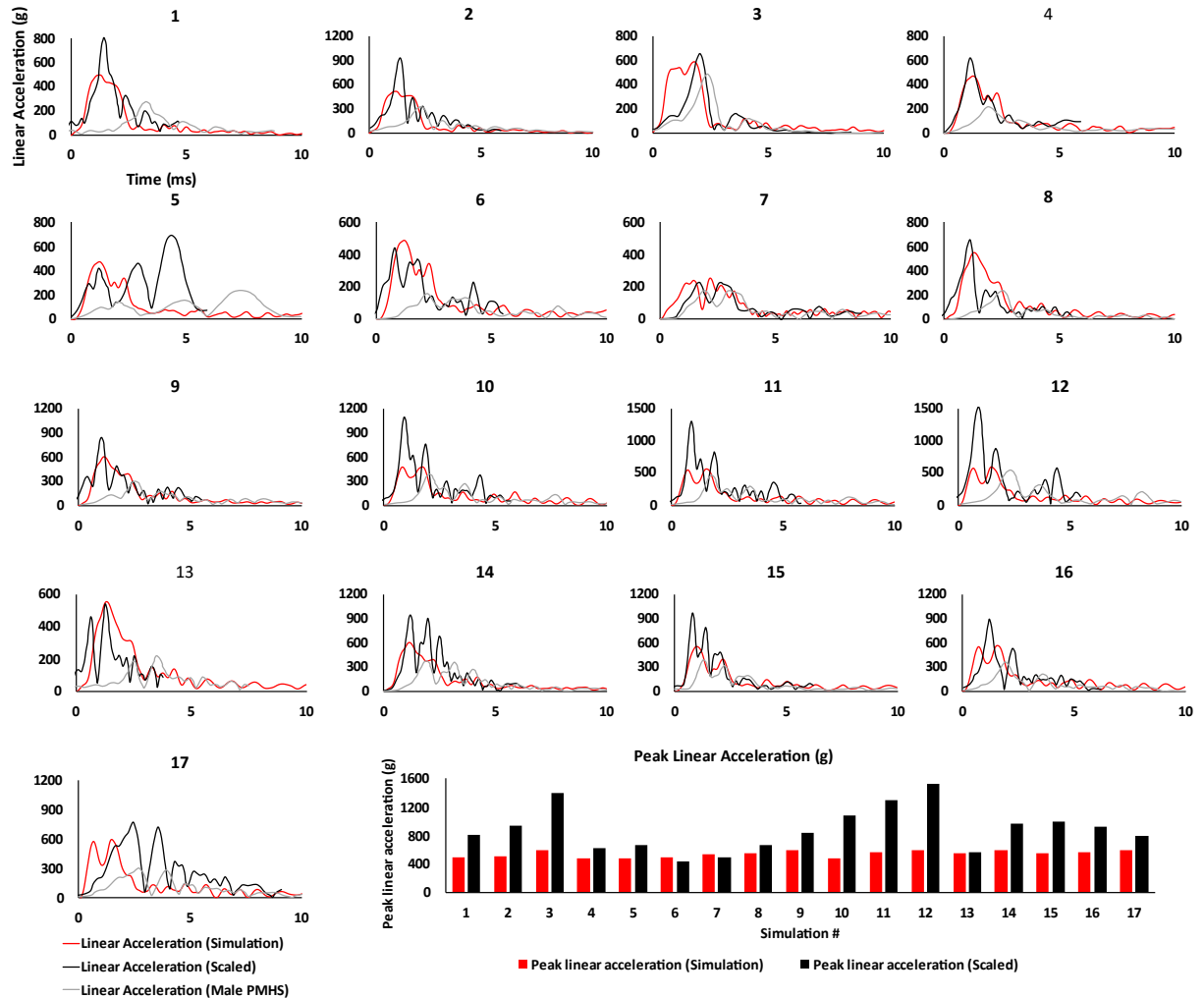


Figure 3-5 Head resultant linear acceleration of 3YO child. Experimental data were scaled digitized PMHS experiments data from ASSURE report.

3.3.2 Resultant head rotational velocity verification

3.3.2.1 10 years old model

In the lateral 0-degree cases (1, 2, and 3 depicted in **Figure 3-6**), the simulations resulted in an overestimation of the peak rotational velocity compared to the scaled PMHS data. Specifically, for case 1, case 2, and case 3, the peak values were respectively 45%, 30%, and 30% higher than the corresponding scaled PMHS data.

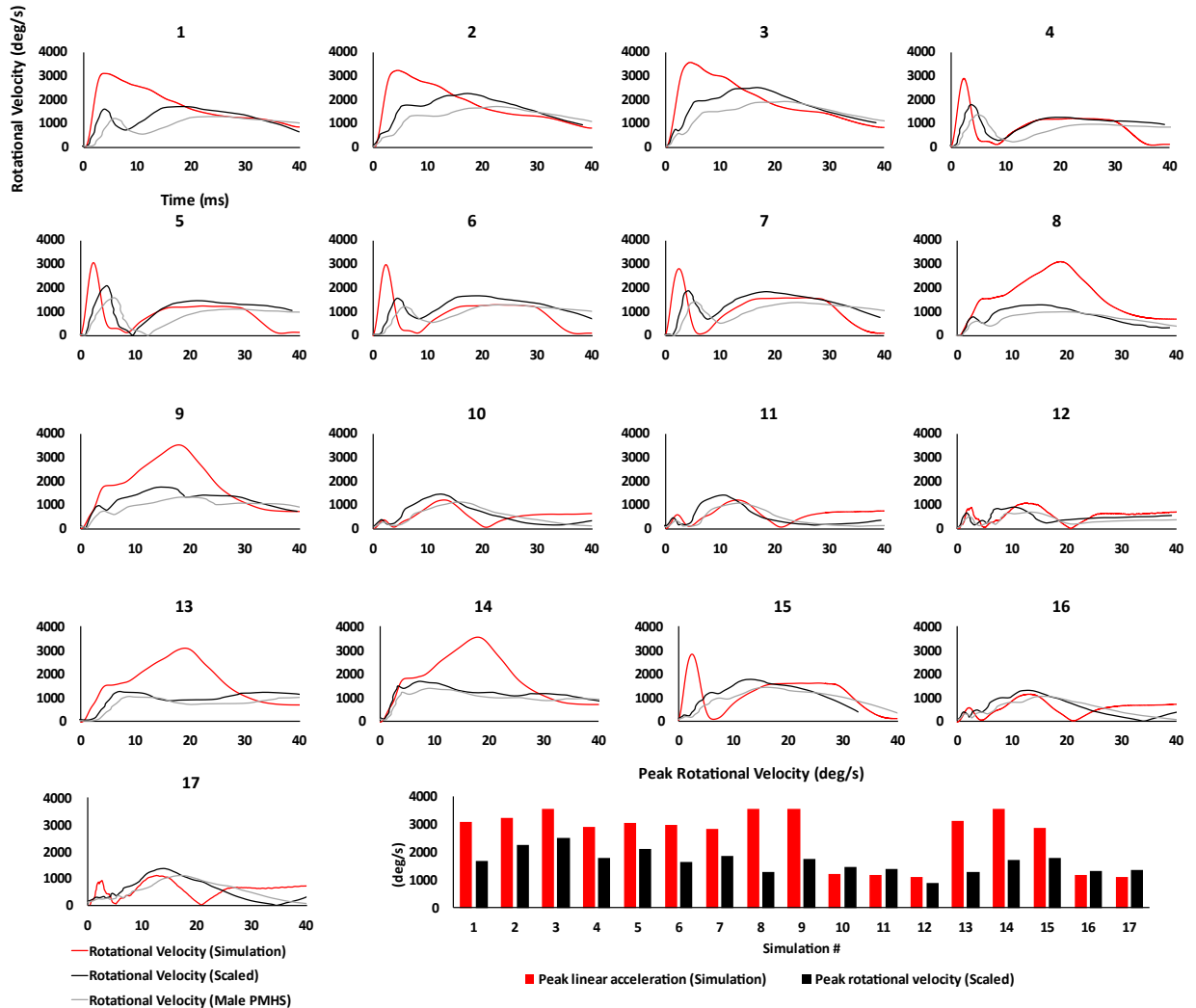


Figure 3-6 Head resultant rotational velocity of 10YO child. The experimental data were scaled digitized PMHS experiments data from ASSURE report.

In the frontal 58-degree impact cases (case 4, 5, 6, and 7 shown in **Figure 3-6**), the simulated time history curves closely resembled the scaled PMHS curves. However, the peak values for cases 4, 5, 6, and 7 were overestimated, with increases of 39%, 31%, 44%, and 34% respectively compared to the corresponding scaled PMHS data.

In the lateral 58-degree impact cases (case 8, 9, 13, and 14 shown in **Figure 3-6**), the simulated peak rotational velocity was overestimated when compared to the corresponding scaled PMHS peak rotational velocity.

In the top 90-degree impact cases (case 10, 11, 12, 16, and 17 shown in **Figure 3-6**), the simulated curve shapes closely resembled those observed in the scaled PMHS experiments. Furthermore, the peak rotational velocity generally matched well with the corresponding scaled data, except for case 17 where the simulated peak value was 25% higher than the scaled PMHS results.

3.3.2.2 6 years old model

In the lateral 0-degree cases (case 1, 2, and 3 shown in **Figure 3-7**), the simulated results for all three cases exhibited an overestimation in terms of peak value compared to the scaled PMHS data. Additionally, the peak values in the simulated results occurred at an earlier stage compared to the scaled peak values.

In the frontal 58-degree impact cases (case 4, 5, 6, and 7 shown in **Figure 3-7**), the shapes of the time histories exhibited a perfect match with the experimental curves. Both the simulated and scaled curves displayed two peaks in their time histories, with the first peak occurring at the initial stage and the second peak occurring around 20 milliseconds. The second peak value closely aligned with the scaled PMHS peak value. However, the first peak rotational velocity in the simulated results was overestimated compared to the corresponding scaled data.

In the cases of lateral 58-degree impact (cases 8, 9, 13, 14 depicted in **Figure 3-7**), the simulated peak rotational velocity was higher than the corresponding experimental peak values, indicating an overestimation in the simulation results.

In the top 90-degree impact cases (case 10, 11, 12, 16, and 17 shown in **Figure 3-7**), the peak value in the simulated time histories was observed earlier compared to the corresponding scaled experimental results. However, the peak value of the simulated peak rotational velocity closely matched the scaled PMHS results, except for case 12 where the simulated result had a 45% higher peak value than the corresponding scaled experimental peak value.

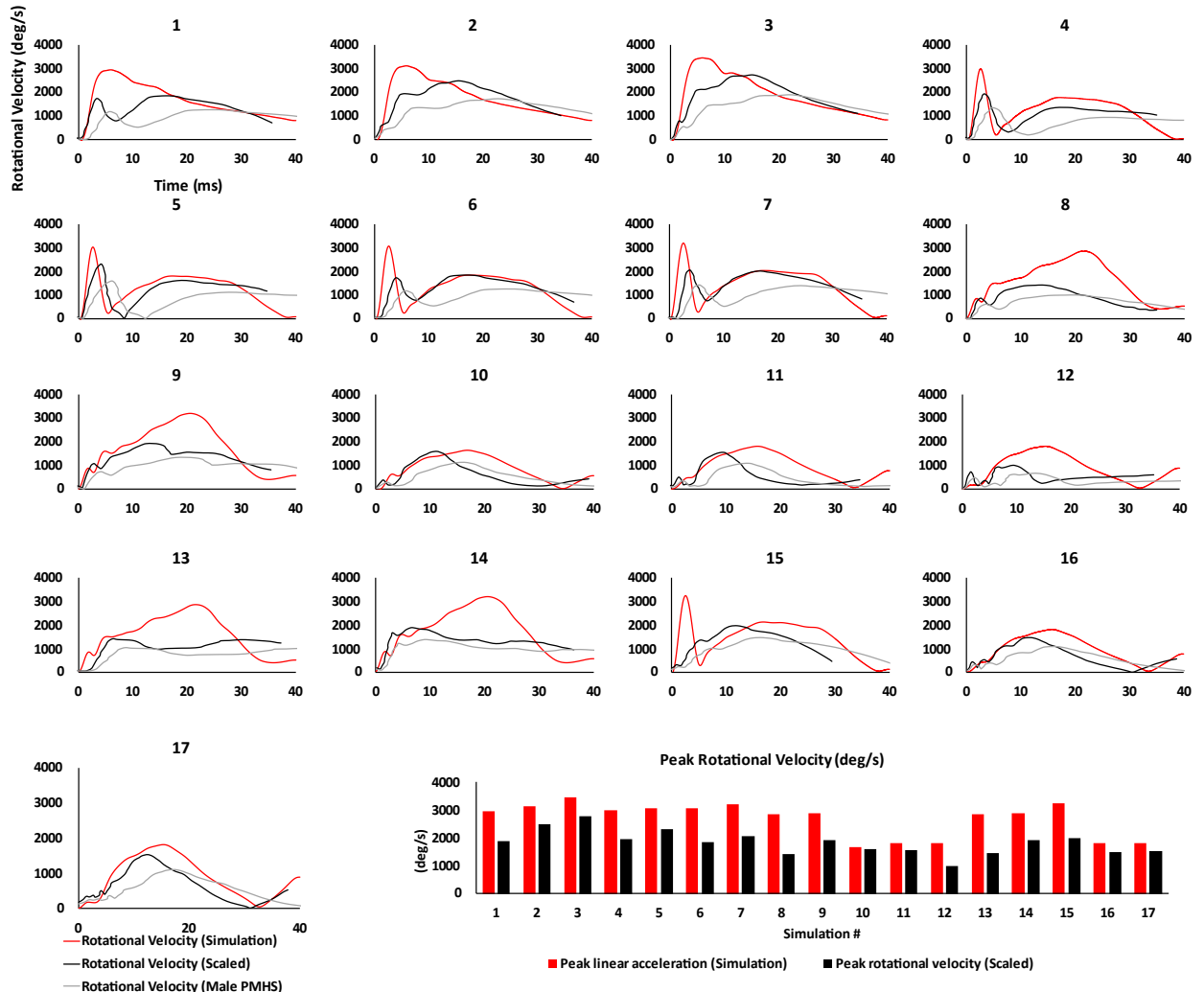


Figure 3-7 Head resultant rotational velocity of 6YO child. The experimental data were scaled digitized PMHS experiments data from ASSURE report.

3.3.2.3 3 years old model

In the lateral 0-degree cases (Case 1, 2, and 3 shown in **Figure 3-8**), the simulation accurately predicted the rotational velocities, closely matching the scaled experimental data. Though in case 1, the simulation result had a 22% higher peak rotational value compared to the corresponding scaled experimental peak value. Overall, the curve shapes in the simulation results matched well with the experimental results, except for case 1.

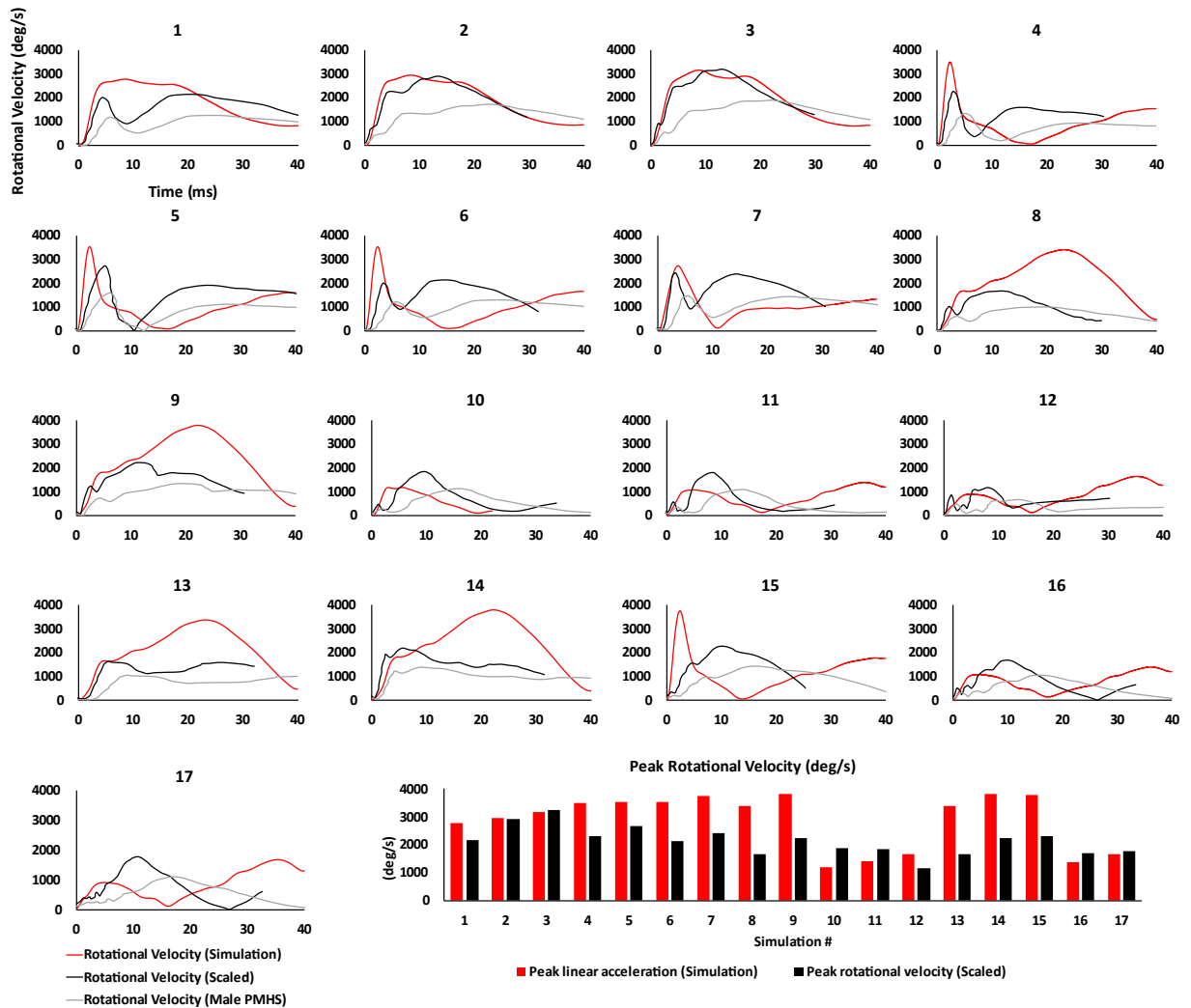


Figure 3-8 Head resultant rotational velocity of 3YO child. The experimental data were scaled digitized PMHS experiments data from ASSURE report.

In the frontal 58-degree impact cases (case 4, 5, 6, and 7 shown in **Figure 3-8**), the simulation accurately predicted the rotational velocities, closely matching the patterns observed in the scaled data. Although the simulated peak values tended to be higher than the corresponding scaled experimental results, except for case 7 where the peak rotational velocity matched the scaled PMHS data.

In the lateral 58-degree impact cases (8, 9, 13, and 14 shown in **Figure 3-8**), the peak value in the simulation occurred at approximately 5 milliseconds, whereas for the scaled PMHS results, the peak value occurred at around 22 to 24 milliseconds, which is a much

later stage of the impact. In all the impact cases, the simulation results consistently overestimated the peak rotational velocity compared to the corresponding scaled experimental results.

In the top 90-degree impact cases (case 10, 11, 12, 16, and 17), the simulated curves closely resembled the scaled PMHS experiments. However, the peak rotational velocities occurred earlier in the simulations. Case 10, 11, and 16 had higher peak values (57%, 28%, and 23% respectively), while case 12 had a lower peak value (30%) compared to the scaled experimental data.

3.3.3 Skull stress

Out of the total 17 cases, this study focused on 4 cases with very high impact velocity to compare skull stress among the 3 child models (**Figure 3-9**). Specifically, cases 3, 7, and 14 demonstrated that the von Mises stress was greater for the 10-year-old child model compared to the 6-year-old and 3-year-old child models. This indicates that the 10-year-old model experienced the highest level of skull stress. However, there was an exception in case 17, which involved a Top 90-degree impact. In this particular scenario, the 3-year-old child model exhibited the highest skull stress compared to the 6-year-old and 10-year-old models.

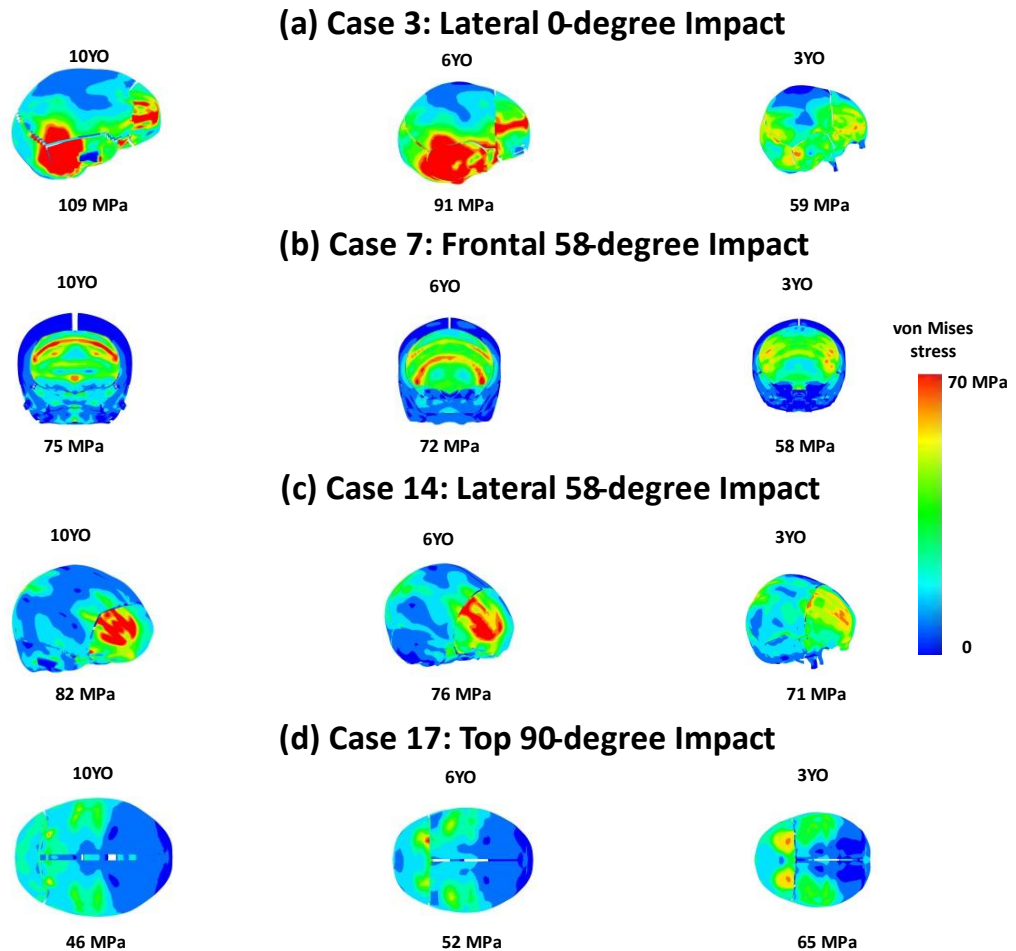


Figure 3-9 Skull stress contours comparison of three child models

3.3.4 Comparing average values among child models of different ages

Figure 3-10 and **Figure 3-11** display the average values of all 17 cases for three child models of varying ages. Notably, the data from **Figure 3-10** demonstrates a trend where, as the age of the child model increased, the average values tended to decrease. The 6-year-old child model exhibited 7.04% lower peak linear acceleration, 22.04% lower HIC, 6.54% lower peak rotational velocity, and 2.44% lower BrIC compared to the 3-year-old child model. Additionally, the 10-year-old child model showed 24.84% lower peak linear acceleration, 26.08% lower HIC, 9.54% lower peak rotational velocity, and 7.32% lower BrIC than the 3-year-old child model.

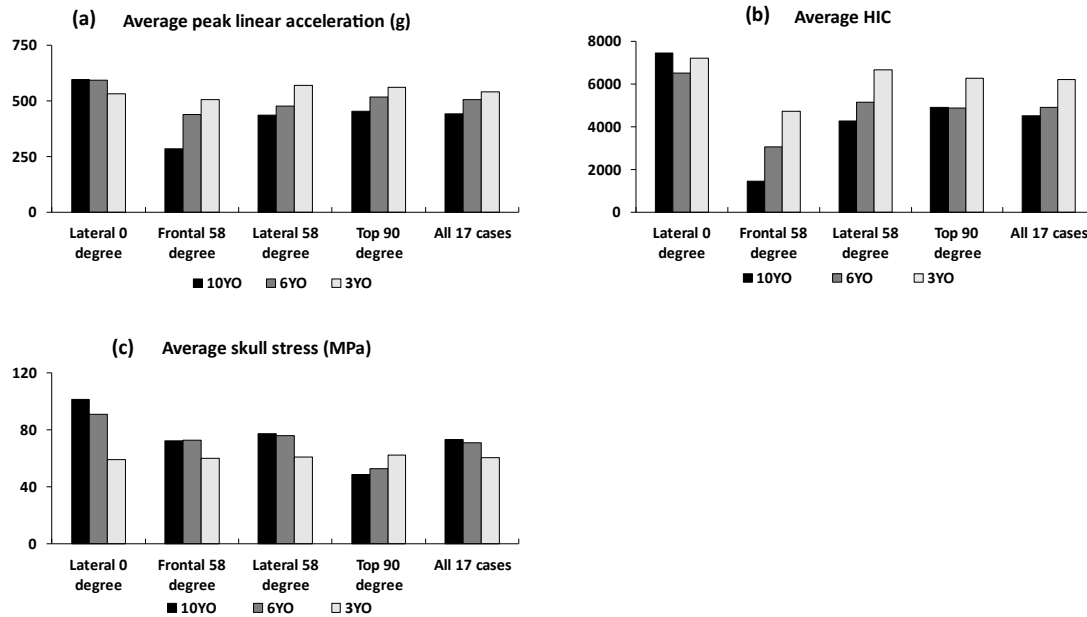


Figure 3-10 Average peak linear acceleration, Average HIC and Average skull stress comparisons of all three-child model.

However, despite experiencing higher linear acceleration and HIC, the 3-year-old model exhibited lower skull stress when compared to both the 10-year-old and 6-year-old models. A similar pattern was observed between the 10-year-old and 6-year-old models as well. Despite the 6-year-old model having higher peak linear acceleration and HIC, it still showed lower skull stress than the 10-year-old model. The 6-year-old child model experienced higher strain compared to the 10-year-old model, as indicated by higher peak rotational velocity and BrIC. CSDM10, and CSDM15 all showed higher values for the 6-year-old model compared to the 10-year-old model (**Figure 3-11**). Surprisingly, the 3-year-old model displayed lower brain MPS than both the 10-year-old and 6-year-old models. CSDM10, and CSDM15 exhibited lower values for the 3-year-old model in comparison to both the 10-year-old and 6-year-old child models.

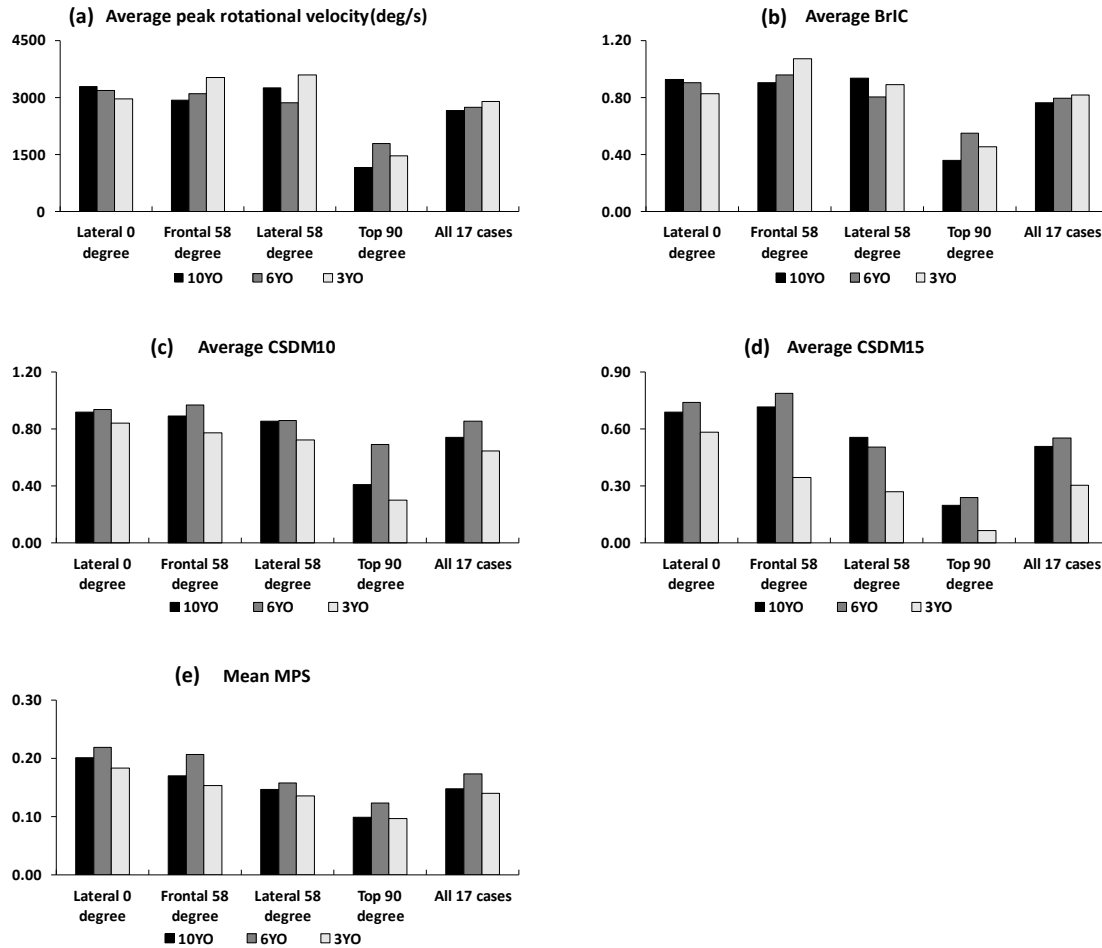


Figure 3-11 Average peak rotational velocity, Average BrIC, Average CSDM and Average mean MPS comparisons of all three-child model.

3.4 Discussion

The findings of this research provide valuable insights into the head injury risks associated with drone impacts, especially for vulnerable populations such as children. The observed variations between simulated and scaled data may be attributed to differences in head geometry and material properties between the FE models and PMHS experiments. Despite these differences, the simulations were generally successful in predicting the trends and providing valuable injury risk information.

To assess the potential risks posed by small Remotely Piloted Aircraft Systems (sRPAS) to vulnerable populations, such as children, an established and validated FE (Finite

Element) model of sRPAS was employed. This model was utilized to investigate the potential head impacts of sRPAS on children. Given the scarcity of child PMHS experiments, the model was verified by scaling head linear acceleration and rotational velocity data from experiments conducted on male PMHS. Weng et al. (2021) verified the female model using head linear acceleration and rotational velocity data that were scaled from male PMHS experiments [68]. This research represents the pioneering effort in examining the effects of sRPAS on child head impacts and providing critical insights into brain strains and von Mises skull stresses. In general, these findings suggest that children may be at heightened risk of injury in scenarios involving sRPAS-related head impacts, thus emphasizing the necessity for enhanced protective measures.

The comparative analysis conducted across the three distinct age groups yielded insightful findings. As the age of the child increased, the mean values of critical parameters, including linear acceleration, Head Injury Criterion (HIC), peak rotational velocity, and Brain Injury Criterion (BrIC) generally exhibited a diminishing trend, indicating a prevailing pattern of decreasing impact severity with advancing age. Our study encompassed four conventional impact scenarios: lateral 0 degrees, frontal 58 degrees, lateral 58 degrees, and top 90 degrees.

Zhang et al. in his study found that linear acceleration greatly affected intracranial pressure [33]. The head injury criterion (HIC) has gained significant acceptance as a primary metric for assessing head injuries in automotive safety [85]. Among these impact scenarios, the results consistently indicated that the lateral 0-degree impact was the most vulnerable, manifesting the highest levels of linear acceleration and HIC. In addition, except for the 3-year-old child model, where the top 90-degree impact exhibited the highest skull stress, the lateral 0-degree impact consistently induced the highest skull stress.

Researchers proposed the brain's maximum principal strain (MPS) as a predictor for concussion and diffuse axonal injury (DAI) [86]. In all impact cases across the three child models, brain strains generally exhibited elevated levels. Notably, among the four impact scenarios, the lateral 0-degree impact consistently resulted in particularly elevated brain

strains. Specifically, for the 10-year-old model, the average brain strain (Mean MPS) observed was approximately 0.20. Similarly, for the 6-year-old model, the average brain strain was approximately 0.22. In the case of the 3-year-old model, the lateral 0-degree impact led to an average brain strain of around 0.18. These outcomes underscore the significance of frontal and lateral impacts in relation to brain injury risks, indicating that such impacts merit heightened attention compared to top impacts.

The comparison of the Cumulative Strain Damage Measures (CSDM10 and CSDM15) across the three child models revealed noteworthy trends. The 6-year-old model consistently exhibited higher values in comparison to the 10-year-old model, signifying potentially elevated brain injury risks in the former. The 3-year-old model consistently displayed lower brain strain levels in relation to both the 6-year-old and 10-year-old models across these metrics, indicating a relatively lower susceptibility to brain injury.

3.5 Conclusion

The developed sRPAS FE model was utilized to simulate impacts on child models of 10, 6, and 3 years old, totaling 51 simulations. The model's predictions for linear acceleration and rotational velocity generally aligned well with scaled PMHS data. With the increasing age of the child model, the average values for all impact cases, including linear acceleration, HIC, peak rotational velocity, and BrIC, tended to decrease. Despite the 3-year-old model showing higher linear acceleration and HIC, it displayed lower von Mises stress compared to the 10-year-old and 6-year-old models. Notably, the 6-year-old model consistently demonstrated higher brain strain than the 10-year-old model, and the 3-year-old model exhibited lower brain strain compared to both the 6-year-old and 10-year-old models. The findings underscore the importance of age-specific considerations in safety design and establish a solid basis for further exploration in this critical domain.

Chapter 4

4 Investigating Head Injury Dynamics in Small Remotely Piloted Aircraft System(sRPAS) to Head Collisions: A Comparative Study of sRPAS Models

Abstract

The increasing prevalence of drone usage has raised concerns regarding the safety of individuals on the ground, particularly in cases of drone malfunctions leading to collisions. This study delves into the intricate dynamics of drone-to-human impacts, with a specific focus on small remotely piloted aircraft systems (sRPAS). Using a highly detailed finite element (FE) model, the head kinematics resulting from sRPAS impacts and verified the model's accuracy against cadaveric data from impact scenarios were investigated. The research extended to a comparative analysis of head injuries caused by two different sRPAS models: the Mavic Pro and the Phantom 3, considering frontal 58-degree impacts at varying speeds. The FE model accurately predicted head linear accelerations and rotational velocities, confirming its reliability in capturing real-world impact dynamics. Comparing the impacts of the Mavic Pro and the Phantom 3, the Mavic Pro exhibited higher linear accelerations, Head Injury Criterion (HIC), skull stress, and brain strain, highlighting its potential to cause more severe injuries. In contrast, the Phantom 3 impact yielded greater rotational velocities. The findings emphasize the importance of thorough safety measures in drone design and operations to mitigate potential risks to individuals on the ground. This research contributes to aviation regulatory efforts by providing insights into head injury risks during impacts with two types of sRPAS and aiding the establishment of effective safety protocols.

4.1 Introduction

Numerous incidents involving drone malfunctions resulting in ground collisions have highlighted a significant safety concern. In May 2015, an unmanned aircraft flying over a crowd during a Memorial Day parade in Marblehead, MA, struck a building and subsequently crashed, causing minor injuries to two individuals [87]. Similar risks are present in any scenario involving unmanned aircraft and people, as malfunctioning drones have the potential to descend onto individuals on the ground. For instance, in early April 2014, an unmanned aircraft collided with a female athlete during a triathlon in Geraldton, Western Australia, resulting in a head laceration [88]. Emergency personnel had to remove a piece of the propeller from the athlete's head. Tragically, operator errors have led to fatal outcomes as well. In April 2003, an out-of-control model aircraft claimed the life of a 14-year-old girl in England [76], while a radio-controlled helicopter struck and severely injured a 41-year-old operator in Switzerland in 2013 [89].

Numerous studies that explore the impact of drones on humans utilize a probabilistic methodology, involving a sequence of estimations and assumptions. This complex matter can be broken down into distinct components. One crucial aspect is identifying the worst-case impact scenario, encompassing factors such as kinetic energy, drone orientation, and approach angle. Additionally, evaluating collision outcomes for a human involves considerations like energy transfer or absorption and human vulnerability. Practical testing utilizing Anthropomorphic Test Devices (ATDs), Post-Mortem Human Surrogates (PMHS), or computational modeling plays a pivotal role in establishing foundational datasets for assessing potential consequences. Both cadaveric experiments and Finite Element (FE) models have significantly contributed to the understanding of head injuries caused by such incidents. Koh et al. (2018) employed practical tests to validate finite element models, utilizing a simplified Anthropomorphic Test Device (ATD) to assess head impacts [90]. Another study revealed an AIS2 skull linear fracture resulting from a quadcopter-type sRPAS impacting the head in various scenarios. The utilization of the Advanced Human Body Models for injury prediction (PIPER) scalable child model shed light on the correlation between skull stress and fracture in children [91]. This study highlighted that stress responses predicted by the model, such as von Mises stress, are

more effective in forecasting skull fractures compared to kinematic-based injury measures. Similarly, Weng et al. (2021) validated an sRPAS model against 17 experimental studies from the ASSURE report [56].

Aviation regulatory authorities grapple with the intricate task of balancing the benefits of Small Remotely Piloted Aircraft Systems (sRPAS) with the inherent safety risks posed to individuals on the ground. To address this multifaceted issue, these authorities are actively proposing and implementing a range of solutions to ensure the safety of individuals on the ground. In recent years, the Federal Aviation Administration (FAA) supported a substantial project aimed at comprehending the impact of sRPAS on human heads. The Alliance for Safety of UAS through Research Excellence (ASSURE) employed automotive criteria and limits for evaluation, drawn from an extensive array of empirical data commonly utilized in certifying vehicle safety for occupants during collisions [15]. Still, caution is warranted during the transition due to discrepancies in impact masses, velocities, and materials between drones and Unmanned Aircraft Systems (UASs). Empirical data from sRPAS tests involving Post-Mortem Human Surrogates (PMHS) emphasize the need for this cautious approach.

The ASSURE A4 report, comprising 26 tests involving a DJI Phantom 3 standard drone impacting an ATD, incorporated various automotive criteria to assess injury severity. The most comprehensive dataset to date is encapsulated in the ASSURE A14 Report, which encompasses a total of 315 tests involving diverse UASs subjected to various impact scenarios, utilizing distinct impact partners such as simplified ATDs and PMHS [15]. However, it is important to note that detailed data and test results are available only for 149 tests, which constitute the focus of this study.

There are sRPAS with various structures and masses available. While in previous chapters, head responses to one specific quadcopter sRPAS were studied. This study aimed primarily to create a new quadcopter sRPAS FE model and verify it using cadaveric data through four distinct frontal impact scenarios. After confirming the impact simulations and verifying the human head model, skull von Mises stress and brain maximum principal strain were studied and compared to the previous sRPAS model

(Phantom 3) in similar impact scenarios. Furthermore, various injury metrics, including HIC and BrIC, were compared between the two sRPAS models.

4.2 Methods

4.2.1 Mavic Pro model development

A representative quadcopter-style Mavic Pro FE model was developed (**Figure 4-1**). The FE model comprised various structural parts, including chassis upper portion, chassis lower portion, drone frame, battery, propeller assembly, hover arms, camera assembly, and gimble cover. In total, the FE model was made up of 56,512 1D-2D shell elements, including 961 1D beam elements and 55,551 2D shell elements. Overall, the model weighed 1.641lbs, which is 1.2% different from the physical model. High-quality meshes were used in this model to ensure accuracy. The shell element composition in the analyzed model consisted of 55,147 2D quadrilateral elements, accounting for 99.27% of the total shell elements. Additionally, there were 404 2D triangular elements, representing a mere 0.037% of the total shell elements. Among the 2D shell elements, a mere 3% exhibited a warpage value exceeding 5, with the highest recorded value reaching 46.45. Remarkably, all 2D shell elements maintained an aspect ratio below 5.

Furthermore, a fraction of 3% of the 2D elements displayed a Jacobian value below 0.7, with the minimum recorded value being 0.43. Notably, every 2D element exhibited a length greater than 1mm, with the minimum length measured at 1.07 mm and the maximum length at 3.86 mm. These stringent mesh quality requirements were upheld to ensure the accuracy of the finite element model, while the dimensions of the model were verified against the specifications of the Mavic Pro Quadcopter, as per the established standards.

The Mavic Pro FE model was meshed using HyperMesh (Altair, Troy MI, USA), with the frame and battery components being separated. Spotwelds were used to connect the different parts. The arm joint with the main frame and battery components being separated. Spotwelds were used to connect the different parts. The arm joint with the main frame was one complicated part of this model. The arm in the physical model is flexible and can rotate to a certain extent. Hence, the

*CONSTRAINED_JOINT_REVOLUTE was defined to reinforce the connection between the frame and the arms. This *CONSTRAINED_JOINT_REVOLUTE is a function defined in Ls-Dyna, which specifies the revolution axis and the stiffness. The revolute joint was implanted at four drone arms to better represent these features in the FE model, allowing the arms of the drone to be flexible and rotate in the z direction.

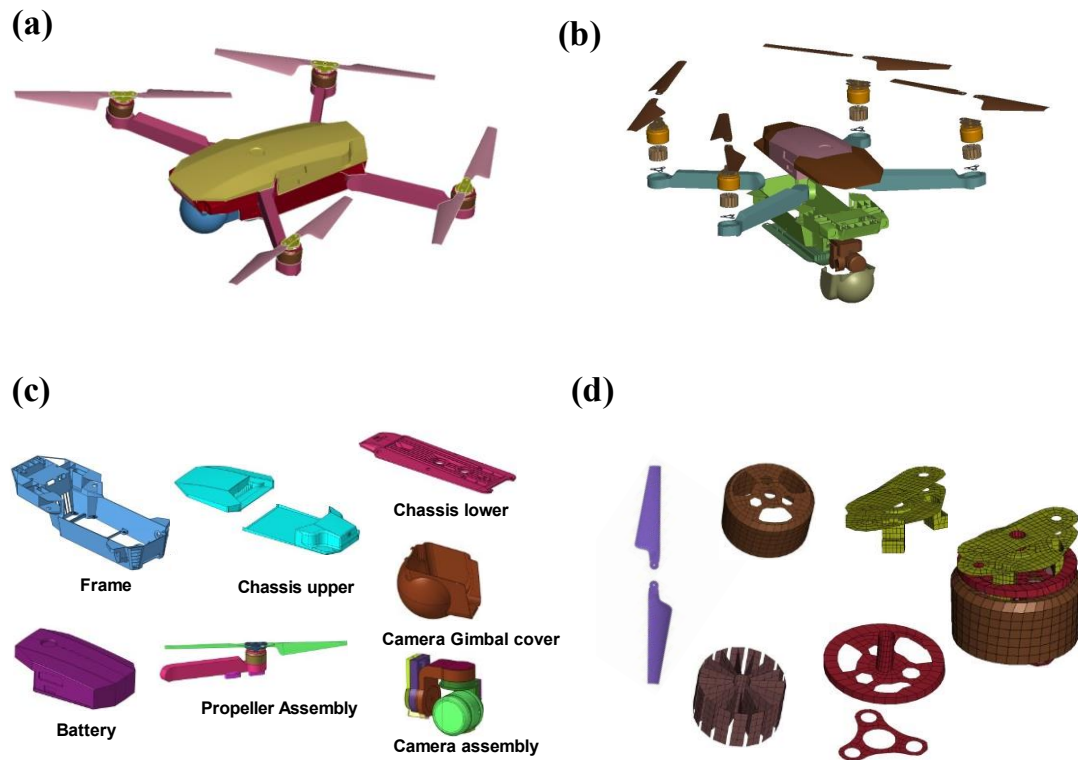


Figure 4-1 Mavic Pro finite element model. (a) Full FE model of Mavic Pro. (b) Exploded view. (c) Parts of Mavic Pro. (d) Motor assembly

Based on the material information from the ASSURE report [15], which is presented in **Table 4-1**, the material properties of various components of the Mavic Pro FE model were determined. Polycarbonate material was assigned to the body frame, upper & lower chassis, arm, and propeller blades. The gimble was modeled using G10 Fiber glass. The Motor casing, clamp & blade clamp were modeled using Case Aluminum 520F. Motor Windings were modeled using Steel 4030. However, it was discussed during the later model verification stage that the Gimbal cover was removed when sRPAS is under

operation. So, the Gimbal cover was removed for later sRPAS-to-head simulations, even though it was developed.

The sRPAS frame shell was deemed the most important part because it made direct contact with the human head. The energy of the moving drone would be transferred from the body shell, which was stopped during impacts, to the head, which was driven. As a result, the material properties of the shell were believed to play a significant role in the impact simulations. In general, the shell was made of polycarbonate plastic, a strong and durable material commonly used in engineering structures. According to the ASSURE report, the Johnson-Cook model was found to be suitable for simulating shells. **Table 4-3** summarized the material properties of polycarbonate based on the ASSURE report.

Table 4-1 Parts and material types

Drone parts	Material
Frame	Polycarbonate
Upper & Lower Chassis	Polycarbonate
Arm	Polycarbonate
Propeller Blades	Polycarbonate
Battery Pack	Battery
Motor Casing	Case Aluminum 520F
Clamp	Case Aluminum 520F
Motor Windings	Steel 4030

Table 4-2 General material properties

Material	Young's modulus (MPa)	Poisson's ratio	Density (ton/mm³)
Cast Aluminum 520F	66,600	0.33	2.87E-09
Steel 4030	200,500	0.29	8.65E-09
G10 Fiber glass	13,790	0.12	1.98E-09
Battery	500	0.33	5.477E-09

Table 4-3 Detailed material properties of polycarbonate

Density (kg/m³)	Young's Modulus (GPa)	Shear Modulus (GPa)	A (MPa)	B (MPa)	C	m	n	Cv (KJ/kgK)	Tmelt (K)
1197.8	2.59	0.93	80	75	0.0052	0.548	2	1.3	562

4.2.2 Available cadaver data for verification

The comprehensive ASSURE report provides access to cadaveric test data involving sRPAS-to-human collisions [15]. These experiments, overseen by Ohio State University, employed various sRPAS for testing purposes. Notably, Weng et al. (2021) previously validated their FE model using data from 17 quadcopter-style sRPAS (Phantom 3) experiments found within the detailed ASSURE report [56]. This study focused on data from 4 experiments involving quadcopter-style sRPAS (Mavic Pro) sourced from the same report. These experiments yielded detailed head kinematics time histories during impacts and were conducted using frontal 58-degree impact configurations. Two male cadaver subjects participated, with body masses of 143lb and 193lb, respectively. Each PMHS subject was equipped with head kinematics sensors, allowing for the measurement

of head linear acceleration, head rotational velocity, and head rotational acceleration at the head's center of gravity during impact.

4.2.3 sRPAS to head impact

4.2.3.1 THUMS human body model

This study employed both the 50th percentile male adult model and the 5th percentile small female model from Total Human Model for Safety (THUMS) version 4.02. A comprehensive depiction of these two models is provided in chapter 2, specifically in sections **2.2.1.1** and **2.2.1.1**.

4.2.3.2 Simulation of Mavic Pro to human head impact

In the preprocessing phase, the integration of the Mavic Pro model and the THUMS was accomplished through the utilization of HyperMesh and LS-Prepost version 4.5 (LSTC/ANSYS, Livermore, CA). Paramount to establishing the initial boundary and loading conditions were various considerations. These encompassed the strategic positioning of the Mavic Pro FE model relative to the human head, the determination of the Mavic-Pro's flying speeds, and the precise definition of contact conditions governing the interaction between the sRPAS and the human head.

The initial positioning and velocities of the drone were established based on empirical data obtained from Ohio State University (OSU) PMHS experiments (**Table 4-4**). Specifically, the Mavic Pro model focused exclusively on the Frontal 58-degree scenario. In total, four cadaveric experiments were reported in the ASSURE Report [15]. For comparing the head kinematics and injury metrics between males and females, identical impact conditions were applied to the THUMS female model (**Figure 4-2**). Two simulations were performed for females, mirroring the ones conducted for males, employing the initial loading conditions outlined in the ASSURE report (**Table 4-5**). Since female cadaveric data were absent from the ASSURE report, consistency in impact locations was ensured for both average males and small females using a proportional approach. By using a vertical line through the head's center of gravity as a reference, impact locations were determined based on the angles between the vertical center line

and the approaching directions of the sRPAS. To impart the desired velocity to the drone, the *INITIAL_VELOCITY command available in LS-DYNA was employed. Additionally, the *AUTOMATIC_SURFACE_TO_SURFACE command was utilized to accurately define the contact interaction between the Mavic Pro and the human head model.

To collect linear acceleration and rotational velocity data at the head's center of gravity, numerical accelerometers were placed on the human head model. However, it was observed that the resultant acceleration output from the middle to later stages of LS-DYNA's LS-Direct PrePost generated spurious values. In order to obtain accurate linear acceleration values, a low-pass channel frequency class (CFC) 1000 Hz filter was applied to the x, y, and z axes linear acceleration data, and the resultant acceleration was then calculated from the filtered data. Rotational velocities were filtered using a 180 Hz filter.

By implementing this meticulous preprocessing methodology, the integration of the Mavic Pro model and the THUMS is upheld with a high degree of reliability and precision. Consequently, it guarantees the accurate acquisition of linear acceleration and rotational velocity data, thereby facilitating precise and reliable data for subsequent analytical investigations.

Table 4-4 sRPAS to head impact setups. FPS: Foot per second. OSU: Ohio State University

Case #	Impact Direction	Impact Angle (degree)	Sex	Impact Velocity m/s (FPS)	Cadaver subject
1	Frontal	58	Male	18.6 (61)	4
2	Frontal	58	Male	21.6 (71)	3
3	Frontal	58	Male	18.6 (61)	4
4	Frontal	58	Male	21.6 (71)	3

Table 4-5 sRPAS to female head setups. FPS: Foot per second

Case #	Impact Direction	Impact Angle (degree)	Sex	Impact Velocity m/s (FPS)
1	Frontal	58	Female	18.6 (61)
2	Frontal	58	Female	21.6 (71)

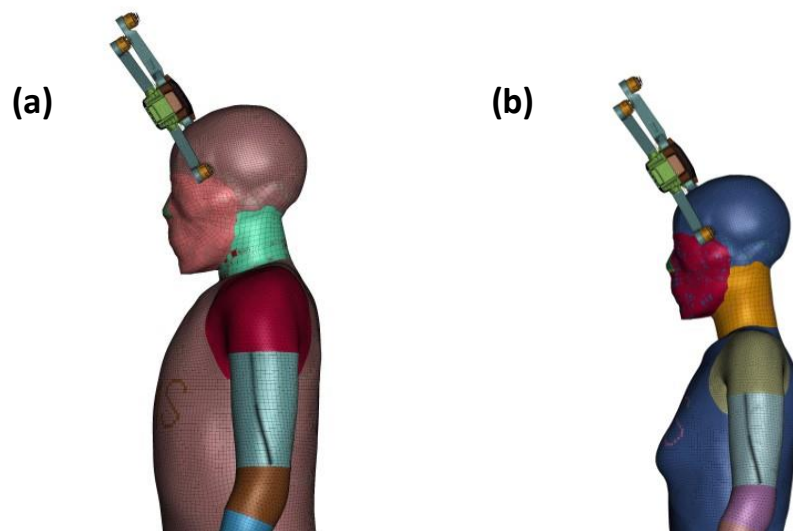


Figure 4-2 Mavic Pro Frontal 58-degree Impact setting. (a) THUMS 4.02 50th percentile male model. (b) THUMS 4.02 5th percentile female model

4.2.4 Mavic Pro vs Phantom 3

This section delves into the effects of head impacts from the Mavic Pro and Phantom 3 drones, examining the resulting head responses. Notably, these sRPAS differ in weight and structure, with the Mavic Pro weighing 0.74kg and the Phantom 3 weighing 1.2kg (shown in **Figure 4-3**). For the assessment, a frontal impact at a 58-degree angle was chosen as the impact setting, with two distinct impact velocities of 61fps and 71fps.

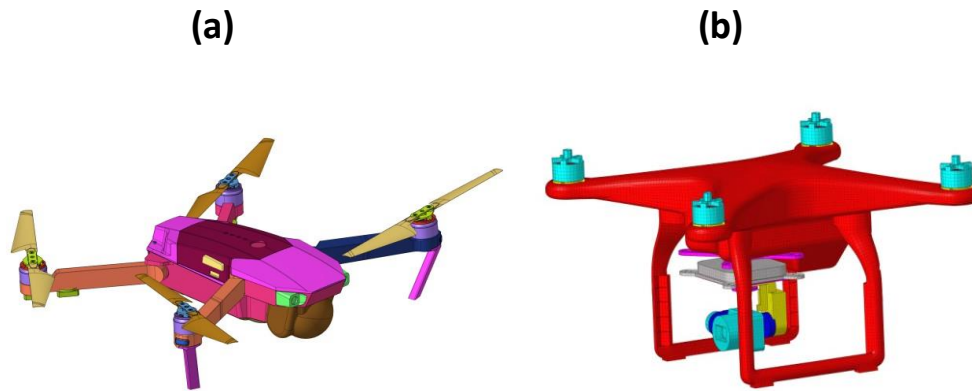


Figure 4-3 (a) Mavic Pro. (b) Phantom 3

4.3 Results

4.3.1 Resultant linear acceleration verification

All four cases were verified (**Figure 4-4**) using frontal 58-degree drone impact. It needs to be noted that the direction of frontal was referred to the human head. During the impact, one peak linear acceleration appeared in all the impact cases. The impact duration was approximately 2 milliseconds. The simulated peak linear acceleration matched the cadaver experiments well, though the simulated results slightly underestimated the peak value by around 14% in case 1 and 12% in case 2. The peak linear acceleration of the simulation matched well with the experimental results for case 3 and case 4.

4.3.2 Resultant rotational velocity verification

The rotational velocity curves were well-verified (**Figure 4-5**). Except for the first two cases, the curves of simulations and cadaver experiments matched well. The peak values of simulation and experimental values were generally close in the first two cases. For the first two cases, the peak value occurred at around 16 milliseconds. However, in simulation, the rotational velocity peaked at around 5 milliseconds. In case 3 and 4, the peak rotational values were 34% and 27% higher than those of experiments.

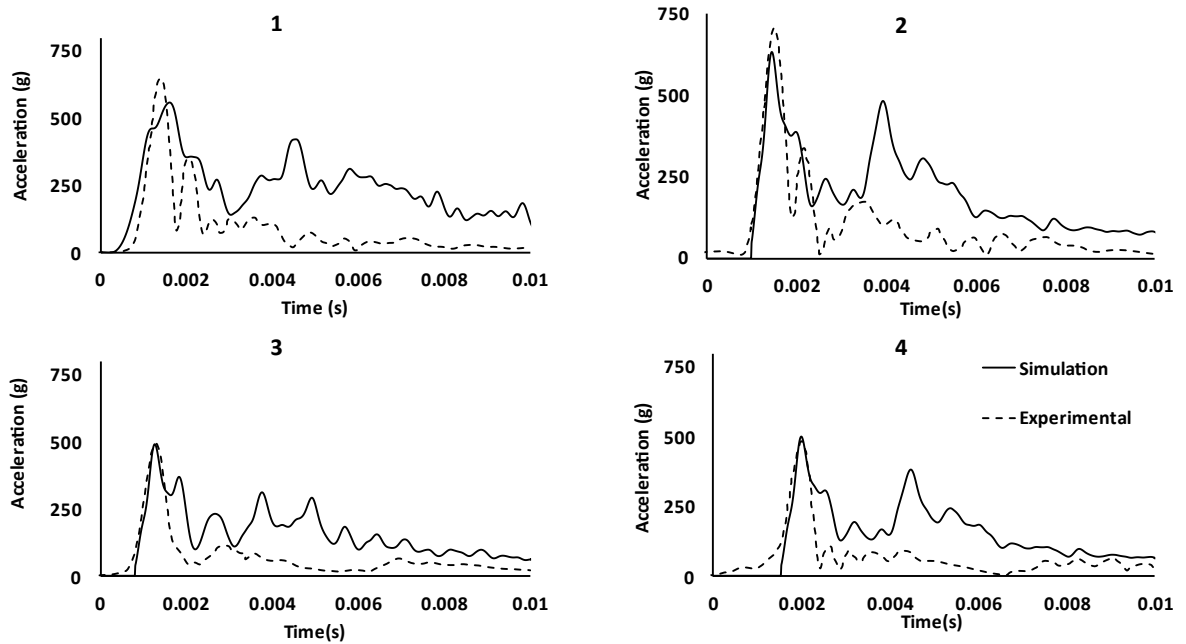


Figure 4-4 Head resultant linear acceleration verification. Experimental data were digitized based on ASSURE report.

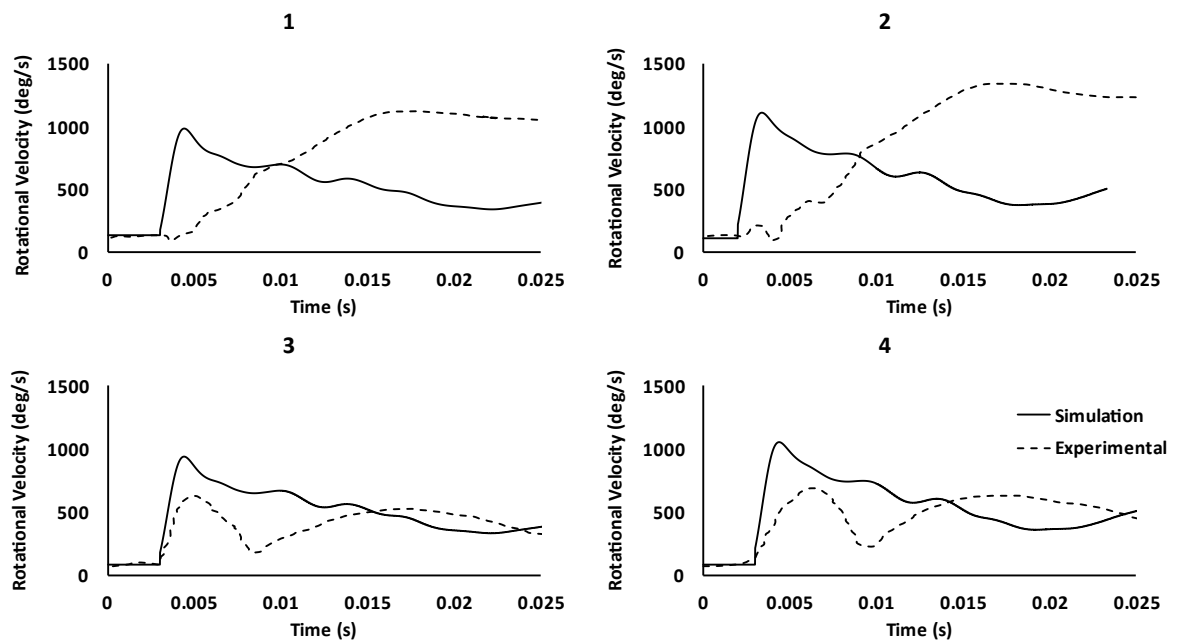


Figure 4-5 Head resultant rotational velocity verification. Experimental data were digitized based on ASSURE report.

4.3.3 Comparison of DJI Phantom and Mavic Pro

An analysis of two separate impact scenarios was conducted to understand the kinematic effects of head-on collisions involving two different drone models: the Mavic Pro and the Phantom 3. Notably, by maintaining consistent impact parameters for both drones, an opportunity emerges to outline the differences in injury kinematics resulting from these distinct impacts.

Figure 4-6(a) shows that both male and female individuals experienced increased levels of linear acceleration, Head Injury Criterion (HIC), and skull stress under Mavic pro impact situations. Pertinently, in the context of head impact by the Mavic Pro at 61fps, the male exhibited a noteworthy peak linear acceleration of 492g. In stark contrast, when subjected to the impact of the Phantom 3, the average male experienced a markedly reduced peak linear acceleration of 218g, signifying a substantial 55% lower than the Mavic Pro impact. Analogous trends were witnessed amongst female subjects, who registered an almost 49% reduction in peak linear acceleration consequent to the Phantom 3 impact in comparison to the Mavic Pro's.

The HIC results followed these patterns (**Figure 4-6(b)**), with the Mavic Pro impact manifesting higher HIC values relative to the Phantom 3 impact across both average male and small female subjects. The same pattern observed when examining skulls stress (**Figure 4-6(c)**). For average male, the Mavic Pro impact resulted in a skull stress of 117MPa, while the Phantom 3 impact led to a lower value of 97MPa. This pattern was true for the small female as well, with the Mavic Pro impact causing more skull stress than the Phantom 3 impact.

At a higher impact speed of 71fps, a similar pattern was observed. The Mavic Pro impact led to much higher peak linear acceleration of 502g for average males and 598g for small females (**Figure 4-7(a)**). In contrast, the impact associated with the Phantom 3 yields comparatively lower results, with the average male experiencing a peak linear acceleration of 194g and the small female encountering 254g. In terms of the Head Injury Criterion (HIC), the Mavic Pro impact yields notably higher values when compared with the Phantom 3 impact (**Figure 4-7(b)**).

The delineation of skull stress data mirrors these recurring trends. Specifically, the average male subjected to the Mavic Pro impact demonstrated a skull stress of 124MPa, while the corresponding value for the small female stood at 143MPa. By contrast, the Phantom 3 impact resulted in lower skull stress values, with the average male experiencing 98MPa and the small female registering 127MPa (**Figure 4-7(c)**).

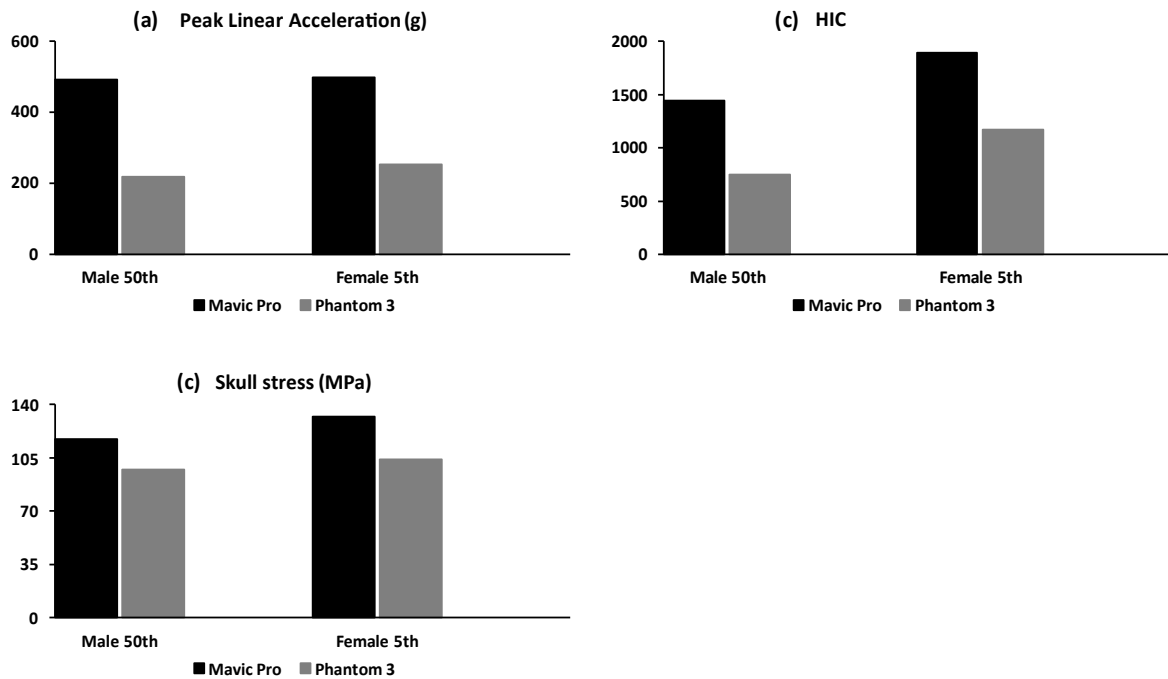


Figure 4-6 Comparison of Mavic Pro Vs Phantom 3 impact at 61fps (a) Peak linear acceleration, (b) HIC, (c) Skull stress.

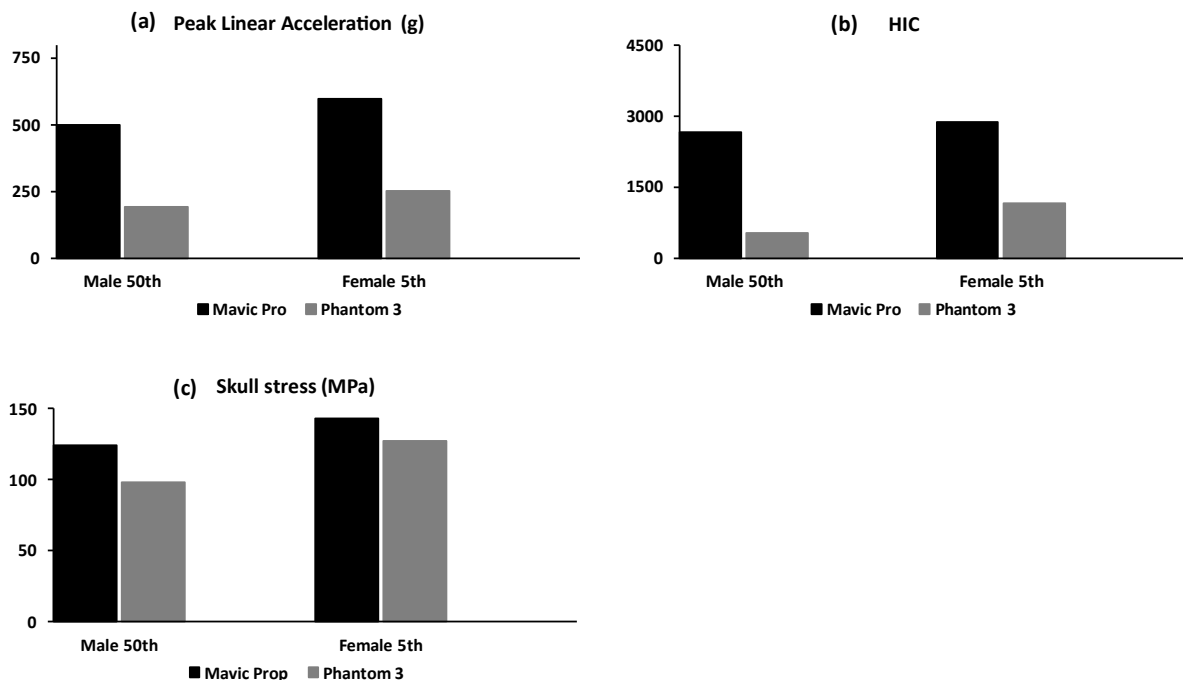


Figure 4-7 Comparison of Mavic Pro Vs Phantom 3 impact at 71fps (a) Peak linear acceleration, (b) HIC, (c) Skull stress.

Upon examining the rotational velocity, distinctive patterns were identified. (**Figure 4-8**). At a 61fps impact speed, the Mavic Pro impact on the head resulted in lower rotational velocities for both average males and females compared to the Phantom 3 impact. The peak rotational velocity recorded for the Mavic Pro impact was 809 degrees per second, marking a 24% decrease in comparison to the peak rotational velocity observed with the Phantom 3 impact. This same trend was observed in small females, where the impact of the Mavic Pro led to approximately 27% lower rotational velocity compared to the Phantom 3 impact. This pattern continued even as the impact velocity increased to 71fps, with both male and female subjects experiencing reduced rotational velocities from the Mavic Pro impact relative to the Phantom 3 impact (**Figure 4-9**).

Shifting to the BrIC calculation, at a 61fps impact speed, the values were nearly indistinguishable for both the Mavic Pro and Phantom 3 impacts. However, in the case of small females, the BrIC value was approximately 7% lower for the Mavic Pro impact compared to the Phantom 3 impact. This pattern held true at higher speeds as well, with male subjects exhibiting near-identical BrIC values for both Mavic Pro and Phantom 3

impacts. Conversely, small females demonstrated lower BrIC values for the Mavic Pro impact compared to the Phantom 3 impact.

Consideration of Brain MPS revealed consistent trends at both 61fps and 71fps. In both instances, the Mavic Pro impact elicited higher MPS values for both male and female subjects relative to the Phantom 3 impact. Specifically, at 61fps, the male subjects experienced nearly 90% higher MPS due to the Mavic Pro impact compared to the Phantom 3 impact. Similarly, small females exhibited an approximate 54% higher MPS resulting from the Mavic Pro impact in contrast to the Phantom 3 impact. This congruence in trends extended to the 71fps speed, where both average male and female subjects encountered elevated MPS values due to the Mavic Pro impact in comparison to the Phantom 3 impact.

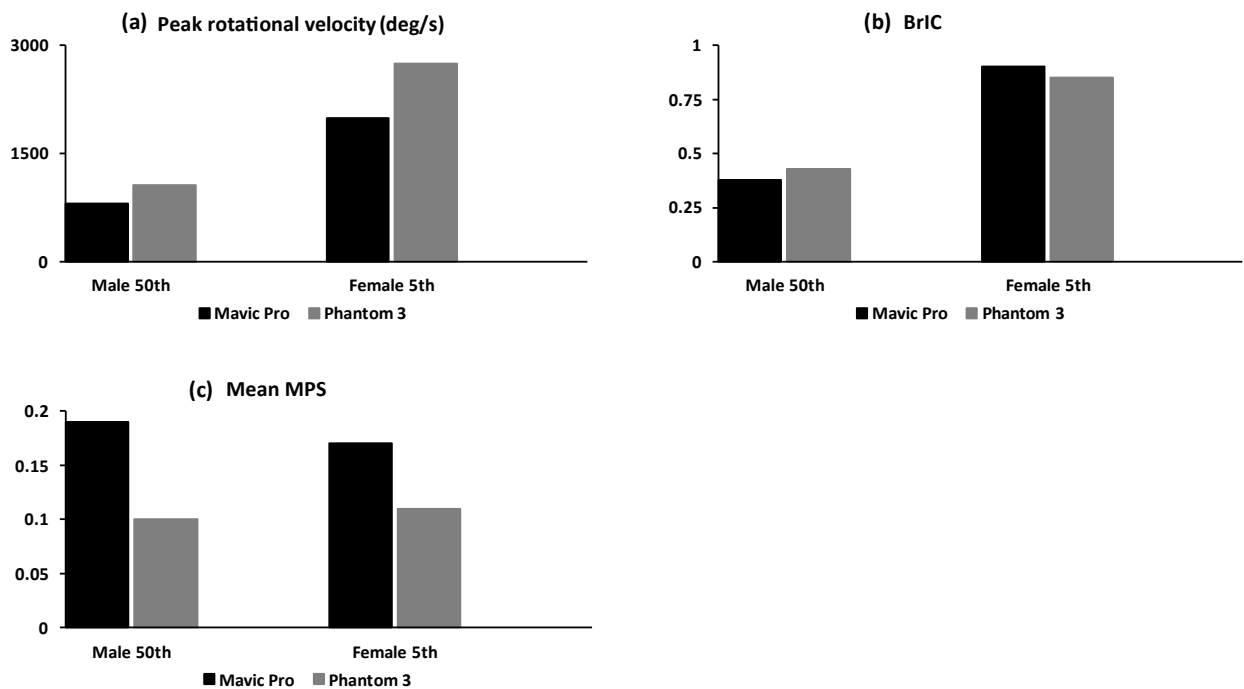


Figure 4-8 Comparison of Mavic Pro Vs Phantom 3 impact at 61fps (a) Peak rotational velocity, (b) BrIC, (c) Mean MPS

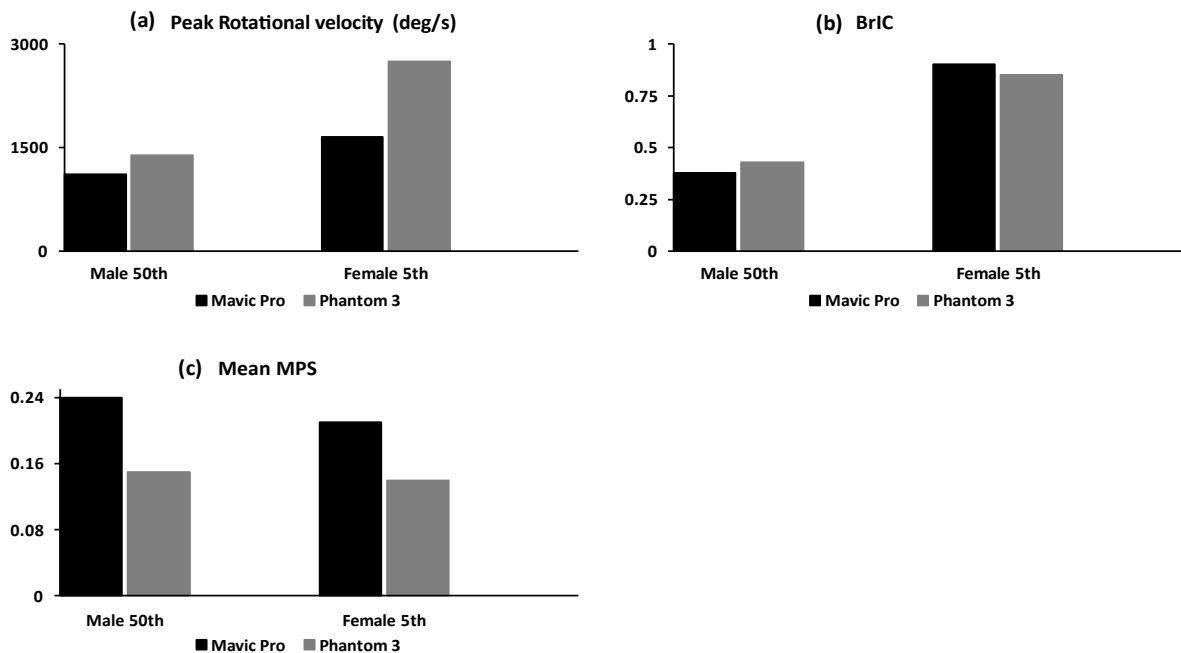


Figure 4-9 Comparison of Mavic Pro Vs Phantom 3 impact at 71fps (a) Peak rotational velocity, (b) BrIC, (c) Mean MPS.

4.4 Discussion

This study focused on comprehending the human head's responses when exposed to impacts from sRPAS to humans. To achieve this, a highly detailed finite element (FE) model of a representative quadcopter-style sRPAS was developed, specifically the Mavic Pro. To verify the accuracy of the model, a meticulous comparison was made between its predictions and data obtained from four separate sRPAS-to-human-head impact scenarios. The model's predictions for head linear acceleration and rotational velocity closely matched real-world data collected from cadaveric heads.

The research was expanded to examine head-on collisions involving the Mavic Pro and the Phantom 3 drones, along with an exploration of how head responses vary due to impacts on these two distinct drone models. In their previous work, Weng et al. (2021) focused on the Phantom 3, creating a model for it, and validated it against 17 cases of drone-to-human head impacts [56]. This study underscored variations in the impact of these two drones on human head responses.

The increasing occurrences of drones malfunctioning and colliding with individuals on the ground have raised significant safety concerns. Through simulations, this study emphasizes potential hazards arising from scenarios involving impacts of the human head by both Mavic Pro and Phantom 3 sRPAS. These collisions can lead to varying degrees of injury severity, highlighting the crucial need for a comprehensive understanding of injury mechanisms to formulate effective safety protocols.

Linear kinematics have been established as factors contributing to concussion injuries. Notably, research by Pellman et al. (2003) indicated that concussed sports players experienced peak linear acceleration of $98 \pm 28g$ [92], while Zhang et al. (2004) reported peak linear acceleration ranging from 61 to 144g [33]. Analysis of linear acceleration showcased marked distinctions between the impacts of the Mavic Pro and the Phantom 3. Specifically, impacts at velocities of 61fps and 71fps involving the Mavic Pro induced significantly higher peak linear accelerations compared to those involving the Phantom 3. This dissimilarity in acceleration levels underscores the potential for more severe head injuries stemming from Mavic Pro impacts, thus underscoring the importance of careful drone design considerations and operational regulations.

Head Injury Criterion (HIC) is a pivotal parameter in assessing the severity of injuries resulting from head impacts. The findings consistently indicated elevated HIC values for impacts involving the Mavic Pro, relative to those involving the Phantom 3. These higher HIC values underscore the heightened risk of head injury posed by Mavic Pro collisions. Similarly, the analysis of Von Mises skull stress underscores the greater potential of the Mavic Pro to cause significant damage. Higher Von Mises stress values observed in Mavic Pro impacts underscore its propensity to lead to severe head injuries.

An intriguing observation emerged from a cadaveric study wherein a frontal 58-degree impact at 70.5fps resulted in an AIS 2 level, 13cm linear skull fracture [93]. Scientific literature has associated Von Mises stress values with injury prediction, specifically establishing a critical threshold of 110.9 MPa as indicative of skull fractures [91]. The investigation revealed that both male and female subjects demonstrated Von Mises stress exceeding this threshold during impacts from the Mavic Pro at 61fps and 71fps. This

strongly implies a significant likelihood of skull fractures resulting from Mavic Pro impacts, thereby underscoring the potential for severe head injuries.

Rotational velocity has also been identified as a critical factor in predicting head injuries. This study demonstrates that Mavic Pro impacts yield lower rotational velocities compared to Phantom 3 impacts. However, data on brain MPS reveals higher values in the context of Mavic Pro impacts relative to Phantom 3 impacts.

The Mavic Pro weighs 0.74kg, whereas the Phantom 3 has a weight of 1.2kg. Despite its lower weight, the Mavic Pro leads to greater head impact effects in terms of HIC and skull stress. This prompts an investigation into the structural dissimilarities between these two sRPAS. While the Phantom 3's impact involves direct head contact with its frame shell, the Mavic Pro's impact involves battery contact. This structural variance, coupled with differing material properties, likely contributes to varied head responses.

Additionally, BrIC values show a lower reading for the Mavic Pro impact compared to the Phantom 3, possibly due to variations in rotational velocity. Intriguingly, brain strain analysis contradicts expectations, showing higher strain for the Mavic Pro than the Phantom 3. This complexity underscores the need for more impact scenarios and sensitivity studies, as this investigation only considers a single impact scenario.

Due to the complexity of these collisions, it is necessary to account for various factors like drone orientation, impact velocity, and human vulnerability. Practical approaches, such as cadaveric experiments and computational modeling, assume a pivotal role in establishing foundational datasets for comprehending potential injury outcomes.

Regulatory authorities face the challenging task of balancing the benefits of sRPAS with associated safety concerns. This study contributes to this ongoing discourse by offering a comprehensive analysis of head impacts from distinct drone models. The integration of realistic finite element models, verified using cadaveric data, underscores the imperative role of reliable datasets in shaping regulatory decisions.

Despite the thoroughness of this study, it's important to acknowledge certain limitations. The primary emphasis on frontal impact scenarios somewhat limits the scope of address collisions from different angles and scenarios. Additionally, the divergent impact

conditions between the two drone models—particularly how the body shell of the Phantom 3 and the battery of the Mavic Pro impact the head—might introduce variations in results. This underscores the importance of nuanced interpretation when considering differences in material structure. Although there are limitations as mentioned earlier, it's important to emphasize the efforts in creating a well-verified sRPAS model and studying head kinematics during sRPAS-to-human impacts have yielded valuable and original insights. Furthermore, there is a need for more experimental and computational research in light of the expected rapid growth in sRPAS utilization.

4.5 Conclusion

A finite element model representing a quadcopter-style sRPAS was developed and performed four impact simulations, focusing solely on frontal 58-degree impacts. The model accurately predicted head linear accelerations and rotational velocities, aligning well with data obtained from cadaveric experiments. This study compared the injury kinematics of two distinct sRPAS models: the previously developed Phantom 3 and the newly developed Mavic Pro, under two different impact speeds. Comparing the impacts, the Mavic Pro showed higher linear acceleration, HIC, skull stress, and brain strain compared to the Phantom 3. Notably, rotational velocity differed, with the Mavic Pro impact resulting in less rotation than the Phantom 3 impact. These findings underscore the vital necessity of implementing robust safety measures in both drone design and operation. This study significantly contributes to the ongoing endeavors of aviation regulatory authorities, aiding in the delicate balance between the advantages and hazards of sRPAS operations. Ultimately, this work serves to ensure the safety of individuals on the ground.

Chapter 5

5 Conclusion

5.1 Summary and Conclusions

With the growing utilization of sRPAS, ensuring the safety of individuals on the ground from head impacts caused by sRPAS has become a significant priority. Regulatory bodies are actively engaged in comprehending the impact of sRPAS on human heads to facilitate the development of safety regulations. This includes considering how the general population on the ground could be affected by such impacts.

The project commenced by verifying the THUMS V4.02 female pedestrian head model, and the computational outcomes demonstrated strong concordance with experimental results. The THUMS head model verification encompassed 9 cadaveric experiments. Subsequently, a comparison between the head responses of an average male and a small female was conducted in response to a Phantom 3 impacting on the head. A total of 17 simulations were executed for small female, utilizing loading conditions consistent with the male impact case outlined in the ASSURE report. Notably, the small female exhibited lower skull stress in comparison to the average male, despite experiencing higher linear acceleration and HIC values. In terms of brain strain, the small female encountered greater strain than the male under the same impact conditions.

The comprehension of sRPAS-to-head impact has primarily centered around the male and female populations. However, there exist other vulnerable groups, such as children, who could be at a heightened risk of injury from sRPAS impacts. To address this, we verified sRPAS-to-child models representing ages 10, 6, and 3 years old. These models were subjected to impact scenarios similar to those applied to males. As direct cadaveric data for child models were lacking, we employed scaling laws based on male PMHS results. Generally, the simulation results exhibited consistent curve patterns and peak values with the scaled outcomes. Remarkably, the 3-year-old model demonstrated greater linear acceleration and HIC values yet exhibited lower von Mises stress in comparison to the 10-year-old and 6-year-old models. Specifically, the 6-year-old model consistently

displayed higher brain strain than the 10-year-old model, while the 3-year-old model showcased lower brain strain compared to both the 6-year-old and 10-year-old models.

Additionally, the project advanced by creating a new representative quadcopter sRPAS FE model. Subsequently, this sRPAS model was integrated with the THUMS human body model. The determination of contact conditions between the sRPAS and human body model involved numerous trials, aligning simulations with experimental results. Leveraging the invaluable experimental data from PMHS, the developed sRPAS model was fine-tuned to correspond with measurements from four cadaveric experiments. This study compared the impact of the previously developed drone (Phantom 3) with the impact of the newly developed drone (Mavic Pro) on both male and female models. This comparison highlighted that the Mavic Pro induced higher linear acceleration, HIC, skull stress, and brain strain in contrast to the Phantom 3, despite the less mass of Mavic Pro. Notably, the two drones also diverged in terms of rotational velocity, with the Mavic Pro generating less rotation than the Phantom 3 upon impact.

5.2 Limitations

The first limitation arises from the scarcity of cadaveric data for head impact, primarily due to the novelty of this emerging research direction. The absence of cadaveric experiments involving vulnerable groups such as females and children hampers the verification of models concerning the impacts of sRPAS on these populations. The verification of female and child simulations relied on scaled data from male PMHS experiments, a common approach that might not fully account for the intricate interplay of gender and age disparities in head injury responses. Although extensive verification on head kinematics was conducted for male models, direct validation on head responses like brain strain and skull stress during sRPAS head impacts was lacking. Future research could bolster accuracy by incorporating data specifically collected from female and child cadavers to refine female head models. Nonetheless, the human model used in this study underwent verification against brain-skull relative motion data which has been extensively employed in automotive and sports collision contexts.

Additionally, there is a limitation concerning the study's emphasis solely on frontal impacts at a 58-degree angle, possibly overlooking a broader range of collision scenarios possible with the Mavic Pro model. Hence, a comparison between the impacts of the two drones could only be made for a single impact setting, limiting the scope. Additionally, variations in impact angles, speeds, and directions could yield diverse outcomes, underscoring the need for comprehensive coverage.

The study's FE model relies on simplifications and assumptions that could potentially compromise the accuracy of the results. Differences between the Phantom 3 and Mavic Pro models' impact characteristics, where the body shell or battery hits the head first, further introduced complexity and potential limitations. Moreover, the use of simplified material models, especially for the battery component, contrasts with the intricate structure of physical Lithium-ion batteries typically used in sRPAS. This simplification could impact the overall mechanical properties and deformation behaviors during impact.

The sensitivity of FE simulations to model parameters and assumptions also poses a limitation. Minor alterations in input parameters can lead to disparate outcomes. The absence of real-world cadaveric data for child and female models necessitated reliance on scaled male cadaver data for verification, introducing potential variability due to the proportional approach used for impact settings.

The scaling of experimental cadaveric data based on mass also posed a limitation. Ideally, the detailed medical scans of tested head could be used, which, however, were not available for early cadaveric experiments. Meanwhile, the dimensions of specimen heads could be adopted in the future to develop specimen-specific FE model for improved verification and validation.

Acknowledging these constraints, it is important to recognize the necessity for further research, encompassing experimental validation and a broader range of impact scenarios, to gain a more comprehensive understanding of the safety implications of drones on individuals.

5.3 Future Work

Collaborative research efforts are essential to further investigate brain injuries caused by sRPAS head impacts. Building upon this study, numerous avenues for future research are apparent, enabling a deeper understanding of the risks associated with sRPAS impacts.

This section will delve into the potential research directions that can be pursued using this study as a foundation.

5.3.1 Expanded Impact Scenarios

The study has focused on specific impact scenarios, but there's room for future research to broaden its scope. This could involve examining various collision situations with different impact angles, velocities, and directions. This expanded approach would offer a more thorough understanding of how small remotely piloted aircraft system (sRPAS) impacts affect head injuries. For example, the study looked at four impact settings for the Phantom 3 model and one for the Mavic Pro. To enhance future investigations, it would be valuable to extend the impact scenarios for the Mavic Pro using the same four settings as the Phantom 3. This would allow for a direct comparison of impact severity and injury outcomes between the two sRPAS models. Additionally, the current study didn't include cases of free-falling impacts. In the future, there's potential for research to incorporate different free-falling scenarios from varying heights. Exploring these scenarios could provide important insights into the potential injuries caused by sRPAS accidents. By considering a wider range of collision and impact scenarios, future research can deepen the understanding of head injuries from sRPAS impacts and contribute to injury prevention strategies and safety regulations.

5.3.2 Advanced sRPAS modeling and Material selection

The developed finite element system for sRPAS-to-human head impacts offers a practical avenue for manufacturers to devise strategies safeguarding against sRPAS collisions. One potential approach is to consider a slight reduction in the stiffness of the sRPAS shell. This change could help reduce the kinematics effects and, in turn, decrease the risks of injury. Furthermore, refining the precision of finite element models through enhanced

material modeling for various components, including the shell thickness and optimal battery material selection, could lead to more accurate injury prediction.

5.3.3 Impact analysis for vulnerable populations

Further investigation is required concerning the effects of sRPAS impacts on small females and children. The data gathered from Phantom 3 impact scenarios suggests that vulnerable groups like children and small females might be more susceptible to severe injuries compared to adults. Extending research to the newly developed sRPAS model, such as the Mavic Pro, could provide a more comprehensive understanding of how sRPAS impacts affect small females and children. This extension could encompass a variety of impact cases, considering all possible directions of impact. Due to their lighter body and head mass and less rigid neck structure compared to adults, it's crucial to delve deeper into these specific population groups to comprehend the potential risks associated with sRPAS impacts.

5.3.4 Cadaveric study

Acquiring additional real-world cadaveric data, especially for females and children, would enhance the accuracy of the small female head model. Incorporating more diverse and representative data would lead to more reliable injury predictions, particularly for vulnerable populations.

5.3.5 Sensitivity analysis and Injury metrics

This study highlights the significant impact of structural variations in sRPAS on injury kinematics, particularly HIC and BrIC. The location of sRPAS interaction with the head plays a crucial role in shaping these results. Significantly, there are cases where the statistical significance of the relationship between HIC and skull stress, as well as between BrIC and brain strain, is not strong. Even slight alterations in angles can yield vastly different HIC and BrIC values, underscoring the importance of sensitivity studies. These investigations serve to unveil how minor changes in angle or kinetic energy can translate into variations in injury kinematics outcomes. Moreover, the injury metrics utilized for assessing sRPAS impacts draw heavily from the realm of automotive safety,

which significantly differs from the dynamics of sRPAS impacts. As a result, the quest for new injury metrics becomes imperative to accurately capture the nuances of lightweight sRPAS impacts.

5.4 Novelty, significance, and impact of work

- 1) The THUMS 4.02 small female head model for pedestrians underwent verification through several cadaveric experiments. Subsequently, an exploration into the distinctions between average males and small females was conducted. The study's finding that small females experience higher injury metric values compared to males provides critical insights for designing gender-specific head protection strategies. This acknowledgment of gender differences in injury response can lead to more inclusive and effective safety measures.
- 2) The study's uniqueness lies in its focus on different age groups of children (10-year-old, 6-year-old, and 3-year-old), recognizing that children of varying ages may have different responses to head impacts. This age-specific analysis adds a novel dimension to the study, serves as the first study on children to the best of the author's knowledge.
- 3) The research holds significant importance due to its focus on the safety of children, who are particularly susceptible to head injuries. By examining age-related differences in injury risk, the study contributes to a better understanding of how children of varying ages might respond to head impacts, leading to improved protective.
- 4) The study highlights the importance of considering rotational kinematics, such as rotational velocities, in assessing head injuries. Additionally, the emphasis on brain strain metrics (BrIC, CSDM10, CSDM15, and CSDM20) offers a deeper insight into the mechanisms of injury beyond traditional linear acceleration metrics.
- 5) The research stands out by conducting a comparative analysis between two distinct sRPAS models (Mavic Pro and Phantom 3) in terms of impact dynamics and potential injury mechanisms. This comparative approach provides a nuanced

understanding of how different drone designs can lead to varying injury outcomes.

- 6) The research's findings have direct implications for drone design and regulatory efforts. The insight into how different sRPAS models can lead to distinct injury patterns can guide manufacturers in designing safer drones. Moreover, aviation regulatory bodies can use this information to formulate safety protocols and standards for sRPAS operations.
- 7) Overall, this study provides a unique understanding of the head kinematics, injury metrics and injury mechanism under sRPAS to head impact. The insights gained from this research can contribute to the establishment of industry standards for drone impact safety. This has the potential to shape the direction of drone technology development and usage, ensuring safety is prioritized.

References

- [1] L. K. Chung, Y. Cheung, C. Lagman, N. Au Yong, D. Q. McBride, and I. Yang, “Skull fracture with effacement of the superior sagittal sinus following drone impact: a case report,” *Child’s Nervous System*, vol. 33, no. 9, 2017, doi: 10.1007/s00381-017-3485-z.
- [2] STRATEGIC MARKET RESEARCH LLP, “Commercial Drone Market,” 2022.
- [3] S. Gorucu and Y. Ampatzidis, “Drone Injuries and Safety Recommendations,” *EDIS*, vol. 2021, no. 3, 2021, doi: 10.32473/edis-ae560-2021.
- [4] N. Spitzer and J. K. Singh, “Pediatric ocular trauma caused by recreational drones: two case reports,” *Journal of AAPOS*, vol. 22, no. 3, 2018, doi: 10.1016/j.jaapos.2017.11.010.
- [5] A. I. King, *The Biomechanics of Impact Injury*. 2018. doi: 10.1007/978-3-319-49792-1.
- [6] L. K. Paul *et al.*, “Agenesis of the corpus callosum: Genetic, developmental and functional aspects of connectivity,” *Nature Reviews Neuroscience*, vol. 8, no. 4. 2007. doi: 10.1038/nrn2107.
- [7] J. A. Hobson, R. W. Mccarley, and P. W. Wyzinski, “Sleep cycle oscillation: Reciprocal discharge by two brainstem neuronal groups,” *Science (1979)*, vol. 189, no. 4196, 1975, doi: 10.1126/science.1094539.
- [8] D. L. Sparks, “The brainstem control of saccadic eye movements,” *Nat Rev Neurosci*, vol. 3, no. 12, 2002, doi: 10.1038/nrn986.
- [9] E. Skoe, J. Krizman, S. Anderson, and N. Kraus, “Stability and plasticity of auditory brainstem function across the lifespan,” *Cerebral Cortex*, vol. 25, no. 6, 2015, doi: 10.1093/cercor/bht311.

- [10] C. Giordano and S. Kleiven, "Evaluation of Axonal Strain as a Predictor for Mild Traumatic Brain Injuries Using Finite Element Modeling," *Stapp Car Crash J*, vol. 58, 2014.
- [11] T. W. McAllister *et al.*, "Maximum principal strain and strain rate associated with concussion diagnosis correlates with changes in corpus callosum white matter indices," *Ann Biomed Eng*, vol. 40, no. 1, 2012, doi: 10.1007/s10439-011-0402-6.
- [12] A. Post, T. Blaine Hoshizaki, M. D. Gilchrist, and M. D. Cusimano, "Peak linear and rotational acceleration magnitude and duration effects on maximum principal strain in the corpus callosum for sport impacts," *J Biomech*, vol. 61, 2017, doi: 10.1016/j.jbiomech.2017.07.013.
- [13] H. Mao, "Modeling the Head for Impact Scenarios," in *Basic Finite Element Method as Applied to Injury Biomechanics*, 2017. doi: 10.1016/B978-0-12-809831-8.00012-X.
- [14] Anatomy Info, "Skull Bone Anatomy & Clinical Significances."
- [15] J. B. R. P. and S. D. G. Olivares, "Task A14: UAS Ground Collision Severity Evaluation," 2019.
- [16] A. Radi, "Human injury model for small unmanned aircraft impacts," 2013.
- [17] T. Green and T. Barth, "Injury evaluation and comparison of lateral impacts when using conventional and inflatable restraints," in *Proceedings - Annual SAFE Symposium (Survival and Flight Equipment Association)*, 2006.
- [18] Humanetics, "FAA Hybrid III 50M."
- [19] J. Kerrigan *et al.*, "Kinematic comparison of the POLAR-II and PMHS in pedestrian impact tests with a sport-utility vehicle," in *International Research Council on the Biomechanics of Impact - 2005 International IRCOBI Conference on the Biomechanics of Impact, Proceedings*, 2005.

- [20] J. R. Kerrigan, D. B. Murphy, D. C. Drinkwater, and J. R. Crandall, "Kinematic corridors for PMHS tested in full-scale pedestrian impact tests," in *Proceeding in 19th International Technical Conference on the Enhanced Safety Vehicle (ESV)*, 2005.
- [21] J. S. Ruan, T. B. Khalil, and A. I. King, "Finite element modeling of direct head impact," in *SAE Technical Papers*, 1993. doi: 10.4271/933114.
- [22] H. S. Kang, R. Willinger, B. M. Diaw, and B. Chinn, "Validation of a 3D anatomic human head model and replication of head impact in motorcycle accident by finite element modeling," in *Stapp Car Crash Conference Proceedings*, 1997.
- [23] S. Kleiven and H. Von Holst, "Consequences of head size following trauma to the human head," *J Biomech*, vol. 35, no. 2, 2002, doi: 10.1016/S0021-9290(01)00202-0.
- [24] E. G. Takhounts, R. H. Eppinger, J. Q. Campbell, R. E. Tannous, E. D. Power, and L. S. Shook, "On the Development of the SIMon Finite Element Head Model," in *SAE Technical Papers*, 2003. doi: 10.4271/2003-22-0007.
- [25] H. Mao *et al.*, "Development of a finite element human head model partially validated with thirty five experimental cases," *J Biomech Eng*, vol. 135, no. 11, 2013, doi: 10.1115/1.4025101.
- [26] S. Ji *et al.*, "Group-wise evaluation and comparison of white matter fiber strain and maximum principal strain in sports-related concussion," *J Neurotrauma*, vol. 32, no. 7, 2015, doi: 10.1089/neu.2013.3268.
- [27] T. J. Horgan and M. D. Gilchrist, "The creation of three-dimensional finite element models for simulating head impact biomechanics," *International Journal of Crashworthiness*, vol. 8, no. 4, 2003, doi: 10.1533/ijcr.2003.0243.
- [28] C. Deck and R. Willinger, "Head injury prediction tool for predictive systems optimization," *7th European LS-DYNA Conference*, 2008.

- [29] E. S. Gurdjian, V. L. Roberts, and L. M. Thomas, "Tolerance curves of acceleration and intracranial pressure and protective index in experimental head injury," *Journal of Trauma - Injury, Infection and Critical Care*, vol. 6, no. 5, 1966, doi: 10.1097/00005373-196609000-00005.
- [30] E. S. Gurdjian, H. R. Lissner, V. R. Hodgson, and L. M. Patrick, "Mechanism of head injury.," *Clin Neurosurg*, vol. 12, 1964, doi: 10.1097/00000658-194304000-00006.
- [31] C. W. Gadd, "Use of a weighted-impulse criterion for estimating injury hazard," in *SAE Technical Papers*, 1966. doi: 10.4271/660793.
- [32] A. Bartsch, E. Benzel, V. Miele, and V. Prakash, "Impact test comparisons of 20th and 21st century American football helmets: Laboratory investigation," *J Neurosurg*, vol. 116, no. 1, 2012, doi: 10.3171/2011.9.JNS111059.
- [33] L. Zhang, K. H. Yang, and A. I. King, "A Proposed Injury Threshold for Mild Traumatic Brain Injury," *J Biomech Eng*, vol. 126, no. 2, 2004, doi: 10.1115/1.1691446.
- [34] F. , E. R. H. , H. M. , K. N. , K. S. , M. M. , N. T. , S. R. , S. E. , and T. E. Bandak, "Development of Improved Injury Criteria for the Assessment of Advanced Automotive Restraint Systems - II," 1999.
- [35] H. R. LISSNER, M. LEBOW, and F. G. EVANS, "Experimental studies on the relation between acceleration and intracranial pressure changes in man," *Surg Gynecol Obstet*, vol. 111, 1960.
- [36] A. J. Padgaonkar, K. W. Krieger, and A. I. King, "Measurement of angular acceleration of a rigid body using linear accelerometers," *Journal of Applied Mechanics, Transactions ASME*, vol. 42, no. 3, 1975, doi: 10.1115/1.3423640.
- [37] E. G. Takhounts, M. J. Craig, K. Moorhouse, J. McFadden, and V. Hasija, "Development of brain injury criteria (BrIC).," *Stapp Car Crash J*, vol. 57, 2013.

- [38] A. S. and S. O. E. Lee, "NHTSA Oblique Test Data Analysis Method by LSDYNA Modeling," 2020.
- [39] J. A. Newman, "A GENERALIZED ACCELERATION MODEL FOR BRAIN INJURY THRESHOLD (GAMBIT)," in *International Conference on the Biomechanics of Impact IRCOBI*, 1986.
- [40] R. M. Greenwald, J. T. Gwin, J. J. Chu, and J. J. Crisco, "Head impact severity measures for evaluating mild traumatic brain injury risk exposure," *Neurosurgery*, vol. 62, no. 4, 2008, doi: 10.1227/01.neu.0000318162.67472.ad.
- [41] L. F. Gabler, J. R. Crandall, and M. B. Panzer, "Development of a Metric for Predicting Brain Strain Responses Using Head Kinematics," *Ann Biomed Eng*, vol. 46, no. 7, 2018, doi: 10.1007/s10439-018-2015-9.
- [42] C. R. Summers, B. Ivins, and K. A. Schwab, "Traumatic brain injury in the United States: An epidemiologic overview," *Mount Sinai Journal of Medicine*, vol. 76, no. 2, 2009. doi: 10.1002/msj.20100.
- [43] K. M. Tse, S. P. Lim, V. B. C. Tan, and H. P. Lee, "A review of head injury and finite element head models," 2014.
- [44] C. H. Hardy and P. V. Marcal, "Elastic analysis of a skull," *Journal of Applied Mechanics, Transactions ASME*, vol. 40, no. 4, 1973, doi: 10.1115/1.3423172.
- [45] T. A. Shugar, "TRANSIENT STRUCTURAL RESPONSE OF THE LINEAR SKULL-BRAIN SYSTEM.," in *Stapp Car Crash Conference Proceedings*, 1975.
- [46] L. E. Miller, J. E. Urban, and J. D. Stitzel, "Development and validation of an atlas-based finite element brain model," *Biomech Model Mechanobiol*, vol. 15, no. 5, 2016, doi: 10.1007/s10237-015-0754-1.
- [47] W. N. Hardy *et al.*, "A study of the response of the human cadaver head to impact.," *Stapp Car Crash J*, vol. 51, 2007.

- [48] A. M. Nahum, R. Smith, and C. C. Ward, "Intracranial pressure dynamics during head impact," in *SAE Technical Papers*, 1977. doi: 10.4271/770922.
- [49] L. Zhang *et al.*, "Recent Advances in Brain Injury Research: A New Human Head Model Development and Validation," in *SAE Technical Papers*, 2001. doi: 10.4271/2001-22-0017.
- [50] F. A. O. Fernandes, D. Tchepel, R. J. Alves de Sousa, and M. Ptak, "Development and validation of a new finite element human head model: Yet another head model (YEAHM)," *Engineering Computations (Swansea, Wales)*, vol. 35, no. 1, 2018, doi: 10.1108/EC-09-2016-0321.
- [51] M. Iwamoto and Y. Nakahira, "Development and Validation of the Total Human Model for Safety (THUMS) Version 5 Containing Multiple 1D Muscles for Estimating Occupant Motions with Muscle Activation During Side Impacts," *Stapp Car Crash J*, vol. 59, 2015.
- [52] D. Jenkins and B. Vasigh, "The Economic Impact of Unmanned Aircraft Systems Integration in the United States," 2013.
- [53] M. B. Forrester, "Drone-related injuries treated at emergency departments," *American Journal of Emergency Medicine*, vol. 37, no. 11, 2019. doi: 10.1016/j.ajem.2019.07.006.
- [54] J. A. Johnson, M. R. Svach, and L. H. Brown, "Drone and Other Hobbyist Aircraft Injuries Seen in U.S. Emergency Departments, 2010–2017," *Am J Prev Med*, vol. 57, no. 6, 2019, doi: 10.1016/j.amepre.2019.06.023.
- [55] D. , E. M. , P. R. , Z. F. , & F. D. Arterburn, "FAA UAS Center of Excellence task A4: UAS ground collision severity evaluation," 2017.
- [56] Y. Weng, K. Bian, K. Gunasekaran, J. Gholipour, C. Vidal, and H. Mao, "Modeling small remotely piloted aircraft system to head impact for investigating craniocerebral response," *J Biomech*, vol. 128, 2021, doi: 10.1016/j.jbiomech.2021.110748.

- [57] L. XIN, "MATHEMATICAL MODELLING OF HUMAN INJURY LEVELS DUE TO UNMANNED AERIAL VEHICLE (UAV) IMPACT".
- [58] T. Magister, "The small unmanned aircraft blunt criterion based injury potential estimation," *Saf Sci*, vol. 48, no. 10, 2010, doi: 10.1016/j.ssci.2010.04.012.
- [59] J. T. Eckner, K. L. O'Connor, S. P. Broglio, and J. A. Ashton-Miller, "Comparison of Head Impact Exposure Between Male and Female High School Ice Hockey Athletes," *American Journal of Sports Medicine*, vol. 46, no. 9, 2018, doi: 10.1177/0363546518777244.
- [60] C. C. Giza *et al.*, "Summary of evidence-based guideline update: Evaluation and management of concussion in sports: Report of the Guideline Development Subcommittee of the American Academy of Neurology," *Neurology*, vol. 80, no. 24, 2013, doi: 10.1212/wnl.0b013e31828d57dd.
- [61] K. G. Harmon *et al.*, "American Medical Society for Sports Medicine position statement: concussion in sport.," *British journal of sports medicine*, vol. 47, no. 1. 2013. doi: 10.1136/bjsports-2012-091941.
- [62] Z. Y. Kerr *et al.*, "Epidemiologic measures for quantifying the incidence of concussion in national collegiate athletic association sports," *J Athl Train*, vol. 52, no. 3, 2017, doi: 10.4085/1062-6050-51.6.05.
- [63] J. M. Hootman, R. Dick, and J. Agel, "Epidemiology of collegiate injuries for 15 sports: Summary and recommendations for injury prevention initiatives," *Journal of Athletic Training*, vol. 42, no. 2. 2007.
- [64] T. Covassin, R. Moran, and R. J. Elbin, "Sex differences in reported concussion injury rates and time loss from participation: An update of the national collegiate athletic association injury surveillance program from 2004-2005 through 2008-2009," *Journal of Athletic Training*, vol. 51, no. 3. 2016. doi: 10.4085/1062-6050-51.3.05.

- [65] G. L. Garcés, D. Medina, L. Milutinovic, P. Garavote, and E. Guerado, “Normative database of isometric cervical strength in a healthy population,” *Med Sci Sports Exerc*, vol. 34, no. 3, 2002, doi: 10.1097/00005768-200203000-00013.
- [66] N. Yoganandan and F. A. Pintar, “Deflection, acceleration, and force corridors for small females in side impacts,” *Traffic Inj Prev*, vol. 6, no. 4, 2005, doi: 10.1080/15389580500256888.
- [67] T. Wu, J. Antona-Makoshi, A. Alshareef, J. S. Giudice, and M. B. Panzer, “Investigation of Cross-Species Scaling Methods for Traumatic Brain Injury Using Finite Element Analysis,” *J Neurotrauma*, vol. 37, no. 2, 2020, doi: 10.1089/neu.2019.6576.
- [68] Y. Weng, “Investigation of Small Remotely Piloted Aircraft System (sRPAS) to Human Head Impact,” Electronic Thesis and Dissertation Repository. 7978, 2021. Accessed: Aug. 07, 2023. [Online]. Available: <https://ir.lib.uwo.ca/etd/7978>
- [69] T. M. Corporation, “Documentation: Total Human Model for Safety (THUMS) AF05 pedestrian/occupant model academic version 4.02_ 20181226,” 2018.
- [70] W. N. Hardy, C. D. Foster, M. J. Mason, K. H. Yang, A. I. King, and S. Tashman, “Investigation of Head Injury Mechanisms Using Neutral Density Technology and High-Speed Biplanar X-ray,” in *SAE Technical Papers*, 2001. doi: 10.4271/2001-22-0016.
- [71] N. Yoganandan, J. Zhang, and F. A. Pintar, “Force and acceleration corridors from lateral head impact,” *Traffic Inj Prev*, vol. 5, no. 4, 2004, doi: 10.1080/15389580490510336.
- [72] R. W. Nightingale, J. H. McElhaney, D. L. Camacho, M. Kleinberger, B. A. Winkelstein, and B. S. Myers, “Dynamic responses of the cervical spine: Buckling, end conditions, and tolerance in compressive impacts,” in *Stapp Car Crash Conference Proceedings*, 1997.

- [73] C. J.D. *et al.*, “Incidence, risk factors and prevention of mild traumatic brain injury: Results of the WHO Collaborating Centre Task Force on Mild Traumatic Brain Injury,” *J Rehabil Med Suppl*, no. 43, 2004.
- [74] C. A. Hawley, A. B. Ward, J. Long, D. W. Owen, and A. R. Magnay, “Prevalence of traumatic brain injury amongst children admitted to hospital in one health district: A population-based study,” *Injury*, vol. 34, no. 4, 2003, doi: 10.1016/S0020-1383(02)00193-6.
- [75] Federal Aviation Administration, “AC 107-2A - Small Unmanned Aircraft System (Small UAS),” 2021.
- [76] “Girl, 14, killed by model plane after near-misses,” *Telegraph Media Group*, 2003. Accessed: Aug. 15, 2023. [Online]. Available: <https://www.telegraph.co.uk/news/uknews/1447013/Girl-14-killed-by-model-plane-after-near-misses.html>
- [77] E. E. Moskowitz, Y. M. Siegel-Richman, G. Hertner, and T. Schroepfel, “Aerial drone misadventure: A novel case of trauma resulting in ocular globe rupture,” *Am J Ophthalmol Case Rep*, vol. 10, 2018, doi: 10.1016/j.ajoc.2018.01.039.
- [78] K. Ito, M. Tokuyama, H. Miyazaki, S. Hayashi, Y. Kitagawa, and T. Yasuki, “Development of Child Finite Element Models and Vehicle-to-Pedestrian Collision Simulations,” *Paper Knowledge . Toward a Media History of Documents*, 2013.
- [79] T. , Y. Y. , Y. T. , & U. H. Katsuhara, “Analysis Of Kinematics And Head Injury Mechanisms In Car To Child Cyclist Collision Simulation Using Human Fe Model,” *In 26th International Technical Conference on the Enhanced Safety of Vehicles (ESV): Technology: Enabling a Safer Tomorrow National Highway Traffic Safety Administration (No. 19-0030).*, 2019.
- [80] T.M. Corporation, “Total Human Model for Safety (THUMS) 10YO Pedestrian/Occupant Model Version 4,” 2021.

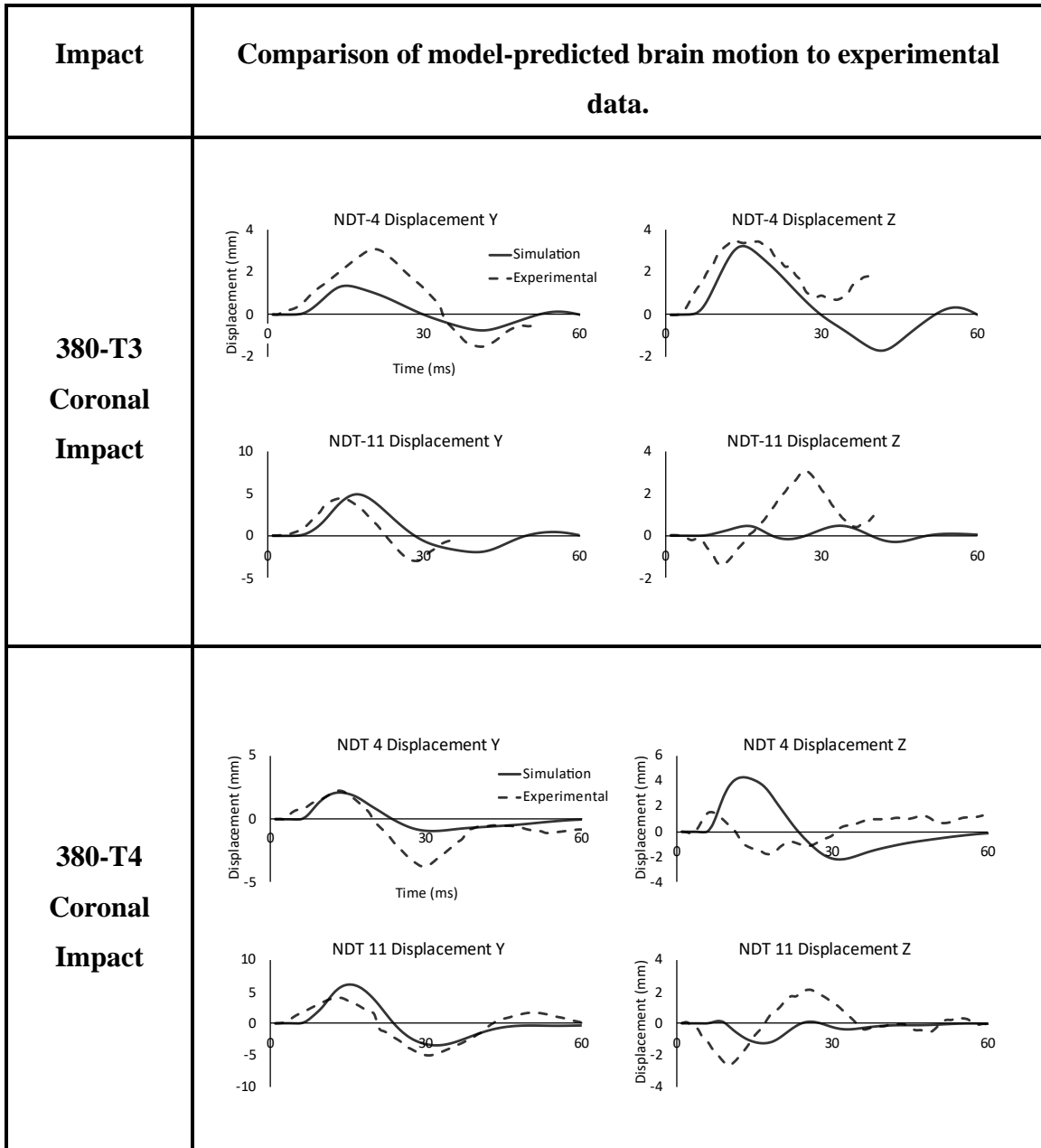
- [81] T.M. Corporation, “Total Human Model for Safety (THUMS) 6YO Pedestrian/Occupant Model Version 4,” 2021.
- [82] T.M. Corporation, “Total Human Model for Safety (THUMS) 3YO Pedestrian/Occupant Model Version 4,” 2021.
- [83] A. M. Loyd, “Studies of the Human Head from Neonate to Adult: An Inertial, Geometrical and Structural Analysis with Comparisons to the ATD Head,” *ProQuest Dissertations and Theses*, 2011.
- [84] J. F. Luck, “The Biomechanics of the Perinatal, Neonatal and Pediatric Cervical Spine: Investigation of the Tensile, Bending and Viscoelastic Response,” *ProQuest Dissertations and Theses*, 2012.
- [85] N. H. T. S. Administration, “Occupant crash protection—head injury criterion,” *Washington, DC: NHTSA.(S6. 2 of FMVSS 571.208), 1972, 1972.*
- [86] A. C. Bain and D. F. Meaney, “Tissue-level thresholds for axonal damage in an experimental model of central nervous system white matter injury,” *J Biomech Eng*, vol. 122, no. 6, 2000, doi: 10.1115/1.1324667.
- [87] Molinet, “Drone crashes into crowd at Memorial Day Parade in Marblehead, Mass.,” *New York Daily News*, 2015. [Online]. Available: <https://www.nydailynews.com/news/national/drone-crashes-crowd-memorial-day-parade-mass-article-1.2235360>
- [88] “Triathlete injured as drone filming race falls to ground,” *ABC News*, 2014. [Online]. Available: <https://www.abc.net.au/news/2014-04-07/triathlete-injured-as-drone-filming-race-drops-to-ground/5371658>
- [89] Curtis, “Operator of remote control helicopter dies,” *The Local Switzerland*, 2013. Accessed: Aug. 15, 2023. [Online]. Available: <https://www.thelocal.ch/20130711/remote-control-helicopter-kills-operator-in-lucerne>

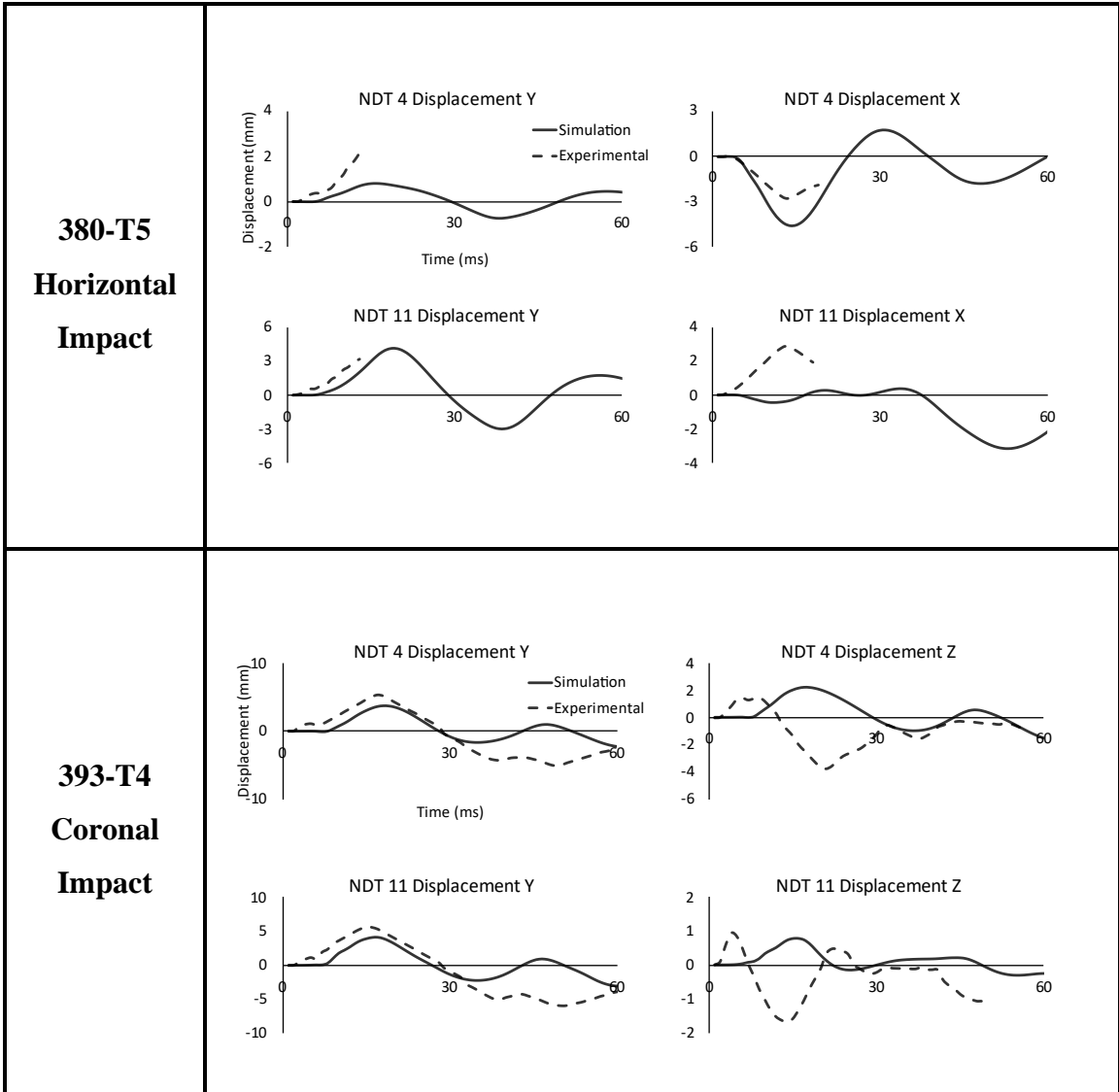
- [90] C. H. Koh *et al.*, “Weight threshold estimation of falling UAVs (Unmanned Aerial Vehicles) based on impact energy,” *Transp Res Part C Emerg Technol*, vol. 93, 2018, doi: 10.1016/j.trc.2018.04.021.
- [91] C. Giordano, X. Li, and S. Kleiven, “Performances of the PIPER scalable child human body model in accident reconstruction,” *PLoS One*, vol. 12, no. 11, 2017, doi: 10.1371/journal.pone.0187916.
- [92] E. J. Pellman *et al.*, “Concussion in professional football: Reconstruction of game impacts and injuries,” *Neurosurgery*, vol. 53, no. 4, 2003, doi: 10.1093/neurosurgery/53.3.799.
- [93] D. B. Stark *et al.*, “Human Response and Injury Resulting from Head Impacts with Unmanned Aircraft Systems,” *Stapp Car Crash J*, vol. 63, 2019, doi: 10.4271/2019-22-0002.

Appendices

Appendix A: THUMS V4.02 small Female Head model verification Result

Figure A 1 Brain Model Verification Results





Appendix A

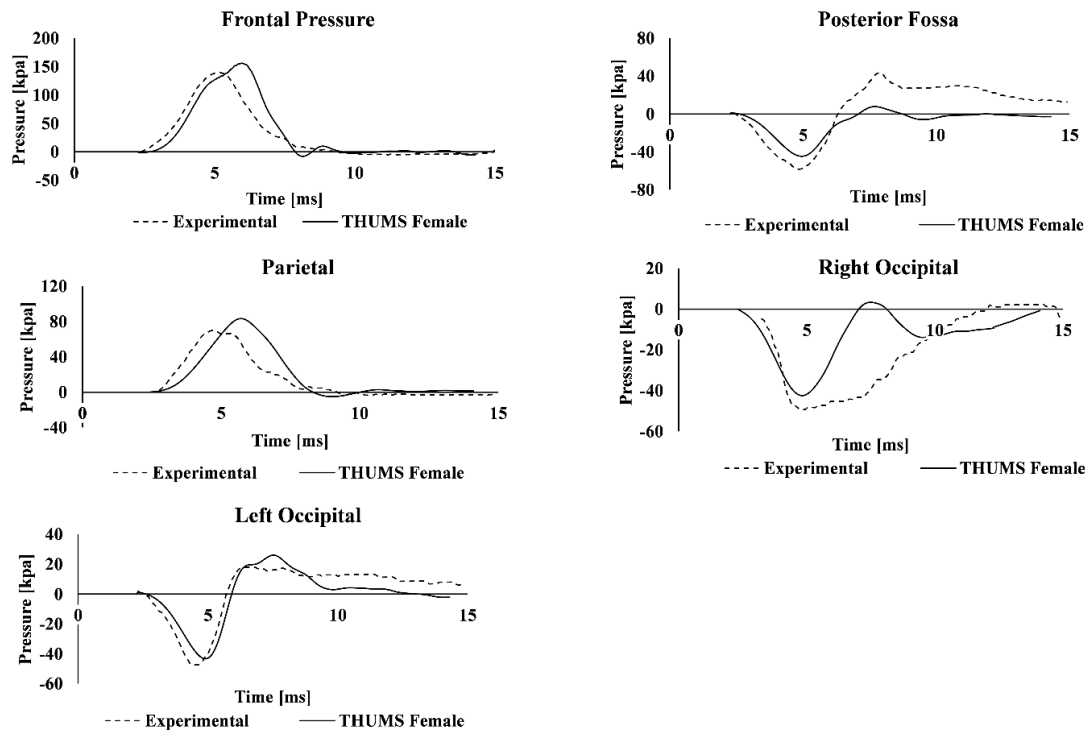


Figure A 2 Comparison of model-predicted brain pressure to experimental data (Nahum et al.[48])

Appendix A

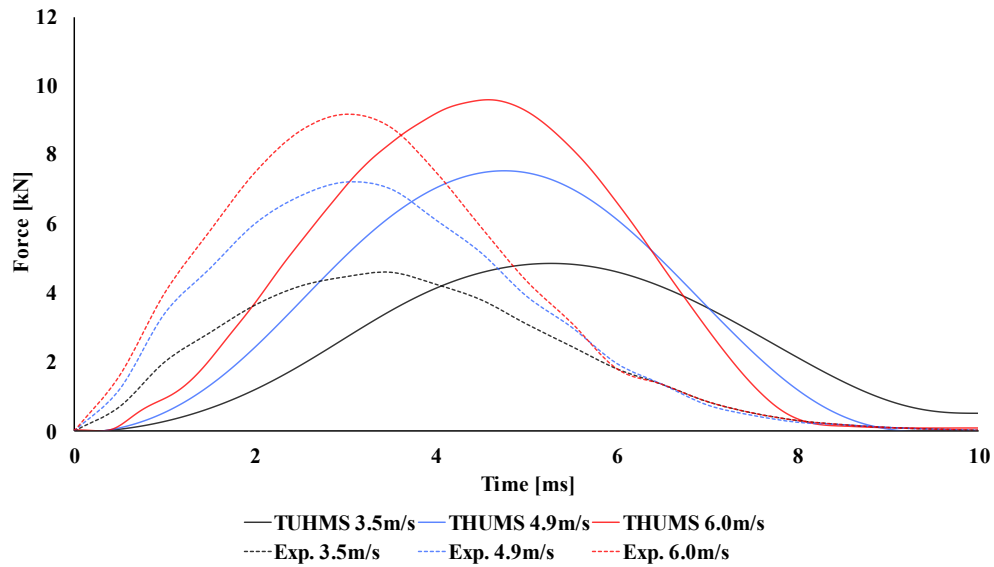


Figure A 3 Force deflection in lateral drop (Yoganandan et al. [71])

Appendix A

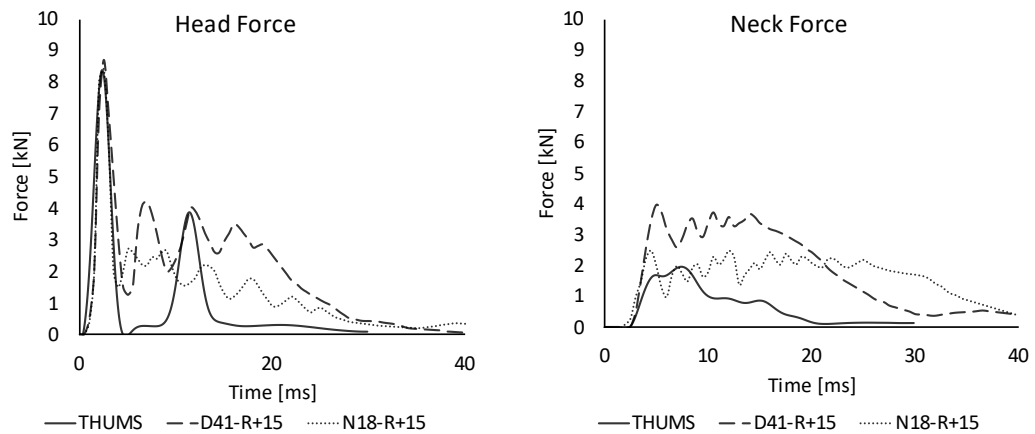


Figure A 4 Comparison of model-predicted force deflection to experimental data
(Nightingale et al. [72])

Appendix B: Material Property of Finite Element model

Table B 1 Material Property of THUMS FE model

Head component			Density (kg/m ³)	Bulk Modulus (MPa)	Shear Modulus		Decay Constant (1/s)	Material Type
					Short- term Shear Modulus (kPa)	Long- term Shear Modulus (kPa)		
Brain	Cerebrum	White Matter	1,000	2,160	12.5	6.125	0.06	Viscoelastic
		Gray Matter	1,000	2,190	10	5	0.06	Viscoelastic
	Cerebellum	White Matter	1,000	2,160	12.5	6.125	0.06	Viscoelastic
		Gray Matter	1,000	2,190	10	5	0.06	Viscoelastic
	Brainstem	White Matter	1,000	2,190	22.5	4.5	0.06	Viscoelastic
		Gray Matter	1,000	2,019	10	5	0.06	Viscoelastic
			Density (kg/m ³)	Bulk Modulus (MPa)	Poisson Ratio	Yield Stress (MPa)		
Skull	Frontal	Cortical	2,120	11,000	0.22	48		Elastic- Plastic
		Trabecular	1,000	100	0.22	0.35		Elastic- Plastic
	Parietal	Cortical	2,120	11,000	0.22	48		Elastic- Plastic
		Trabecular	1,000	100	0.22	4.8		Elastic- Plastic
	Temporal	Cortical	2,120	11,000	0.22	48		Elastic- Plastic
		Trabecular	1,000	100	0.22	4.8		Elastic- Plastic

Appendix C: The summarized head kinematics, injury metrics, skull von Mises stress and brain strain value child model

Table C 1- 10 YO Child Model Results

Case #	Peak Linear acceleration (g)	Peak rotational velocity (deg/s)	HIC	BrIC	Maximum skull stress (MPa)	CSDM10	CSDM15	Mean MPS
1	532	3090	5815	0.87	93.23	0.8976	0.6318	0.19071
2	591	3239	6999	0.9091	102.1	0.9122	0.7001	0.19788
3	669	3553	9521	1.0051	108.98	0.9387	0.7386	0.21321
4	268	2903	1417	0.899	78.53	0.8321	0.5923	0.15966
5	281	3061	1589	0.95	76.41	0.8657	0.6972	0.16405
6	278	2981	1481	0.9226	71.47	0.8876	0.7002	0.16526
7	297	2837	1365	0.8781	75.01	0.9341	0.7866	0.17826
8	474	3539	4887	0.9916	81.2	0.8145	0.3808	0.14206
9	492	3539	5926	0.9916	82.8	0.8678	0.5998	0.16144
10	431	1227	4057	0.3799	61.96	0.3898	0.0676	0.09662
11	454	1198	4862	0.3712	46.04	0.3989	0.2568	0.0966
12	464	1097	5384	0.3402	46.38	0.4355	0.3011	0.09962
13	472	3111	4851	0.8732	85.21	0.8124	0.4465	0.10264
14	492	3539	5926	0.9916	81.9	0.8787	0.5487	0.16144
15	302	2852	1391	0.8832	60.48	0.9322	0.7981	0.18058
16	451	1172	4841	0.363	42.72	0.3898	0.0676	0.09962
17	464	1097	5385	0.3402	46.38	0.4355	0.3011	0.10264

Table C 2- 6 YO Child Model Results

Case #	Peak Linear acceleration (g)	Peak rotational velocity (deg/s)	HIC	BrIC	Maximum skull stress (MPa)	CSDM10	CSDM15	Mean MPS
1	508	2966	4537	0.84	91.57	0.9131	0.6954	0.2041
2	577	3144	5895	0.893	91.01	0.9355	0.7329	0.2155
3	691	3450	9108	0.9861	90.76	0.9633	0.7933	0.2364
4	427	2986	2916	0.923	77.13	0.9558	0.7458	0.1938
5	434	3053	3039	0.94	74.52	0.9600	0.7598	0.1979
6	434	3067	3014	0.9482	68.07	0.9620	0.7657	0.1996
7	454	3207	3189	0.9913	71.9	0.9781	0.8288	0.2197
8	478	2860	5228	0.8004	71.28	0.8384	0.4518	0.1502
9	477	2877	5135	0.8051	75.73	0.8851	0.5626	0.1664
10	487	1651	3809	0.5112	55.1	0.5884	0.1376	0.1094
11	515	1814	4757	0.562	53.91	0.6985	0.2351	0.1229
12	536	1816	5551	0.5622	58.23	0.7358	0.2854	0.1290
13	477	2860	5135	0.8004	80.32	0.8336	0.4449	0.1492
14	477	2877	5135	0.8051	75.73	0.8851	0.5626	0.1664
15	448	3229	3170	0.9978	71.39	0.9798	0.8383	0.2228
16	514	1816	4757	0.5617	45.3	0.7058	0.2427	0.1239
17	536	1816	5551	0.5622	52.1	0.7358	0.2854	0.1290

Table C 3- 3YO Child Model Results

Case #	Peak Linear acceleration (g)	Peak rotational velocity (deg/s)	HIC	BrIC	Maximum skull stress (MPa)	CSDM10	CSDM15	Mean MPS
1	492	2786	5542	0.77	58.46	0.8188	0.5511	0.1751
2	515	2962	6714	0.8238	59.15	0.8387	0.5857	0.1830
3	588	3171	9389	0.8849	59.44	0.8662	0.6124	0.1909
4	475	3499	4263	1.0825	58.8	0.7623	0.3308	0.1531
5	476	3508	4295	1.085	61.79	0.7710	0.3389	0.1545
6	486	3536	4410	1.1	61.82	0.7771	0.3469	0.1556
7	537	3734	4845	1.155	57.76	0.8540	0.4750	0.1728
8	549	3381	5850	0.9517	59.25	0.6944	0.2320	0.1305
9	591	3810	7509	1.07	55.5	0.8015	0.3667	0.1478
10	475	1194	4778	0.3721	55.97	0.2548	0.0512	0.0866
11	565	1419	6158	0.44	62.87	0.2874	0.0592	0.0974
12	600	1661	7144	0.5154	65.45	0.3323	0.0743	0.0999
13	552	3386	5827	0.44	58.46	0.6997	0.2374	0.1312
14	591	3810	7509	1.1	71.2	0.6997	0.2374	0.1312
15	555	3770	4901	1.17	58.34	0.8658	0.5010	0.1762
16	564	1389	6211	0.4317	61.47	0.2887	0.0587	0.0984
17	600	1661	7144	0.5154	65.45	0.3323	0.0743	0.0999

Curriculum Vitae

Name: MD Farhan Hoque Sagar

Post-secondary Education and Degrees: Military Institute of Science and Technology
Dhaka, Bangladesh
2014-2017 BSc

The University of Western Ontario
London, Ontario, Canada
2020-2021 MEng

The University of Western Ontario
London, Ontario, Canada
2021-2023 M.E.Sc

Related Work Experience Teaching Assistant
The University of Western Ontario
2021-2023

Research Assistant
The University of Western Ontario
2021-2023